Experimental and numerical investigation of cluster morphologies and dynamics during biphasic flow in porous media

Atta-Ul Monem Ayaz

UNIVERSITÉ DE STRASBOURG

ÉCOLE DOCTORALE 413

Géophysique expérimentale

Institut de Physique du Globe de Strasbourg

en cotutelle avec l'Université d'Oslo

THÈSE

présentée par:

Atta-ul Monem Ayaz

soutenue le : **16 décembre 2019**

pour obtenir le grade de: **Docteur de l'université de Strasbourg**

Discipline/ Spécialité: Géophysique

Experimental and numerical investigation of cluster morphologies and dynamics during biphasic flow in porous media

THÈSE dirigée par :

M. TOUSSAINT Renaud	Directeur de Recherche CNRS, Université de Strasbourg
M. MÅLØY Knut Jørgen	Professeur, University of Oslo
M. SCHÄFER Gerhard	Professeur, Université de Strasbourg

RAPPORTEURS :

M. SANTUCCI Stephane	Chargé de Recherche CNRS, HDR, ENS de Lyon
Mme. NEUWEILER Insa	Professeur, Leibniz University of Hannover

---

AUTRES MEMBRES DU JURY :

M. ACKERER Philippe	Directeur de Recherche CNRS, Université de Strasbourg

Contents

List of papers

Paper.1: Influence of gravity and finite-size effects on pressure-saturation curves
M.Ayaz, R.Toussaint, K.J Måløy and G.Schäfer
Water Resources Research (submitted manuscript)

Paper.2: Avalanche dynamics and pressure variations during drainage in gravity stabilized flow
M.Ayaz, R.Toussaint, K.J Måløy and G.Schäfer
Physical Review E (proposed paper to be submitted)

Paper.3: Snap-off displacement during slow drainage
M.Ayaz, R.Toussaint, K.J Måløy and G.Schäfer
Frontiers in Physics (proposed paper to be submitted)

Paper.4 (co-author): Frictional Fluid Dynamics and Plug Formation in Multiphase Millifluidic Flow
G.Dumazer, B.Sandnes, M.Ayaz, K.J Måløy and E.Flekkøy
Physical Review Letters (2016), Vol: 117, issue:2, pages: 28002-28007
Doi: 10.1103/PhysRevLett.117.028002

Paper.5 (co-author): Self-Structuring of Granular material under Capillary Bulldozing
G.Dumazer, B.Sandnes, M.Ayaz, K.J Måløy and E.Flekkøy
Powder and Grains 2017 (EPJ), Vol: 140, Article Number: 09016
Doi: 10.1051/epjconf/201714009016

Résumé

Dans notre première étude, nous étudions expérimentalement, numériquement et analytiquement l'influence de la gravité et des effets de taille finie sur les dépendances et mesures de pression-saturation pendant des drainages lents, où le fluide le moins dense envahit le système depuis le haut. Les hydrologues, modélisateurs de réservoirs et les pédologues utilisent beaucoup cette relation pour la fermeture des équations de Darcy généralisées utilisées dans la modélisation continue de tels écoulements.

Nous réalisons des expériences en utilisant des milieux poreux quasi- bidimensionnels, constitués dune monocouche de billes de verre polydisperses disposées en sandwich entre deux plaques de confinement. Les frontières sont scellées avec une couche de gel de silicone avec un côté ouvert la phase d'invasion (air). La différence de pression relative entre la phase non mouillante et la phase mouillante est mesurée l'aide de capteurs piézoélectriques, tandis que la saturation des deux phases est extraite par seuillage de cartes en niveaux de gris partir d'images prises intervalles de temps réguliers. Le fluide visqueux est extrait à débit constant et lent, rendant les effets visqueux négligeables pour le processus d'invasion. En parallèle aux expériences, nous effectuons des simulations numériques en utilisant un algorithme de percolation d'invasion. Dans de tels modèles, l'invasion est représentée par un processus de croissance d'amas sur un réseau aléatoire, dépendant uniquement de la pression hydrostatique globale dans chaque phase et des propriétés capillaires locales, i.e. des seuils de pression capillaire dans les constrictions des pores le long de l'interface. On modifie systématiquement l'effet de gravité en inclinant le système par rapport à la configuration horizontale, ce qui stabilise le processus d'invasion par gravité. La structure de déplacement qui émerge est composée d'amas de fluide mouillant qui restent piégés après que l'interface d'invasion soit passée dans le système et sont donc construits par le mouvement de l'interface. En exploitant la nature fractale de la structure de déplacement, nous sommes en mesure d'obtenir une relation entre la saturation finale, et les nombres sans dimension caractérisant la compétition entre les forces visqueuses, capillaires et gravitationnelles, en utilisant la théorie de la percolation.
Dans le cas 2D (bidimensionnel), cette relation a été vérifiée par les simulations et les expériences. Dans le cas 3D (tridimensionnel), nous avons comparé notre relation avec des expériences réalisées par Nouri et al.[30] Ici, la saturation et la pression ont été mesurées à l'aide d'une colonne suspendue pour quatre types de sols diffrents, démontrant la compatibilité avec nos relations obtenues. De

plus, la saturation, la pression et le nombre de Bond sont fonctionnellement reliés, ce qui permet le regroupement des courbes de pression-saturation en une seule courbe maîtresse.

Dans notre deuxième étude, nous étudions la connectivité du réseau d'écoulement secondaire qui émerge lors de drainages lents. Ce réseau consiste en éléments de films de fluide mouillant piégés, reliés par des ponts capillaires. Une compréhension accrue de ces chemins et des mécanismes par lesquels ils se dconnectent est importante pour comprendre et finalement contrôler le piégeage dans des milieux poreux.Nous effectuons nouveau des expériences dans un milieu poreux synthétique bidimensionnel. Par acquisition optique lors du processus d'invasion, nous sommes en mesure d'identifier les ponts capillaires et cartographier leur connectivité aux amas piégés de fluide mouillant. L'augmentation de la composante gravitationnelle agissant sur le système induit des forces de stabilisation dont l'effet est de modifier la fraction des pores et l'ordre dans lequel l'espace poral est exploré par le fluide d'invasion. Pour répondre à la question de la croissance de ces réseaux et de sa possible dépendance directionnelle à la gravité, on a utilisé une caractérisation par boîtes dinclusion, qui forment le plus petit rectangle entourant un amas. En étudiant la distribution de leurs dimensions le long de la direction moyenne d'écoulement et le long de la direction perpendiculaire, nous avons conclu à labsence d'anisotropie des éléments de ces réseaux. Nous avons utilisé le cadre de la théorie des réseaux pour transformer l'ensemble des ponts capillaires reliés en graphe. Chaque lien correspond un pont capillaire reliant deux grains, et est caractérisé par sa longueur, i.e. la longueur du pont capillaire ou par la distance au centre de masse de l'amas de fluide mouillant piégé. Nous avons caractrisé le réseau en calculant les mesures typiques associées aux graphes, telles que le coefficient de regroupement et l'efficacité. Durant le processus d'invasion, il a parfois été observè que des ponts liquides se fragmentent, ce qui est aussi appelé rupture. Il a été mis en évidence que cette rupture se produit statistiquement plus fréquemment pour les ponts capillaires les plus longs, et la majeure partie des évènements de rupture a lieu près de la position moyenne de l'interface. De plus, la largeur du front entre les deux fluides et la zone d'activité de ruptures se comportent de manière couplée dans l'espace.

De nombreux systèmes réagissent à une condition externe variant de manière lente, non pas par une réaction continue et lente, mais sous forme d'une série d'événements discrets regroupés en ensembles couvrant une large gamme de tailles. De telles avalanches sont observes pour de nombreux systèmes diffrents, entre autres pour le drainage en régime capillaire. Ici, la différence de pression entre les deux fluides est seule responsable du déplacement, et de tels systèmes présentent une évolution de pression caractrisée par des avalanches, également désignés dans la littérature comme des sauts de Haines. Le signal de pression est caractèrisé par des montées lentes suivies de soudaines chutes de pression. L'influence de la gravité dans de tels systèmes a été montrée comme conduisant à des corrélations à longue portée le long de l'interface, réduisant ainsi l'écartement entre les deux phases, et ainsi, limitant l'extension spatiale

du front d'invasion. De plus, la variation de la gravité effective modifie la proportion et la manière dont l'espace poral est envahi, comme c'est la capacité de l'interface à faciliter l'exploration des pores pour le fluide d'invasion qui entraîne les avalanches. Ceci est important pour la dynamique, puisque le nombre de pores accessibles est diminué avec une augmentation de la gravité effective. Au cours des expériences, la pression dans la phase liquide est mesurée en même temps qu'un suivi optique numérique est effectué. Nous montrons en corrélant les deux quantités mesurées que l'évolution intermittente du signal de pression peut être lié à l'invasion de pores multiples sous forme d'avalanches. En outre, nous étudions l'influence de la gravité sur les statistiques d'invasion et d'avalanches de pression, et nous mettons en évidence une relation linéaire entre la taille des sauts de pression et le nombre de pores envahis durant une avalanche, et nous sommes en mesure d'extraire le temps de relaxation moyen de la variation de pression associée à une avalanche.

Enfin, l'étude découlements multiphasiques dans un confinement cylindrique est un sujet important avec un large éventail d'intrêts de recherche, d'un point de vue géophysique, biologique ou d'ingniérie: du transport des cellules sanguines travers les artères et les veines, à celui de pétrole et de gaz par conduites (pipelines). Même le cas simple de découlement biphasique air et eau à travers des tubes et capillaires présente un comportement d'écoulement complexe, avec des transitions communément observées entre écoulement stratifié, bulleux, piston et annulaire, en fonction des vitesses d'écoulements des phases respectives. Les écoulements triphasiques grain-liquide-gaz génèrent également des écoulements complexes, pour les études où l'échelle de longueur caractéristique du système est de l'ordre de la longueur capillaire, ce qui signifie qu'il existe un ménisque d'interface biphasique entre les bords (plaques de confinement). De tels systèmes génrent des motifs causés par l'interaction entre forces capillaires, visqueuses et forces de friction solide, ces dernières existant par le biais d'interactions grain-grain, établissant un réseau de forces qui se connecte à la géométrie de confinement. Pour un confinement quasi-2D, il a été démontr que lorsque de tels systèmes sont amens hors équilibre par une source d'écoulement externe, ils génèrent une varité de motifs.
Dans cette étude, nous étudions plus avant une géométrie de confinement simplifiée: on s'intéresse un tube étroit avec un ménisque capillaire bien défini. Nous regardons les structures qui résultent du déplacement d'une suspension dense constituée d'un granulaire de billes de verre immergé dans l'eau. Au fur et à mesure que le ménisque air/eau passe à travers le tube, soit il évacue les grains de toute la section transversale du tube, soit il laisse derrière lui une structure de matériau granulaire caractérisée par des bouchons granulaires suivis de lacunes.

Summary

In our first this study we experimentally, numerically and analytically study the influence of gravity and finite-size effects on pressure-saturation measurements during slow drainage where the lighter fluid invades the system from the top. This relationship is much used by hydrologist and soil-scientists to give closure to the Darcy equations used in continuum modeling. We experimentally perform tabletop experiments utilizing a quasi two-dimensional (2D) porous medium, made up by a monolayer of poly-disperse glass beads sandwiched between two confining plates. The boundaries are sealed off with a layer of silicon glue with one side open to the invading phase (air). The relative pressure difference between the non-wetting and wetting phase is measured with pressure sensors while the saturation of the two phases is extracted by thresholding the grayscale map from images taken at fixed time lapse. The saturating fluid is withdrawn with a constant slow flow rate, making viscous effects negligible for the invasion process. Coupled with the experiments we perform numerical simulations using an invasion percolation algorithm. In such models the invasion is represented by a cluster growth process on a random lattice, dependent solely on the global homogeneous pressure in each phase and on the local capillary pressure thresholds in the pore throats along the interface. The effect of gravity is systematically varied by tilting the system relative to the horizontal configuration, causing the invasion to be gravity stabilized. The displacement structure that emerges is composed of clusters of defending fluid that stay trapped after the invasion interface has moved through the system and are hence built by the motion of the interface. By exploiting the fractal nature of the displacement structure we are able to obtain a relationship between the final saturation, and the dimensionless capillary and Bond numbers Ca and Bo,characterizing the competition between the viscous, capillary and gravitational forces, using percolation theory. For the 2D case this relation was verified by simulation and experiments. For the 3D case we compared our relation with measurement conducted by Nouri et al[30] Here saturation and pressure were measured using a hanging column apparatus for four different soil types, showing compatibility with our obtained relationship. Moreover the saturation, pressure and Bond number are functionally related allowing for pressure-saturation curves to collapse onto a single master curve.

In our second study we investigate the connectivity of the secondary flow network that emerges during slow drainage. The network consists of clusters of trapped defending fluid in connection to capillary bridges. An increased un-

derstanding of these pathways and mechanism by which they are disconnected is important for the understanding and ultimately controlling entrapment in porous media. We conduct experiments in a two-dimensional synthetic porous medium. By optical monitoring of the invasion process we are able to identify capillary bridges and map their connectivity to trapped clusters. Increasing the gravitational component acting on the system sets up stabilizing forces which in effect changes how much and the sequence by which the pore-space is explored by the invading fluid. To answer the question of possible directional growth of these networks with respect to gravity we utilized a bonding box which is the smallest rectangle that encloses the subnetwork. By studying the distribution of its extension in the l_x direction transverse to the flow direction and l_z parallel to the flow direction, we conclude that the effect of gravity on the structure of the network is not present. Next we utilized the framework of network theory to transform the set of connected capillary bridges and clusters into a graph object. Each edge corresponds to a capillary bridge or the link to its neighboring island of defending fluid. We characterize the network by calculating measures typically associated to networks such as the clustering coefficient and efficiency. During the invasion process liquid bridges were observed to sometimes rupture, also referred to as snap-off. The snap-off was measured to statistically occur more regularly for the longest capillary bridges, and most of the rupturing events took place close to the mean interface position. Furthermore the front width and rupture activity area behave in a coupled manner in space.

Many systems respond to a slowly changing external condition not in a smooth way but in terms of a series of discrete events or bursts spanning a broad range of sizes. Such avalanches are observed for many different systems,including drainage in the capillary regime.

Here the fluid pressure difference between is solely responsible for the displacement, such systems have displayed pressure evolution in terms of avalanches, also referred to in the literature as Haines jumps. The pressure signal is characterized by slow buildups followed by sudden drops in pressure. Influence of gravity in such systems have shown to exhibit long range correlations along the interface, reducing the spread between the two phases, in effect spatially limiting the front of the invading phase. Moreover, varying the effective gravity changes how much and how the pore-space is displaced, while it is the ability of the interface to readjust after a newly invaded area has been displaced which drives the avalanches. This is of importance for the dynamics as the number of pores to redistribute is decreased with an increase in the effective gravity. During experiments the pressure in the phase is measured together with optical monitoring. We show by correlating the two measured quantities that the intermittent evolution of the pressure signal can be related to the invasion of multiple pores in a burst like fashion. Furthermore we investigate the influence of gravity on its statistics, and we found a linear relationship between the size of the bursts and invasion of multiple pores, and we are able to extract the average relaxation time of the pressure decay preceding a burst.

The study of multiphase flows in a cylindrical confinement is an important

topic with a broad range of interest from geophysical, biological and engineering perspective, from transport of blood cells through arteries and veins to flow of oil and gas by pipelines. Even the simple case of two-phase air and water flow through tubes and capillaries displays complex flow behavior, with commonly observed transitions between stratified, bubbly, slug, and annular flow depending on the flow rates of the respective phases. Three-phase grain-liquid-gas flows have shown to generate complex flows. For studies where the characteristic length scale of the system is at the capillary length, meaning there exist an active meniscus between the confining plates. Such systems have shown to generate patterns caused by the interplay between capillary, viscous and the solid frictional forces, the latter existing through grain- grain interactions setting up a force network witch branches onto the confining geometry. For a quasi 2D confinement it has been showed that when such system are driven with an external flow rate out of equilibrium they generate a variety of patterns. In this study we a further investigate a simplified confining geometry: Namely a narrow tube with a well defined capillary meniscus. We look at the structures that arise from the displacement of a dense suspension consisting of a granular bed of glass beads immersed in water. As the meniscus travels through the tube it either evacuates the grains from the whole cross-section of the tube or it seen to leave behind a structure of granular material characterized by its granular plugs followed by gaps

Chapter 1

Introduction

Porous materials widely exist around us and play a role in many aspects of our life. Natural substances such as rocks and soil can often be considered to be porous materials. It is thanks to their porosity that soil allows for precipitation to migrate from the surface to ground water aquifers. Similarly in rocks such as calcite the connected pores set up pathways for mineral water to percolate through stone, allowing for changes of the chemical composition over long time scales. Furthermore, as porous materials have low density of mass and high structural rigidity they are among other found to take shape as skeletal structures. An example is the bones in our body.

The work presented in this thesis is concerned with improving our understanding of the underlying mechanisms by which fluids are transported in porous media and how dense suspensions are transported through a confining geometry [34, 10]. Fluid flow in porous media is a research topic which has been extensively studied for the past decades. An improved understanding of such processes promises economical benefits such as enhanced oil recovery, and great environmental rewards, among other in terms of CO_2 sequestration in sub-sea reservoirs and mapping and controlling of migrating ground water contaminants [31].

From a fundamental perspective flow in porous media is of interest as it displays complex behavior. Such systems responds to a slowly changing external condition not in a smooth way but in the terms of a series of discrete events or bursts spanning a broad range of sizes. Such avalanches are observed for many different systems ranging from earthquakes occurring when slowly moving tectonics plates shear into each other [33], to the tearing of paper [37]. Another example is the motion of a fluid front when it invades a porous medium [8, 35, 28, 15]. Moreover the displacement dynamics is seen to generate fractal structures for certain flow conditions [19, 32, 42, 21].

We will in this study, experimentally investigate two-phase flow in porous media. We will look at the case where the porous medium is allowed to be deformed and for the case where it remains a rigid body. We will utilize two different

confining geometries in our study, namely a cylindrical confinement and a quasi two dimensional porous structure, allowing for reduced system complexity and ease in optical monitoring.
We will study mechanisms governing fluid-displacement during drainage. We show that by combining a detailed description of the pore-scale with parameters acting on the system scale, we are able to find a pressure-saturation relation which allows for upscaling of the system. Furthermore we will increase our understanding of mechanisms by which drainage occurs such as Haines jumps and snap-off. We will look at the case of deformable porous media in a cylindrical confinement within the capillary length, and study how grain-grain interactions and interactions with the confining geometry give rise to the emergence of previously unexplored patterns [10].

Chapter 2

Basic concepts

2.1 Porous media

We begin by defining a porous medium as a rigid material which contains voids. The size of these voids may vary by several orders of magnitude, from the milimetric or centimetric one met in some reservoir rocks, to those of micron size or even smaller in clay soils. The solid skeletal structure is often referred to as the porous matrix and the voids are called pores. The porous material is characterized by its porosity $\phi = V_p/V_{tot}$ which is a ratio between the volume of the pore space V_p and the total volume V_{tot}. Furthermore when studying flow through porous media, we demand the set of pores to be interconnected such that there exists pathways for the flow to percolate from one side of the porous body to the other. If this constraint is met we say that the system is permeable. The ease with which fluid flows through a porous media is characterized by the permeability κ. The permeability is dependent on the porosity but also the geometry of the pores in the medium. It is also directly related to the pressure drop needed to maintain a constant discharge rate over the porous media.

2.2 Leaving Navier-Stokes equation behind

The basic governing equations for the fluid flow of a Newtonian fluid is given by the Navier-Stokes equation. This set of non-linear partial differential equations has no general solution, and only a limited number of exact solutions. For incompressible fluid flow, the continuity equation and Navier-stokes equation is reduced to the form.

$$\nabla \cdot \mathbf{v} = 0 \tag{2.1}$$

$$\frac{\partial \mathbf{v}}{\partial t} + \mathbf{v} \cdot \nabla \mathbf{v} = -\frac{1}{\rho}\nabla p + \nu \nabla^2 \mathbf{v} + \mathbf{g} \tag{2.2}$$

Here $\mathbf{v}$ is the local velocity field, ρ the density, ν the kinemtic viscosity and g the gravitational constant. In addition, for a porous medium there will be a set of complex boundary conditions to consider. Direct modeling can be made by solving simplified version of Navier-Stokes equation, or solving the discrete

Lattice Boltzmann equation [6, 23, 29, 12], among many other methods.

An empirical relationship describing the flow in a porous media was formulated by the French engineer Henri Darcy in 1856 [9]. It has later on been derived from the Navier Stokes equations via averaging [40]. It is analogous to Fourier's law in the field of heat conduction or Fick's law in the field of diffusion theory. Here q is the volume flux per unit of cross sectional area of the sample, κ is the permeability, μ is the dynamic viscosity, p the pressure and ρ is the density of the wetting fluid.

$$q = -\frac{\kappa}{\mu}\nabla\ (p - \rho g z) \tag{2.3}$$

This equation is an important tool for porous media physics and engineering, presenting numerous applications for modeling, among other reservoir rock, and is seen to govern flow in porous media on a macroscale, valid only for stationary slow viscous flow.

2.3 Pore-scale description

In addition to these macroscopic quantities, the porous network is further specified in terms of its local or pore-scale properties, such as the pore-throat size distribution (Fig. 2.1) and the pore-size distribution. This can be defined in multiple ways depending on how the system is probed. For pressure measurements you can define a pore constriction size to be the size of a sudden pressure drop, related via Young-Laplace law (Eq. 2.4) with a threshold pressure being overcome. Similarly for optical monitoring a pore can be defined in multiple geometrical ways, among others by finding the dual of the Delaunay triangulation over the pore-space [27]. Even though the basic physics at a pore-scale is well understood, the collective behavior of the flow in a disorderd system is highly non-trivial [39].

When two immiscible fluids are present in a porous media, there will exist a surface tension between the two fluids. This surface property is caused by the interactions between the fluid molecules trying to minimize the interface area between the two fluids. Hence to increase the interface area work must be performed. Furthermore in equilibrium the curvature of the interface leads to a difference in pressure between the two fluids in contact. The pressure on the concave side exceeds the pressure on the convex side by Δp , which is expressed by the Young-Laplace equation.

$$\Delta p = p_{nw} - p_w = \gamma\Big(\frac{1}{R_1} + \frac{1}{R_2}\Big), \tag{2.4}$$

Here γ is the surface tension between the fluids and R_1 and R_2 are the principal radii of curvatures. We define *wetting*, which is the ability of a liquid to maintain contact with a solid surface. The degree of wetting is determined by a force balance between adhesive and cohesive forces. Macroscopically this is usually defined by the contact angle (see Fig.2.2). If a fluid has a contact

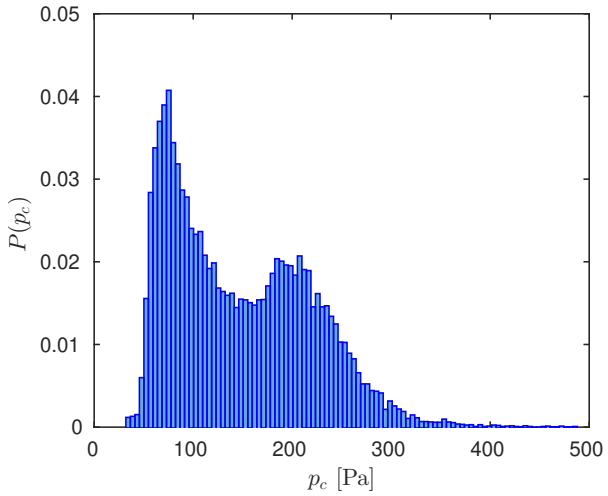

Figure 2.1: Gives the pore-size distribution for the porous matrix used throughout this thesis.

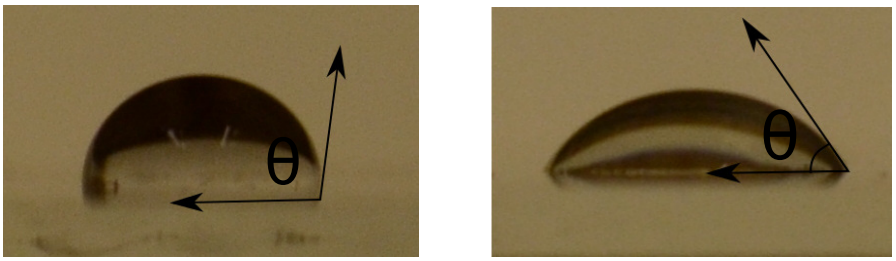

Figure 2.2: The wetting property of the fluid-air-water contact line can be altered, among other by coating the solid surface with silanized fluid. The image to the right shows the droplet before the surface is silanized, having a contact angle of $\theta = 55°$, the image to the left shows the wetting angle after treating the surface with $\theta = 113°$.

angle $\theta < 90$ it is wetting fluid, on the contrary if it has a contact angle $\theta > 90$, it is said to be non-wetting.

Throughout our experiments the interface affinity will be to minimize its surface area. This will oppose the driving force leading to invade the initially saturating fluid in the porous medium. From a pore-scale perspective, for every pore-throat there is an associated capillary threshold pressure p^t_{cap} which needs to be overcome for the subsequent pore to be invaded, under the influence of gravity there will also exist a hydrostatic term caused by relative height differences along the front. Hence the capillary pressure will depend on its position in the gravitational field.

2.4 Two-phase flow

Displacement of one fluid by another in a porous media, comes in two flavors. *Imbibition*, here the wetting phase displaces a non-wetting phase saturating the

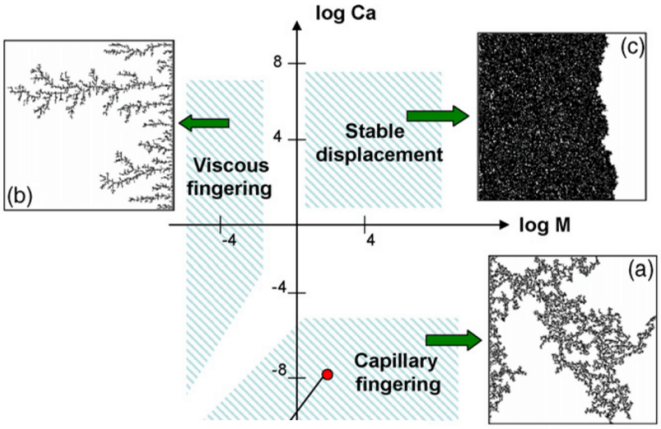

Figure 2.3: The competition between capillary and viscous forces changes within the phase diagram, resulting in three main domains with its distinct pattern formation. Namely capillary fingering viscous fingering and stable displacement.

porous network, such as water displacing air. The opposite order of displacement is called *Drainage*. Lenormand et al [18] performed pioneering experimental work on immiscible displacement on a simplified quasi two-dimensional porous network. They used horizontal models in the absence of gravitational forces. This setup allowed for a simplified porous network, which could more easily be studied and compared. Pairing their experimental work with simulations led to the construction of a phase diagram, where the displacement structures that emerge could be mapped into three different flow regimes namely viscous regime [21], stable displacement [13] and the capillary regime [18], depending on the interplay between the capillary and viscous forces.

A fluid flow is in the viscous regime, as the name suggests, when the viscous forces dominate the structural propagation [20], as a consequence long reaching fingers are formed, this type of structures have successfully been modeled by diffusion limited aggregation (DLA) [32]. These finger-like structures are found to be fractal with a fractal dimension $D = 1.62$ [21]. Stable displacement occurs when the viscosity ratio between the fluid pair is the significant parameter, the pattern presents a flat front with small irregularities spanning at most a couple of pores [17, 13] this regime has been modeled by the anti-DLA scheme [32]. In this study we will focus on the capillary regime. Here the pressure difference across the interface is the driving force for the displacement, for sufficiently low flow rates, the non-wetting phase generates patterns that are similar to that presented by invasion percolation [41] being a dynamic percolation process. In such models the invasion is represented by a cluster growth process on a random lattice, dependent purely by the local capillary pressures. [5]. Moreover such displacement patterns are shown to also be fractal [22] with a fractal dimension of $D_c = 1.83$ for 2D and $D_c = 2.5$ for 3D, experimentally [14, 7].

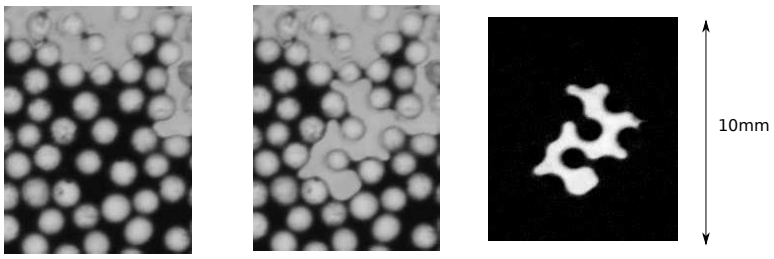

Figure 2.4: The first two images show the displacement caused by a burst, here the lighter colored fluid(air) is seen to invade the wetting fluid which is darker colored. The last image shows the growth obtained by performing an image subtraction between the two gray-scale images.

2.5 Drainage and the capillary regime

Immiscible drainage in a porous medium consists of the displacement of a wetting phase by a non-wetting phase. In the absence of a gravitational gradient and for sufficiently low driving rates, the system dynamics is determined solely by the pressure difference across the interface, defined by the Young-Laplace law.

Drainage of immiscible fluids is found to occur in three different ways.
1) Displacement in terms of Haines Jumps [16] (Fig.2.7) is considered to be the basic mechanism for drainage, occurring as multiple connected pores are invaded as a consequence of a pressure threshold being overcome, the corresponding pressure signal is characterized by slow build up followed by sudden pressure drops, the displacement is seen to occur in a pore filling fashion. The characteristics of slow displacement process is that viscous pressure gradients have time to relax between front movements. Capillary effects govern the displacement. This type of dynamics gives the fingerprint for the temporal evolution of the pressure during drainage.

2) Displacement by capillary bridges. In this case seemingly entrapped fluid migrates back to the bulk by means of a network of capillary bridges. We define a capillary bridge to be a film of liquid held by the surface tension between two glass beads, separated by a distance l (Fig2.5). The capillary bridges are seen to be unstable with respect to length l by which they are formed. The collection of these capillary bridges forms a network which acts as transport highways for the fluid. This type of flow mechanism has yet to be explored in a systematic way.

3) Lastly we have displacement caused by the snapping off of capillary bridges,

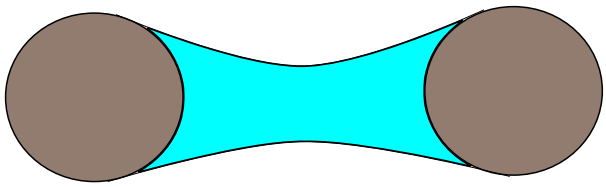

Figure 2.5: Shows the schematics of a capillary-bridge

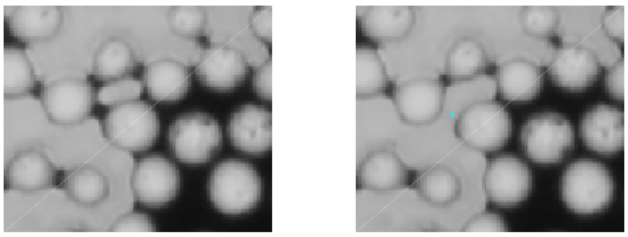

Figure 2.6: The two images show how a capillary bridge is observed to rupture

these are films of wetting fluid trapped in the porous network, having the ability to transport fluid. Most the films that eventually snap-off have a short life-span according to paper 3). (2019). An increased understanding of snap-off as a process is pivotal for determining whether a phase is truly entrapped. On longer time scale evaporation and film flow along the confining plate can become considerable factors. As the time scale of the study has been significantly shorter, such effects have not been taken into consideration.

2.6 Use of invasion percolation to model slow drainage

Modeling of one fluid by another in the capillary regime, have displayed close connection to percolation theory, first studied by De Gennes [4] in the 50s. A dynamical model was proposed by Wilkinson and Wilhelmsen [41] named invasion percolation (IP) for a boundary condition of constant flow rate. Here the advancement of the interface is strictly a ranking problem, where the fluid takes the path of least resistance. As the fluid considered is incompressible, regions surrounded by nonwetting fluid is removed from possible invasion paths. These regions of wetting fluid are referred to as trapped clusters, and have shown a power-law behavior in their cluster size distribution $N(s) \sim s^{-\tau}$, with an exponent $\tau = 2.1 \pm 0.1$ which is close to what is observed from percolation theory [3].

The effect of gravity on the system can be stabilizing or destabilizing depending on the density contrast between the two fluids [24, 1]. In the capillary

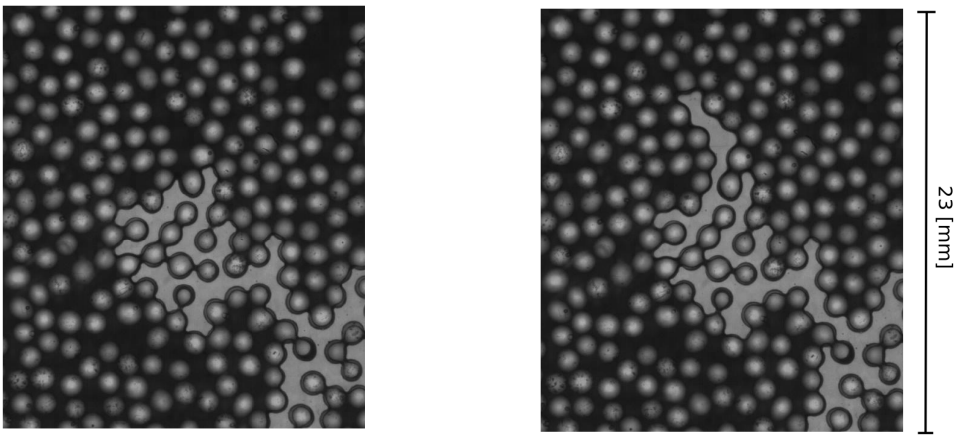

Figure 2.7: As the pressure overcomes a capillary threshold pressure, multiple pores are observed to be invaded in a burst like fashion.

regime where the density of the invading phase is smaller than the defending phase, gravity tends to stabilize the invading front. It has further been shown by both simulation and experiments [2] that the front width w scales with the strength of the gravitational field as $w \sim Bo^{-\nu/(1+\nu)}$. Here Bo is the ratio between the gravitational force and the capillary force for a typical pore, given by $Bo = \Delta\rho g a^2/\gamma$, $\Delta\rho$ is the density difference, γ is the surface tension between the two fluids, g is the gravitational acceleration acting on the system, and a is the typical pore-size. The mechanism behind this stabilization lies in the fact that the pressure needed to overcome the threshold pressure is no longer only dependent solely on the disorder in the capillary pore-throats but also has an hydrostatic pressure difference term. This term suppresses any height variations along the front. Modified Invasion percolation scheme has successfully been used to model such a system configuration [2]. Here the pore-throats are weighted according to their position in the gravitational field. This in turn makes pore-throats with high positions along z statistically easier to invade than pore throats with lower position.

2.7 Avalanche behavior

Certain systems respond intermittently to the continuous flow of energy fed into the system [15]. The textbook example is the stick-slip displacement of a wooden block which is attached to a spring. The spring is pulled with a constant force along a surface with a given friction coefficient. Characteristic for its motion is the presence of stable periods where energy is built up in the system followed by events where energy is dissipated and the wooden block is displaced [11]. Drainage in the capillary regime where fluid phase is withdrawn with a constant flow rate is an analogous process. Here capillaries along the invasion front store up energy in their meniscii up to a threshold in pressure, at which an abrupt event causes the interface to propagate, and the meniscii

which stores up energy, to back-contract. A common feature of these systems is that the statistics of various measures associated to them lack a characteristic scale.

In general the global response function of the system can be analyzed by studying the time series $v(t)$. (In our study this corresponds to the pressure $p(t)$ and optical imaging $I(t)$ in Paper 2). However identifying an avalanche from a time series can be a difficult task, as the time signal often also is subdued to a background noise, which needs to be thresholded away. Statistical properties of avalanches are usually considered by studying the PDF's of various quantities such as the avalanche duration, size, and the waiting-time between successive events.

Because of their lack of a characteristic scale of the system, the distribution of these quantities is power law distributed as.

$$P(x) = x^{\epsilon} f(x/x_o) \tag{2.5}$$

Here ϵ is the exponent characterizing the statistics quantity, and $f(x/x_o)$ is scaling function with x_0 a characteristic size, correlation length or time.

Chapter 3

Methodology

3.1 Experimental setup for two-phase flow

In this section we will present the experimental setup which was used throughout our studies of two-phase flow in porous media.
We have made use of an artificial quasi-two dimensional porous medium. The medium is constructed by pouring poly-disperse glass beads, with bead-size range of $1.0mm < d < 1.2mm$ onto the sticky side of an adhesive contact paper, the monolayer of beads is then clamped between two Plexiglas plates, which are sealed off with a rectangular layer of silicon glue. Hence the voids in between the beads form the porous network. The Plexiglas plate has milled inlet and outlet channels, allowing for injection and withdrawal of the respective fluid phases. From below a pressure cushion forces the porous structure to stay confined. The dimensions of the rectangular system are: Length $L = 14.5cm$ and width $W = 10cm$ and thickness of $d = 1mm$. The porous medium is initially saturated with a wetting fluid which is composed of 80% glycerol and 20% water by weight, having a kinematic viscosity of $\nu = 4.25 \cdot 10^{-5} m^2/s$, density of $\rho_w = 1.205 g/cm^3$ with surface tension $\gamma = 0.064 N/m$. The invading fluid used is air and is withdrawn into the system by a syringe pump at a constant flow rate of $0.004 mL/min$. The system is resting on a lightbox which can be tilted at an angle over the horizontal plane, allowing for tuning of the gravitational component along the system plane $g \sin\theta$.

During experiments the relative pressure difference between the non-wetting and wetting phase is measured by two Honeywell 26PCAFG6G flow-through pressure sensors connected to the model outlet, making measurements every $\Delta t \approx 0.2s$. The dynamical evolution of the displacement structure is captured by images at fixed time lapse $\approx 10s$ with a NIKON D7100 SLR camera, which is mounted perpendicular to the model. An Aladdin syringe pump is used to provide constant flow rates, the fluid was withdrawn from the system with a discharge rate of Q $= 6.6 \cdot 10^{-11} m^3/s$.

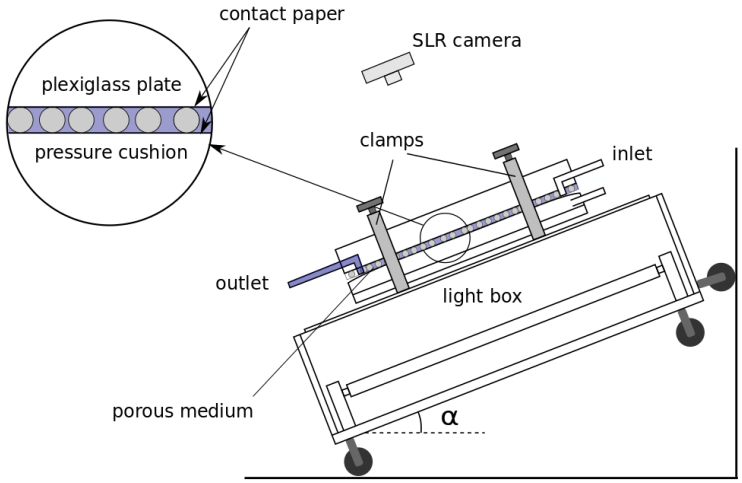

Figure 3.1: Shows a schematics of the experimental setup.

3.2 Experimental setup for three-phase flow in porous media

To build a system which allows for the direct inspection of the displacement dynamics, a simple experimental setup was constructed as shown in Fig.3.2. A camera and a light source was placed on each side of an horizontal glass tube 1.0m in length with a diameter of 2mm. The tube was filled with a granular suspension which slowly settles out of suspension, here grain size diameter was found to lie in the range $d \in [50, 300]\mu m$.
One of the tube openings was connected with plastic tubing to a 30mL plastic syringe, which was mounted onto the pumping system Aladdin-1000, able to supply the system with constant pumping rates. The opposite opening of the glass tube was kept open to the ambient pressure. A three-way junction was connected to the plastic tubing, this extra outlet allowed for the coupling of a pressure sensor, such that pressure measurements in the liquid phase could be made. The measurements were controlled and collected with the help of a computer running a code. The dynamics of the interface was recorded by capturing a sequences of images with a NIKON D7000 SLR camera mounted onto a tripod with a 20mm focal objective.

3.3 Image processing

In this thesis image processing has been extensively used to extract wanted quantities from images captured while conducting experiments. In paper 1) and 2), the signal I(t), which is a time series of the growth of the displacement structure, was obtained by subtracting sequential gray-scale images and then binarizing at a threshold giving us a measurable quantity for the change in

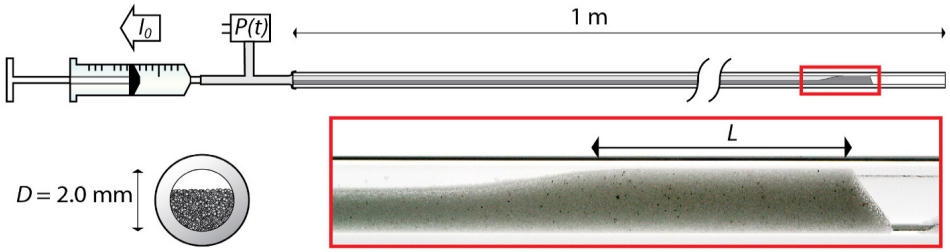

Figure 3.2: Schematics of the experimental setup. The cylinder is filled with a settling suspension which is connected to a syringe, the opposite side is open to the air phase, during experiments the fluid is slowly withdrawn,allowing for the air to displace the frictional fluid.

area. An example of image subtraction is shown in the image sequence below Fig 2.4. Here the first two images display a zoom at the boundary between the two phases. Between the first and second image, air is seen to invade. Captured as the image difference is shown in the last thumbnail.

In paper 3) a routine was constructed to identify and track all the capillary bridges, as displayed in Fig.3.3. Our routine for identifying capillary bridges is based on firstly pinpointing all the pore-throats in the system. This is achieved by a Delaunay triangulation over the porous network, having the centroid of the glass beads act as the vertices. Hence acquiring the set of corresponding triangulated edges is equivalent to finding all the pore-throat sizes in the system. We define the position of the pore-throat as the midpoint of its edge. Fig.3.3.

For every time-step, the midpoint of the pores-throats is assessed, by evaluating its gray-scale value found to lie between [0,255], here the pixel value 0 corresponds to black and 255 to white. The two phases are clearly distinguishable as the wetting phase is dyed with negrosin. We apply a mask over all the trapped clusters such that, the pore-throats are found to be in one of three possible scenarios: 1) The entry pressure to the adjacent pore has been overcome in which case the pore-throat is invaded. 2)The pore-throat can be situated in one of the trapped islands or the bulk. 3) Lastly the pore-throat can be a capillary bridge, in which case the pore on both sides have been invaded by alternative invasion paths.

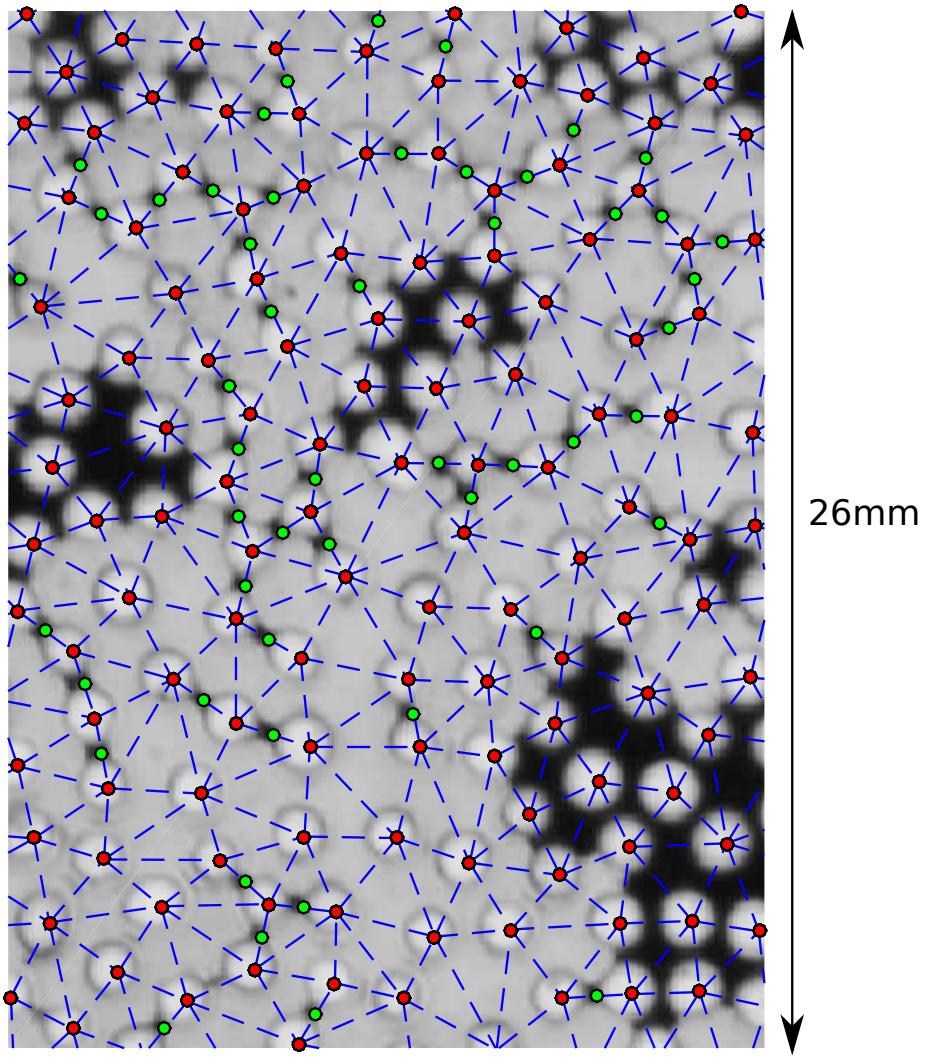

Figure 3.3: Image outcrop, the bead centers are represented by red dots, green dots represents the center of the capillary bridges. Dashed blue grid represents the Delaunay triangulation, by which the capillary bridges are identified.

Chapter 4

Conclusion and Perspectives

We have experimentally and numerically studied influence of gravity during two-phase flow in an artificial quasi 2D porous media. We have obtained pressure-saturation curves and found a relation coupling the saturation to the Bond number using percolation theory. Moreover we have been able to express a relation which allows for upscaling of the system by combining data from the pore-scale with the system scale.

For the cylindrical confinement we have looked at the case of a deformable porous media, here the interface between the air and liquid phase acts as bull-dozer deforming the porous bed. Further we have observed how the interplay between frictional and viscous forces gives rise to pattern formation. We are able to relate the cyclic evolution of plugs being shed by the moving interface to a stress consideration made on a static plug.

We have studied the mechanisms by which drainage displaces a saturating fluid and looked at how the burst-dynamics is affected by gravity, by analyzing its clustering in time and space. The residual saturation is observed to display connective pathways by which the wetting phase can migrate, we have evaluated these fluid pathways in the framework of graph networks.

We have detected snap-off events, where the films between constricting beads rupture, we have shown how this process primarily occurs within the width of the advancing front, and how the occurrence of snap-off events gives rise to waiting-time distributions which are power-law distributed.

The different paths of exploration are numerous, below is a list of possible perspective for a continued study:

- Further investigate the snap-off phenomena, potentially find a relationship between the avalanches and the formation of capillary bridges. .
- Investigate how a chain of capillary bridges can conduct fluid, and how the transport property is affected by the chain length. Study the snap-off as an attack on the secondary network.
- Simulate drainage in the capillary regime by means of invasion percolation, allowing for the formation of paths of capillary bridges.

- Perform experiments where the capillary threshold distribution is a controlled parameter.

Summary of papers

Paper.1: Gravitational and finite-size effects on pressure-saturation curves during drainage
M.Ayaz, R.Toussaint, K.J Måløy and G.Schäfer
Submitted to Water Resources Research

In this study we experimentally, numerically and analytically study the influence of gravity and finite-size effects on pressure-saturation measurements during slow drainage where the lighter fluid invades the system from the top. This relationship is much used by hydrologist and soil-scientists to give closure to the Darcy equations used in continuum modeling. The effect of gravity on these curves is systematically varied by tilting the system relative to a horizontal configuration.

Using a quasi two-dimensional porous media allows for direct spatial monitoring of the saturation. Exploiting the fractal nature of the displacement structure we obtain a relationship between the final saturation and the bond number $S_{nw}^F = Bo^{0.097}$ for the 2D case using percolation theory, which we found to be in agreement with numerical and experimental results. Compatibility for similar arguments in the 3D case was checked with an experimental study conducted by Nouri et al. [30]. Moreover the saturation, pressure and Bond number is functionally related, allowing for pressure-saturation curves to collapse onto a single master curve. Lastly the size distribution of trapped defending fluid is also shown to contain information on the flux while the invasion process took place.

We propose a simple invasion percolation model as a tool for producing pressure saturation curves, depending on the fluid-pair characteristics, system size and on the pore-scale characteristics, given by the pore-size distribution.

Contribution: Conducted the experimental work,simulations and wrote the first version of the manuscript.

Paper.2: Avalanche dynamics and pressure variations during drainage in gravity stabilized flow
M.Ayaz, R.Toussaint, K.J Måløy and G.Schäfer
Preprint to be submitted to Frontiers Of Physics

In this paper we study avalanche dynamics experimentally under the influence of gravity. The experiments are conducted in a Hele-Shaw confinement

where pressure in the wetting phase is measured coupled with optical monitoring of the system. Here we investigate the statistical measures related to the clustering of drainage events in space and time. We show by correlating the two measured quantities that the intermittent evolution of the pressure signal can be related to the invasion of multiple pores in a burst like fashion. Furthermore we investigate the influence of gravity on its statistics. We find a linear relationship between the size of the pressure burst and the optical invasion of multiple pores. Lastly the shape of the bursts was predicted, and measured to be well fitted to an exponentially decaying function.

Contribution: Conducted the experimental work and wrote the first version of the manuscript.

Paper.3: Snap-off displacement during slow drainage in a gradient
M.Ayaz, R.Toussaint, K.J Måløy and G.Schäfer
Preprint to be submitted to Physical Review E

Recent studies of drainage have showed how trapped wetting fluid can migrate back to the bulk of a fluid, through a network of entrapped films found to exist between constricting areas in the porous body [36], forming a secondary transport network.

In this paper we present an experimental investigation on a quasi two-dimensional porous media. We examine the phenomena of snap-off of capillary bridges, defined as films of wetting fluid, trapped in the porous structure. In our study we localize these rupturing events in time and space by optical monitoring. By varying the effective gravity, we are able to identify a scaling relation, where the width of the interface bordering the two phases is related to the area where snap-off activity is most dense, using percolation theory. Next we look at the gravitational dependence on the spatial extension of these transport networks and how the waiting time between successive events are distributed in time. The network of capillary bridges is further analyzed and characterized using network theory. We define our edges to represent transport paths for the fluid and the nodes as the set branching points. These findings indicate that our current conceptual models of drainage are incomplete with implications for future experimental and modeling studies as well as engineering applications.

Contribution: Conducted the experimental work and wrote the first version of the manuscript.

Paper.4: Three-phase flow in cylindrical confinement
G.Dumazer, B.Sandnes, M.Ayaz, K.J Måløy and E.Flekkøy
Published in Physical Review Letters

The study of multiphase flows in a cylindrical confinement is an important topic with a broad range of interest from geophysical, biological and engineering perspective. From transport of blood cells through arteries and veins to flow of oil and gas by pipelines. Even the simple case of two-phase air and

water flow through tubes and capillaries displays complex flow behavior, with commonly observed transitions between stratified, bubbly, slug, and annular flow depending on the flow rates of the respective phases.

Three-phase grain-liquid-gas flows have shown to generate complex flows, in studies where the characteristic length scale of the system is at the *capillary length*, meaning there exists an active meniscus between the confining plates. Such systems have shown to generate patterns caused by the interplay between capillary, viscous and the frictional forces, the latter existing through grain-grain interactions setting up a force network witch branches onto the confining geometry. For a quasi 2D confinement Sandnes et al [34] showed that when such system is driven with an external flow rate out of equilibrium they generate a variety of patterns.

In this study we further investigate a simplified confining geometry, namely a narrow tube with a well defined capillary meniscii. We look at the structures that arise from the displacement of a dense suspension consisting of a granular bed of glass beads immersed in water. As the meniscus travels through the tube it either evacuates the grains from the whole cross-section of the tube or it seen to leave behind a structure of granular material characterized by its granular plugs followed by gaps.

Contribution:Took part in building the experimental setup and conducted experiments

Paper.5: Self-Structuring of Granular material under Capillary Bulldozing
G.Dumazer, B.Sandnes, M.Ayaz, K.J Måløy and E.Flekkøy
Published in Powder and grains (conference paper)

In this paper we make experimental observations of the structuring of a granular suspension under the progress of a gas/liquid meniscus in a narrow tube. The dense granular suspension is displaced and compactified as a growing accumulation front. The frictional interaction with the confining walls increases until the pore capillary entry pressure is reached. The gas then penetrates the clogged granular packing and a further accumulation front is formed at the far side of the plug. This cyclic process continues until the gas/liquid interface reaches the tubes outlet, leaving a trail of plugs in the tube. Such 1D pattern formation belongs to a larger family of patterning dynamics observed in 2D Hele-Shaw geometry. The cylindrical geometry considered here provides an ideal case for a theoretical modeling for forced granular matter oscillating between a long frictional phase and a sudden viscous fluidization.

Contribution:Took part in building the experimental setup and conducted experiments

Appendix

We conduct preliminary experiments for our further study. Here we sandwich a monolayer of poly-dispersed glass beads $\sim 1mm$ in size between two glass plates. The sides are sealed off with a sponge, coated with vacuum grease, preventing the fluid from leaking. The sponge allows for the sides of the cell to be clamped together. We further mount three equally spaced acoustic sensors onto the confining plate. The sensors are of the piezoelectric type, which are mostly sensitive in the range (200-900 kHz) are amplified with a Signal Preamplifier. The data recorded on the shock accelerometers which are mostly sensitive in the range (1Hz-26kHz) are amplified with a Bruel and Kjaer Nexus Charge Amplifier Type 2692-A.

The porous medium is saturated with water as the wetting phase, dyed with negrosin for an increased contrast. The model is kept vertical, forcing the system to be gravity stabilized [24, 1]. From the bottom of the cell, fluid is withdrawn at a constant flow rate of 9ml/min, evacuating the model in 30s. The choice of rapid drainage was set by the limitations of the high speed camera, acquisition of the acoustic signal at high sampling rates. Furthermore rapid invasion generates stronger signal onto the acoustic sensors.

The interface motion during drainage is a complex process. Although the interface motion can appear smooth and continuous, closer inspection of the pore-scale reveals an highly intermittent and non-local dynamics. This irregular signal was first observed by Haines et al. [16]. As the system is drained potential surface energy is stored at the interface up to a given threshold in pressure. For a quasi 2D confinement we expect the energy released to generate elastic waves at its confining plates. Prior research work by Moebius et al. [25, 26] studied different signatures of acoustic emission associated with fluid front displacement by imbibition and drainage.

Waiting time matrix - Pinning of the interface

We expect events where the interface is depinned to be associated with a large energy release. In order to measure the pinning-depinning transition of the interface directly we utilized a waiting time matrix (WTM). This is a robust

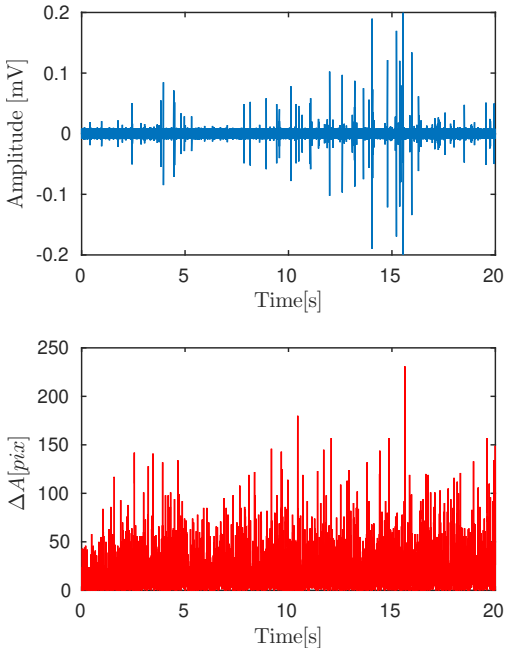

Figure 4.1: The top graph shows the acoustic signal retrieved from one of the sensors situated mounted onto the confining plate. The bottom signal shows the change in area obtained from image subtraction.

procedure which has previously been used to study intermittency in the front propagation for both interfacial crack-propagation [38] and to describe the front evolution of an imbibition front [8]. By extracting the interface $h(x,t)$ from the images and superposing them ontop of each other we are able to construct a spatial map see Fig. 4.3. Here we impose a one-to-one relation between the height h and the length x of the system, not taking into considerations any overhangs that might exist. By superposing all the heights, we can construct a 2D map of the interface motion WTM $= \sum_i h(x,t_i)$. Where each element represents how long in time the interface has stayed pinned for a given (x,y) position. Furthermore we can calculate a map of the local velocities, $V(x,y) = a/w(x,y)\delta t$ here each matrix element is equal to its normal speed parallel to the flow direction over a unit element a.

Results

In Fig.4.1 the obtained acoustic signal is displayed. Here we observe multiple acoustic events occurring at many different scales during the experiment. We notice further that the signal strength is stronger in the second half of the signal. This can be associated with inertial effects and the system coming out of a build up phase [27].

We optically monitor the invasion with an high-speed camera at 500fps, we

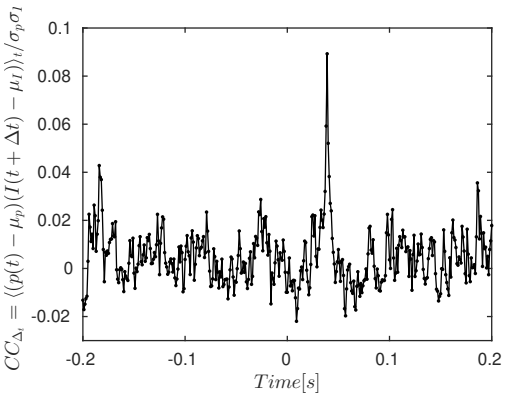

Figure 4.2: correlation between the optically obtained image and the acoustic signal captured with the piezoelectric type sensors.

expect the framrate to provide sufficiently high temporal resolution to detect pore-scale events emanating from the depinning of the interface. To assess the quality of our response signal, we cross-correlate the acoustic measurements with the signal obtained from the image sequence captured during the experiments: see Fig.4.2. Here the growth of the displacement structure is extracted, by performing image subtraction between sequential images and thereafter binarizing. The area where the wetting phase is replaced by non-wetting is assigned positive integers and the opposite order of displacement negative integers. The signal $I(t)$ was retrieved, by summing over all the pixels corresponding to the newly invaded area. We calculate the cross-correlation function $CC_{\Delta t}$ between the summed area signal and the acoustic signal, showing a peak close to the zero-shift, even if the signal over noise ratio is high. The phase shift in the peak is related to the two signals being not being entirely synchronized. Where the maximum of the acoustic signal happens 0.03s after optical signal, as seen from the position of the peak in Fig 5.2.

$$C(\Delta t) = \Big\langle \frac{(p(t) - \mu_p)(I(t + \Delta t) - \mu_I)}{\sigma_p \sigma_I} \Big\rangle_t \tag{4.1}$$

where $p(t)$ is the acoustic sensor signal, and μ_p and μ_I are the averages of the $p(t)$ and $I(t)$ signals, and σ_p and σ_I their root mean square. By stacking the interface of the advancing front we are able to construct a waiting time map Fig. 4.3, We notice regions where the interface is pinned for a longer time, and regions where the interface propagates around as trapped regions. From the local velocity map, Fig. 5.4, we see regions where the interface has progressed in quick manner.

Conclusion

From the preliminary experiments we concluded that we have regions where the interface is accelerated, which should carry an energy release with it. We were able to obtain a cross correlation between the images and the acoustic sensor,

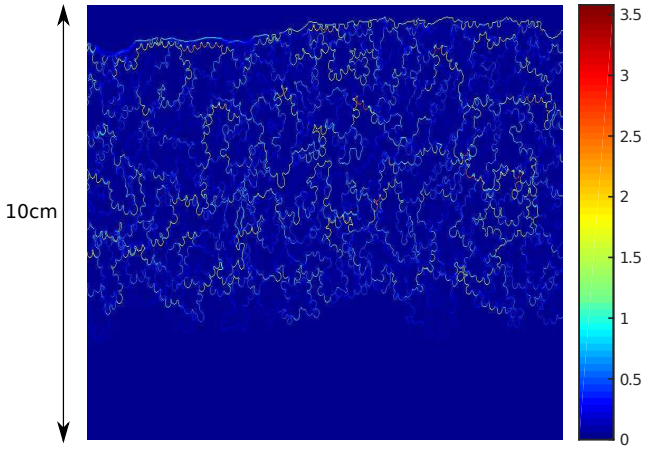

Figure 4.3: Waiting time matrix for an experiment performed at a withdrawal rate of 9ml/min, each element of the map gives the time in seconds, of how long interface has stayed pinned in any given point.The units for the colorbar is [s]

but the signal over noise ratio was not optimal. Thus to achieve better contact we decided to use pressure sensors, sensing directly in the fluid phase.

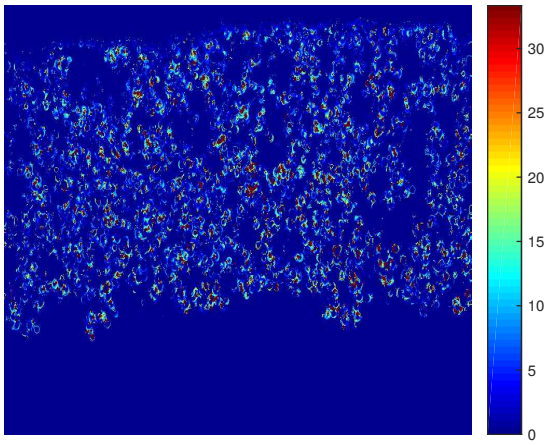

Figure 4.4: By finding the reciprocal of the waiting time matrix we are able to find a map of the local velocities, directed parallel with the flow direction. Units for the colorbar is $[m/s]$

Bibliography

[1] Auradou, Harold ; Måløy, Knut J. ; Schmittbuhl, Jean ; Hansen, Alex ; Bideau, Daniel: Competition between correlated buoyancy and uncorrelated capillary effects during drainage. In: *Phys. Rev. E* 60 (1999), Dec, S. 7224–7234. – URL https://link.aps.org/doi/10.1103/PhysRevE.60.7224

[2] Birovljev, A. ; Furuberg, L. ; Feder, J. ; Jssang, T. ; Mly, K. J. ; Aharony, A.: Gravity invasion percolation in two dimensions: Experiment and simulation. In: *Phys. Rev. Lett.* 67 (1991), Jul, S. 584–587. – URL https://link.aps.org/doi/10.1103/PhysRevLett.67.584

[3] Blunt, Martin ; King, Michael J. ; Scher, Harvey: Simulation and theory of two-phase flow in porous media. In: *Phys. Rev. A* 46 (1992), Dec, S. 7680–7699. – URL https://link.aps.org/doi/10.1103/PhysRevA.46.7680

[4] Bok, Julien ; Prost, Jacques ; Brochard-Wyart, Franoise: *P.G. De Gennes' Impact on Science Volume I.* World Scientific Publishing Company, 2009. – URL https://www.worldscientific.com/doi/abs/10.1142/7317

[5] Chandler, Richard ; Koplik, Joel ; Lerman, Kenneth ; Willemsen, Jorge F.: Capillary displacement and percolation in porous media. In: *J. Fluid Mech.* 119 (1982), 6, S. 249–267. – URL http://journals.cambridge.org/article$_S$0022112082001335.$ISSN$1469−7645Chen, $Shiyi$;Doolen, $Gary\ D.$: In : ***Annual Review of Fluid Mechanics*** 30(1998), $Nr.\ 1, S.\ 329 - -364. - -URL$http://dx.doi.org/10.1146/annurev.fluid.30.1.329

[6] Chen, Songhua ; Kim, Kyung-Hoe ; Qin, Fangfang ; Watson, A.Ted: Quantitative NMR imaging of multiphase flow in porous media. In: *Magnetic Resonance Imaging* 10 (1992), Nr. 5, S. 815 – 826. – URL http://www.sciencedirect.com/science/article/pii/0730725X9290417X. – ISSN 0730-725X

[8] Clotet, Xavier ; Santucci, Stéphane ; Ortín, Jordi: Experimental study of stable imbibition displacements in a model open fracture. II. Scale-dependent avalanche dynamics. In: *Phys. Rev. E* 93 (2016), Jan, S. 012150. – URL https://link.aps.org/doi/10.1103/PhysRevE.93.012150

[9] Darcy, Henry: *Les Fontaines Publiques de la Ville de Dijon.* Dalmont, Paris, 1856

[10] Dumazer, Guillaume ; Sandnes, Bjørnar ; Ayaz, Monem ; Måløy, Knut J. ; Flekkøy, Eirik G.: Frictional Fluid Dynamics and Plug Formation in Multiphase Millifluidic Flow. In: *Phys. Rev. Lett.* 117 (2016), Jul, S. 028002. – URL https://link.aps.org/doi/10.1103/PhysRevLett.117.028002

[11] Feder, Hans Jacob S. ; Feder, Jens: Self-organized criticality in a stick-slip process. In: *Phys. Rev. Lett.* 66 (1991), May, S. 2669–2672. – URL https://link.aps.org/doi/10.1103/PhysRevLett.66.2669

[12] Fiorentino, Eve-Agns ; Toussaint, Renaud ; Jouniaux, Laurence: Two-phase Lattice Boltzmann modelling of streaming potentials: influence of the air-water interface on the electrokinetic coupling. In: *Geophysical Journal International* 208 (2016), 11, S. 1139–1156

[13] Frette, Olav I. ; M ° aløy, Knut J. ; Schmittbuhl, Jean ; Hansen, Alex: Immiscible displacement of viscosity-matched fluids in two-dimensional porous media. In: *Phys. Rev. E* 55 (1997), Mar, S. 2969–2975. – URL https://link.aps.org/doi/10.1103/PhysRevE.55.2969

[14] Frette, Vidar ; Feder, Jens ; Jøssang, Torstein ; Meakin, Paul ; Måløy, Knut J.: Fast, immiscible fluid-fluid displacement in three-dimensional porous media at finite viscosity contrast. In: *Phys. Rev. E* 50 (1994), Oct, S. 2881–2890. – URL https://link.aps.org/doi/10.1103/PhysRevE.50.2881

[15] Furuberg, Liv ; Måløy, Knut J. ; Feder, Jens: Intermittent behavior in slow drainage. In: *Phys. Rev. E* 53 (1996), Jan, S. 966–977. – URL http://link.aps.org/doi/10.1103/PhysRevE.53.966

[16] Haines, William B.: Studies in the physical properties of soil. V. The hysteresis effect in capillary properties, and the modes of moisture distribution associated therewith. In: *The Journal of Agricultural Science* 20 (1930), 1, S. 97–116. – URL http://journals.cambridge.org/article$_S$002185960008864X. – $-ISSN1469-5146$

[17] Lenormand, R: Flow through porous media: limits of fractal pattern. In: *Proc. R. Soc. Lond. A* 423 (1989), Nr. 1864, S. 159–16

[18] Lenormand, R. ; Zarcone, C. ; Sarr, A.: Mechanisms of the displacement of one fluid by another in a network of capillary ducts. In: *Journal of Fluid Mechanics* 135 (1983), 10, S. 337–353. – URL http://journals.cambridge.org/article$_S$0022112083003110. – $-ISSN1469-7645$

[19] Lenormand, Roland ; Zarcone, Cesar: Invasion Percolation in an Etched Network: Measurement of a Fractal Dimension. In: *Phys. Rev. Lett.* 54 (1985), May, S. 2226–2229. – URL https://link.aps.org/doi/10.1103/PhysRevLett.54.2226

[20] Løvoll, Grunde ; Méheust, Yves ; Toussaint, Renaud ; Schmittbuhl, Jean ; Måløy, Knut J.: Growth activity during fingering in a porous Hele-Shaw cell. In: *Phys. Rev. E* 70 (2004), Aug, S. 026301. – URL http://link.aps.org/doi/10.1103/PhysRevE.70.026301

[21] Måløy, K. J. ; Feder, J. ; Jøssang, T.: Viscous fingering fractals in porous media. In: *Phys. Rev. Lett.* 55 (1985), S. 2688–2691

[22] Mandelbrot, Benoit: *The fractal geometry of nature*. San Francisco : W.H. Freeman, 1982. – ISBN 978-0716711865

[23] Martys, Nicos S. ; Chen, Hudong: Simulation of multicomponent fluids in complex three-dimensional geometries by the lattice Boltzmann method. In: *Phys. Rev. E* 53 (1996), Jan, S. 743–750. – URL https://link.aps.org/doi/10.1103/PhysRevE.53.743

[24] Méheust, Yves ; Løvoll, Grunde ; Måløy, Knut J. ; Schmittbuhl, Jean: Interface scaling in a two-dimensional porous medium under combined viscous, gravity, and capillary effects. In: *Phys. Rev. E* 66 (2002), Nov, S. 051603. – URL http://link.aps.org/doi/10.1103/PhysRevE.66.051603

[25] Moebius, Franziska ; Or, Dani: Interfacial jumps and pressure bursts during fluid displacement in interacting irregular capillaries. In: *J. Colloid Interface Sci.* 377 (2012), Nr. 1, S. 406 – 415. – URL http://www.sciencedirect.com/science/article/pii/S0021979712003682. – ISSN 0021-9797

[26] Moebius, Franziska ; Or, Dani: Inertial forces affect fluid front displacement dynamics in a pore-throat network model. In: *Phys. Rev. E* 90 (2014), Aug, S. 023019. – URL http://link.aps.org/doi/10.1103/PhysRevE.90.023019

[27] Moura, M. ; Fiorentino, E.-A. ; Måløy, K. J. ; Schäfer, G. ; Toussaint, R.: Impact of sample geometry on the measurement of pressure-saturation curves: Experiments and simulations. In: *Water Resour. Res.* 51 (2015), Nr. 11, S. 8900–8926. – URL http://dx.doi.org/10.1002/2015WR017196. – ISSN 1944-7973

[28] Moura, M. ; Mly, K. J. ; Toussaint, R.: Critical behavior in porous media flow. In: *EPL (Europhysics Letters)* 118 (2017), Nr. 1, S. 14004. – URL http://stacks.iop.org/0295-5075/118/i=1/a=14004

[29] Neuville, A. ; Flekky, E. G. ; Toussaint, R.: Influence of asperities on fluid and thermal flow in a fracture: A cou-

pled lattice Boltzmann study. In: *Journal of Geophysical Research: Solid Earth* 118 (2013), Nr. 7, S. 3394–3407. – URL https://agupubs.onlinelibrary.wiley.com/doi/abs/10.1002/jgrb.50256

[30] Nouri, Milad ; Homaee, Mehdi ; Bybordi, Mohammed: Quantitative Assessment of LNAPL Retention in Soil Porous Media. In: *Soil and Sediment Contamination: An International Journal* 23 (2014), 05

[31] Nsir, Khalifa ; Schfer, Gerhard ; Chiara Roupert, Raphal di ; Razakarisoa, Olivier ; Toussaint, Renaud: Laboratory experiments on DNAPL gravity fingering in water-saturated porous media. In: *International Journal of Multiphase Flow* 40 (2012), Nr. 0, S. 83 – 92. – ISSN 0301-9322

[32] Paterson, Lincoln: Diffusion-Limited Aggregation and Two-Fluid Displacements in Porous Media. In: *Phys. Rev. Lett.* 52 (1984), Apr, S. 1621–1624. – URL https://link.aps.org/doi/10.1103/PhysRevLett.52.1621

[33] Richter, B. Gutenberg; C. F.: *Seismicity Of The Earth And Associated Phenomena*. Princeton University Press, 1949

[34] Sandnes, B. ; Flekkøy, E.G. ; Knudsen, H.A. ; Måløy, K.J. ; See, H.: Patterns and flow in frictional fluid dynamics. In: *Nat. Commun.* 2 (2011), apr, S. 288. – URL http://dx.doi.org/10.1038/ncomms1289

[35] Santucci, S. ; Planet, R. ; Måløy, K. J. ; Ortín, J.: Avalanches of imbibition fronts: Towards critical pinning. In: *EPL* 94 (2011), may, Nr. 4, S. 46005. – URL http://dx.doi.org/10.1209/0295-5075/94/46005

[36] Singh, Kamaljit ; Menke, Hannah ; Andrew, Matthew ; Lin, Qingyang ; Rau, Christoph ; Blunt, Martin J. ; Bijeljic, Branko: Dynamics of snap-off and pore-filling events during two-phase fluid flow in permeable media. In: *Scientific Reports* 7 (2017)

[37] Stojanova, M. ; Santucci, S. ; Vanel, L. ; Ramos, O.: High Frequency Monitoring Reveals Aftershocks in Subcritical Crack Growth. In: *Phys. Rev. Lett.* 112 (2014), Mar, S. 115502. – URL http://link.aps.org/doi/10.1103/PhysRevLett.112.115502

[38] Tallakstad, Ken T. ; Toussaint, Renaud ; Santucci, Stephane ; Schmittbuhl, Jean ; Måløy, Knut J.: Local dynamics of a randomly pinned crack front during creep and forced propagation: An experimental study. In: *Phys. Rev. E* 83 (2011), Apr, S. 046108. – URL http://link.aps.org/doi/10.1103/PhysRevE.83.046108

[39] Toussaint R. Mly, Mheust Y. Lvoll G. Schfer G Schmittbuhl J. ; Jankov, M.: Two-Phase Flow: Structure, Upscaling, and Consequences for Macroscopic Transport Properties. In: *Vadose Zone Journal* 11 (2011). – URL http://dx.doi.org/10.2136/vzj2011.0123

[40] Whitaker, Stephen: Flow in porous media I: A theoretical derivation of Darcy's law. In: *Transport in Porous Media* 1 (1986), Mar, Nr. 1, S. 3–25. – URL https://doi.org/10.1007/BF01036523

[41] Wilkinson, D. ; Willemsen, J. F.: Invasion percolation: a new form of percolation theory. In: *J. Phys. A: Math. Gen.* 16 (1983), Nr. 14, S. 3365–3376. – URL http://iopscience.iop.org/0305-4470/16/14/028

[42] Yan, Jianzhao ; Luo, Xiaorong ; Wang, Weimin ; Toussaint, Renaud ; Schmittbuhl, Jean ; Vasseur, Guy ; Chen, Fang ; Yu, Alan ; Zhang, Likuan: An experimental study of secondary oil migration in a three-dimensional tilted porous medium. In: *AAPG bulletin* 96 (2012), may, Nr. 5, S. 773–788. – URL http://dx.doi.org/10.1306/09091110140

Paper 1: Influence of gravity and finite-size effects on pressure-saturation curves

Gravitational and finite-size effects on pressure saturation curves during drainage

Monem Ayaz[1,2,3], Renaud Toussaint[1,3,4], Gerhard Schäfer[2], Knut Jørgen Måløy[3]

[1]University of Strasbourg, Institut de Physique du Globe de Strasbourg, CNRS UMR7516, 5 Rue Descartes, F-67000 Strasbourg, France
[2]Université de Strasbourg, CNRS, LHyGeS UMR 7517, 67084 Strasbourg, France.
[3]PoreLab, The Njord Centre, Department of Physics, University of Oslo, PO Box 1048, Blindern, N-0316, Oslo, Norway PoreLab.
[4]Lavrentev Institute of Hydrodynamics, Siberian Branch, Russian Academy of Sciences, Novosibirsk, Russia

Key Points:

- During slow drainage with a lighter fluid invading from the top, the residual saturation can be obtained as a scaling law of the Bond number or the system size.
- The capillary-pressure relationship can be obtained analytically during such drainage from the system size, based on the fractal properties of the invasion front shape and the contribution of the capillary pressure jump and the hydrostatic pressure term inside the system.
- The final saturation after drainage allows to obtain information on the flux while it took place.

Corresponding author: Monem Ayaz, auayaz@fys.uio.no

Abstract

We experimentally and numerically study the influence of gravity and finite-size effects on the pressure-saturation relationship in a given porous medium during slow drainage. The effect of gravity is systematically varied by tilting the system relative to the horizontal configuration. The use of a quasi two-dimensional porous media allows for direct spatial monitoring of the saturation. Exploiting the fractal nature of the displacement structure we obtain a relationship between the final saturation and the bond number $S_{nw}^F = Bo^{0.097}$ using percolation theory. Moreover the saturation, pressure and bond number is functionally related, allowing for pressure-saturation curves to collapse onto a single master curve, parameterized by the Representative Elementary Volume size and by the Bond and Capillary Numbers. This allows to upscale the pressure-saturation curves measured in a laboratory to large representative elementary volumes used in reservoir simulations. The large-scale behavior of these curves follow a simple relationship, depending on Bond and Capillary number, and on the flow direction. The size distribution of trapped defending fluid is also shown to contain information on past fluid flow, and can be used as a marker of past flow speed and direction.

1 Introduction

Displacement of one immiscible fluid by another in a porous media is an important research topic both from a fundamental and an applied perspective. An increased understanding of the basic mechanism that govern the pore-scale description is of interest for multiple disciplines of science such as soil-science, hydrology, physics and biology and has shown industrial importance through applications such as enhanced oil recovery, CO_2 sequestration and by mapping and controlling of migrating ground water contaminants (Nsir et al., 2012). Furthermore it has revealed variety of pattern-forming processes emerging from the pore-scale up to the system scale (Måløy et al., 1985; Lenormand et al., 1983; Méheust et al., 2002; Løvoll et al., 2004; Toussaint et al., 2005), typically governed by the interplay between viscous, capillary and gravitational forces. The structures has shown to exhibit complex behavior, characterized by its rich intermittent dynamics (Clotet et al., 2016; Moura, Måløy, & Toussaint, 2017; Moura, Måløy, Flekkøy, & Toussaint, 2017; Måløy et al., 1992; Furuberg et al., 1988; Planet et al., 2009).

We study two phase flow in a quasi 2D porous confinement and look at the simple case of drainage at pore-scale, where a non-wetting phase displaces a wetting one. Such experiments have shown to generate displacement structures that depend on the density and viscosity contrast between the fluids, surface tension and the flow rates at which the system is driven (Løvoll et al., 2004; Toussaint et al., 2005; Lenormand et al., 1983). Furthermore such structures are assembled by trapped regions of wetting phase, completely surrounded by the invading phase. The trapped islands are characterized by their power law distribution in size with an exponential cut-off directly related to the gravitational forces (Blunt & King, 1990) and the system's finite size.

The forces at play dominate at different length scales and their interplay gives rise to separate scaling regimes allowing for upscaling of the system which consists of relating the pore-scale description to properties defined at the Darcy scale or even at the macroscopic scale (Toussaint et al., 2011; Wilkinson, 1986). In the limit of very slow flow rates, the emerging structure is seen to depend entirely on capillary and gravitational fores (Lenormand et al., 1983; Méheust et al., 2002; Birovljev et al., 1991), and the obtained structure is seen to be well modeled by invasion percolation (Chandler et al., 1982; Wilkinson, 1984). When a low viscous fluid displaces a high viscous one, the unstable displacement pattern that emerges is called viscous fingering. The analogy between DLA and viscous fingering was first proposed by Paterson (1984) and is based on the equivalence between the probability field of diffusing particles and the pressure field in the viscous fluid. On the other hand when a highly viscous fluid is injected into a low viscous fluid, a stable displacement will be observed. This situation is analog to the anti-DLA as proposed by (Paterson, 1984).

Numerical modeling of two-phase displacement in water-saturated porous media using continuum models have been performed by many researchers (Zhang & Smith, 2001; Aggelopoulos & Tsakiroglou, 2009; Kokkinaki et al., 2013; Sleep et al., 2015; Schneider et al., 2015; Nayagum et al., 2004). However, the detailed local description of the invasion front in a porous medium cannot be simulated with these models because they do not explicitly consider the capillary and viscous pressure fluctuations at the pore-scale. To overcome this shortcoming, microscopic approaches such as Stokes' solution for flow in single pores with a specified geometry or lattice Boltzmann methods (LBM) have been investigated to reproduce experiments (Aursjø et al., 2010; Fiorentino et al., 2017; Misztal et al., 2015) . Similarly Pore-scale network models have been developed to study a wide range of displacement processes, including drainage and imbibition (Aker et al., 1998; Nordhaug et al., 2003; Joekar Niasar et al., 2009; Tørå et al., 2012; Sheng & Thompson, 2013; Kallel et al., 2017; Nsir et al., 2018, 2012; Singh & K. Mohanty, 2003; Yang et al., 2019). Ewing and Berkowitz(Ewing & Berkowitz, 1998) developed a generalized growth model based on invasion percolation to simulate immiscible displacement in saturated porous media. Both capillary, viscous and gravity forces were incorporated in their 3D algorithm, where viscous forces were expressed stochastically rather than explicitly. (Glass et al., 2001) developed a macro-modified invasion percolation (MMIP) model, including also the effects of all 3 forces within the invading phase in a macro-heterogeneous porous medium.

In macroscale modeling of two-phase flow, the porous medium and the flow are described by continuous mathematical fields using an empirical functional relationship, coupling the saturation of the wetting fluid S_w to the capillary pressure $p_{nw} - p_w = p(S_w)$ that is the main assumption at hand, where p_{nw} and p_w is the pressure in the non wetting fluid, and p_w the pressure in the wetting one. In practice this relation can be found by conducting experiments on a given porous medium and fluid pair on representative volumes. It is usually parameterized using mathematical models such as Van-Genuchten or Brooks-Corey model (van Genuchten, 1980; Brooks & Corey, 1964). In the case of primary drainage, the Brooks-Corey model introduces several model parameters such as pore size index, entry pressure needed by the invading fluid to displace water, and the residual saturation of the wetting phase. The latter one is an important model parameter because the description of two-phase flow at the macroscopic scale requires also the use of a second constitutive relationship: relative permeabilities as function of saturation of the wetting phase.

In this paper we study the capillary pressure - saturation (PS) relationship during drainage in a system of finite size, taking into account gravitational effects. We examine how this finite size and gravitational forces influence this PS relationship, and how it can be upscaled. First, we propose a simple numerical scheme which produces pressure-saturation curves. In this numerical scheme we take into consideration that we have a gravitational field acting on the system, a distribution of capillary pressure thresholds linked to the pore-scale geometry and the fact that the system has a finite size. Next, we study the relative pressure of the wetting fluid measured at the outlet of a transparent quasi-twodimensional experimental setup with respect to the imposed constant atmospheric pressure of the non-wetting air phase as a function of the saturation, $\Delta P = P_a - p_w = f(S_w)$. From the pressure-saturation relation obtained during the detailed gravity stabilized primary drainage studies, we can then directly derive one of the significant caracteristics of water retention curves which is the residual saturation of the wetting phase $S_w = 1 - S_{nw}$. We further deduce a functional relationship, which couples the final saturation with the pore-scale description under the influence of gravity using percolation theory. This allows to upscale the pressure saturation relationship for a given porous medium, with the help of laboratory drainage tests. We also show how the residual saturation depends on the Bond number and the conditions of drainge flow, in terms of flow angle and flux.

2 Theory

When the viscous forces are negligible for the invasion process (capillary regime) the obtained displacement pattern can be understood by the relative importance of gravity to capillary forces, which is conventionally defined by the Bond number Bo , corresponding to the ratio of buoyancy forces to capillary forces at a pore scale,

$$Bo = \frac{\Delta p_{grav}}{\Delta p_{cap}} = \frac{\Delta\rho\, g\, a \sin\alpha}{\gamma/a} \ , \tag{1}$$

where $\Delta\rho$ is the density contrast between the two fluids, g is the gravitational acceleration, α is the angle between the average flow direction and the horizontal plane, a is the typical pore size , and γ is the surface tension between the two fluids. $ag\sin\alpha$ is the hydrostatic pressure drop on a length scale a, parallel to the flow direction. The typical ratio between viscous and capillary forces over a pore is defined by the capillary number

$$Ca = \frac{\Delta p_{visc}}{\Delta p_{cap}} = \frac{\mu v a^2}{\gamma\kappa} \ , \tag{2}$$

where μ is the viscosity of the most viscous fluid, v is the Darcy velocity, and κ is the permeability of the porous medium. We consider situations where the non-wetting invading fluid has negligible viscosity in front of the defending one. The presence of disorder in the porous medium gives a distribution of capillary thresholds with a well defined spread. In order to capture the relative relevance of these fluctuations we utilize the fluctuation number F as suggested by Meheust et al.(Méheust et al., 2002; Auradou et al., 1999)

$$F = C(Bo - Ca) \ , \tag{3}$$

where the dimensionaless prefactor is $C = \gamma/(aW_t)$, with γ/a the characteristic average capillary pressure threshold, and W_t the standard deviation of the random capillary thresholds in the porous medium. For most media, the average value and the standard deviation of the capillary pressure thresholds are of the same order of magnitude(Toussaint et al., 2005), and C is of order 1. Throughout our study we will consider $Ca \ll Bo$, hence we will utilize the reduced expression $F \sim [\gamma/(aW_t)]Bo \sim Bo$. We define the invasion front as the set of pores bordering the non-wetting phase to the bulk of the defending fluid. From percolation theory the front width σ for a gravity stabilized drainage front is found to scale with the Fluctuation number F as (Wilkinson, 1984, 1986; Birovljev et al., 1991)

$$\sigma/a \propto F^{-\nu/(1+\nu)} \propto Bo^{-\nu/(1+\nu)} \ . \tag{4}$$

Here ν is a critical exponent of the correlation length from percolation theory, $\nu = 4/3$ in 2D(Stauffer & Aharony, 2014) . Since the Fluctuation number depends on the width of the capillary threshold distribution, an increase in its width results in an increase of the front width.

3 Experimental setup

The experiments are performed in a quasi two-dimensional porous medium (cf Fig. 1), which is made up by randomly distributing a monolayer of glass beads between the sticky sides of two sheets of adhesive contact paper in a transparent Hele-Shaw cell with thick walls. The boundaries are sealed off with a rectangular layer of silicon glue. Hence the porous media can be considered as a rectangular box of length $L = 14.5$ cm, width $W = 10$ cm, and thickness $b = 1$ mm. Appended to the system is a filter, positioned between the fixed glass beads and the outlet. The filter consists of a sponge with a typical pore-size much smaller than the pores in the main porous matrix. The resulting difference in entrance pressure makes it necessary to invade all clusters connected to the outlet-filter, before invading the outlet-filter.

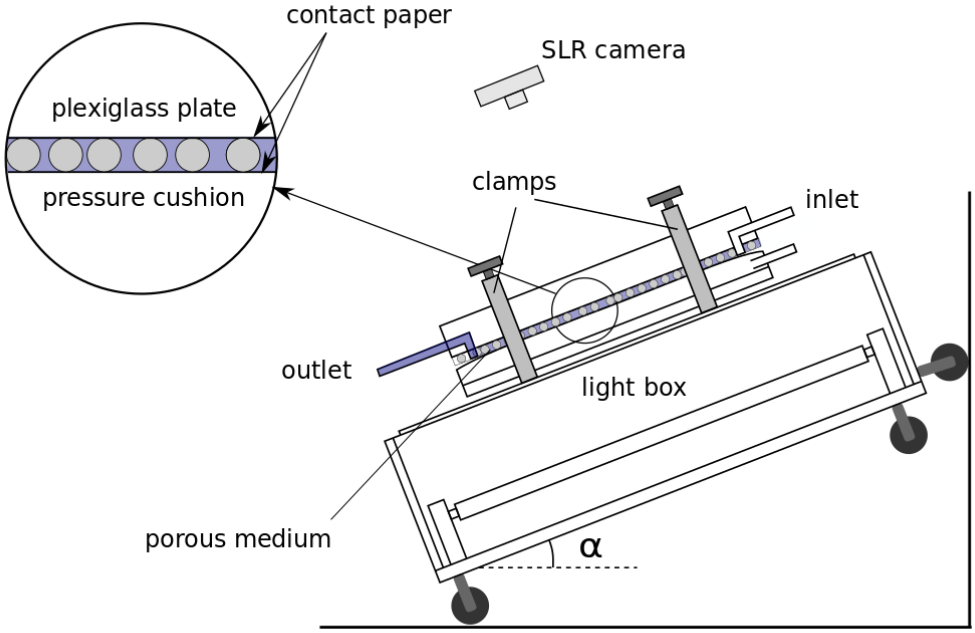

Figure 1. Schematics of the experimental setup. The porous media is sandwiched between two sheets of adhesive contact paper, and kept rigid by clamping it between a water-filled pressure cushion pressed against a rigid transparent plate and a Plexiglass plate. A pulley connected to a light-box is used to provide the desired inclinationα.

To prevent the potential displacement of beads, the porous matrix is kept rigid, by a thick Plexiglas plate from above with milled inlet and outlet channels allowing for the injection and extraction of fluid phases. From below a mylar film is kept under pressure by a 3.5 m water column, acting as a pressurized cushion forcing the glass beads above to stay in place. The rigid model is mounted onto an illuminating light-box that can be tilted by an angle α over the horizontal, allowing for tuning of the gravitational component $g \sin \alpha$.

The invading non-wetting phase used in all the experiments is air. The wetting phase used is a 90-10% by weight glycerol-water solution, dyed with a 0.1% of Negrosine for visual contrast. The wetting fluid has a density of $\rho_w = 1205 kgm^{-3}$ and kinematic viscosity of $\nu = 4.25\ 10^{-5} m^2/s$. The surface tension between the two fluids is $\gamma = 6.4 \cdot 10^{-2} Nm^{-1}$.

During the experiments the relative pressure difference between the non-wetting and wetting phase is measured by two Honeywell® 26PCAFG6G flow-Through pressure sensors, connected to the outlet of the model. The saturation of the two phases is extracted by thresholding the grayscale map from images taken at fixed time lapse with a NIKON® D7100 SLR camera mounted perpendicular to model, similarly to (Moura, Måløy, & Toussaint, 2017). A syringe pump is used to provide constant flow rates, with a discharge rate of $Q = 6.67 \cdot 10^{-11} m^3/s$, corresponding to a capillary number of $Ca = 1.2 \cdot 10^{-4}$. The experiments are terminated once the pores boarding the filter have all been invaded.

4 The network model

Invasion Percolation algorithms (Wilkinson & Willemsen, 1983; Chandler et al., 1982; Moura et al., 2015) have been extensively used to model drainage in the capillary regime between immiscible fluids when the viscous pressure drop and compressibility of the wetting fluid are negligible for the displacement of the fluid-fluid interface, contrarily to cases where viscous forces (Løvoll et al., 2011) or compressibility (Jankov et al., 2010) play an important role. In such models the invasion is represented by a cluster growth process on a random lattice, dependent solely on the global homogeneous pressure in each phase and on the local capillary pressure thresholds in the pore throats along the interface. Such arrangements have been shown to generate displacement structures that are quantitatively similar to what is observed during drainage (Blunt et al., 1992; Lenormand & Zarcone, 1985). In this study we will utilize a bond invasion percolation model. The porous medium is modeled as a completely connected network, where all the pore-sites are interconnected to their neighboring pores through pore-throats. The pore-throats are oriented at 45 degrees from the main flow direction on a rectangular lattice with periodic boundary conditions perpendicular to the flow direction.

Disorder is introduced in the model by letting pore-throats sizes be drawn from a distribution corresponding to the experimental one . First, a random variable is picked from an uniform distribution in [0,1]. Next, a mapping is made transforming the flat distribution to the experimental one, obtained utilizing an imaging based algorithm. The size distribution of the pore-throats channel radii is characterized on the experimental porous matrix, utilizing a Delaunay triangulation over all the constricting beads, as suggested by (Bryant & Blunt, 1992) and detailed by (Moura, Måløy, & Toussaint, 2017). For each pore-throat, the channel radius R fixes the corresponding capillary threshold pressure needed to be overcome in order to invade the adjacent pore-site, from Young Laplace law, $\Delta P_c^t = \gamma/2R$.

The algorithm of Invasion Percolation (IP) in a Gradient to describe drainage in a gravitational field follows the principles introduced by (Sapoval et al., 1985; Birovljev et al., 1991). Gravity is accounted for by linearly weighting the capillary throat thresholds with the hydrostatic pressure difference between the two fluids, taking into account that the pressure in the wetting phase at elevation z above the outlet is $P_w = P_{outlet} - \rho_w g z$.

Initially the network is fully saturated with a wetting fluid. For each iteration the interface of the non trapped part of the defending structure moves where the capillary pressure threshold adjusted by the hydrostatic pressure drop is lowest (see Eq. (8)). This movement involves both the invasion of the pore throat and of the connecting pore. The parts of the interface that enclose (trap) entirely a connected part of the defending fluid will be locked due to the incompressibility assumption of the defending fluid: no further invasion is allowed into these trapped clusters. The invasion is stopped once all the sites bordering the outlet of the model have been fully invaded, effectively blocking any further displacement of the wetting phase. The aspect ratio of the IP lattice was equal to the experimental system for all the simulations performed. The size of the lattice was 232×330 sites.

5 Results

Figure 2 shows a selected set of snapshots captured for different bond numbers, displaying the growth of the displacement structure from the start of the invasion up to the end of the experiments, when all the pores bordering the outlet channel have been invaded and the final saturation S_{nw}^F is reached. For comparison snapshots from the simulations are presented in Fig. 3. We observe that an increase of the gravitational component leads to a denser displacement structure, i.e. a lower S_{nw}^F. The invasion front which refers to the set of pores bordering the bulk of the wetting phase shows a reduced spread

σ along the flow direction, i.e. when the Bond number increases, the system tends to become more stabilized and the fronts is hence closer to a horizontal flat structure. The hydrostatic pressure gradient suppresses the maximum height difference between points along the front.

5.1 Measuring pressure-saturation curves

The saturation of the non-wetting phase S_{nw} is extracted by image analysis from the sequence of captured images. The saturation increases linearly in accordance with the constant flow rate imposed on the system. The pressure drop across the model is at any time such that it maintains the constraint by the flow rate. The pressure ΔP is the difference between the atmospheric pressure P_a and the pressure in the wetting phase at the outlet

$$\Delta P = P_a - P_{outlet} \tag{5}$$

Combining the extracted saturation with the pressure measurements, a series of pressure–saturation curves are obtained, as shown in Fig. 4. The first datapoint on this curves is related to the varying hydrostatic pressure ΔP_h accross the system, which scales as the gravitational term $g \sin \alpha$ for different inclinations. The respective initial values of the pressure offsets are followed by a pressure buildup without any pore invasion. As the initially flat interface begins to fill the local geometry of the pore-throats, the capillary pressure ΔP_c starts to build up. Pore throats have widths that are spatially uncorrelated and thereby each pore-throat exhibits an associated capillary threshold pressure P_c^t which is the minimum pressure needed for the interface to penetrate its respective pore-throat. For a given porous structure, fluid pair and wettabilities there will be a distribution of capillary pressure thresholds associated to the system.The condition for invasion is that the local pressure difference between two phases along the front satisfies $\Delta P_c > P_c^t$. In the presence of gravity, height differences along the invasion front give rise to a hydrostatic term. When accounted for, this gives the following invasion criterion:

$$\Delta P_c = P_a - (P_{outlet} - \Delta \rho g z) = \Delta P + \Delta \rho g z > P_c^t \, , \tag{6}$$

where $z = z' \sin \alpha$ the elevation of the pore throat considered above the cell bottom, with z' the linear upwards coordinate along the cell. z' varies between 0 at the outlet, at the bottom of the cell, and L at the inlet at the top of the cell. This can also be expressed as

$$\Delta P > P_c^t - \Delta \rho (g \sin \alpha) z' \, . \tag{7}$$

Therefore, the front will move at the place with the lowest modified capillary pressure threshold

$$P_c^t - \Delta \rho (g \sin \alpha) z' \tag{8}$$

When this criterion is met the smallest capillary-threshold is invaded followed by a rapid decrease in pressure during the instable Haines jump where pores are invaded until the interface stabilizes on smaller pore-throats. As the porous boundary is horizontal, the initial pressure buildup associated with the invasion of the first pores is independent of gravitational effects, i.e. it is invariant with respect to the Bond number. Once the average capillary threshold pressure is reached, it is observed to fluctuate around an average slowiy increasing with the invading fluid saturation. These fluctuations consist in many build ups followed by sudden relaxations (occurring at many time scales), allowing for the invasion of multiple pores during one burst (Måløy et al., 1992; Furuberg et al., 1996; Haines, 1930). The hydrostatic pressure gradient tends to suppress any height differences between two points along the front. Two distinct features of the pressure-saturation curve is observed. The pressure difference is seen to fluctuate, the aforementioned capillary-threshold pressure displays disorder at the invasion front. We further see that the pressure difference ΔP increases because the hydrostatic pressure difference $\Delta \rho g sin \alpha z$ decreases linearly as the invading phase approaches the outlet.

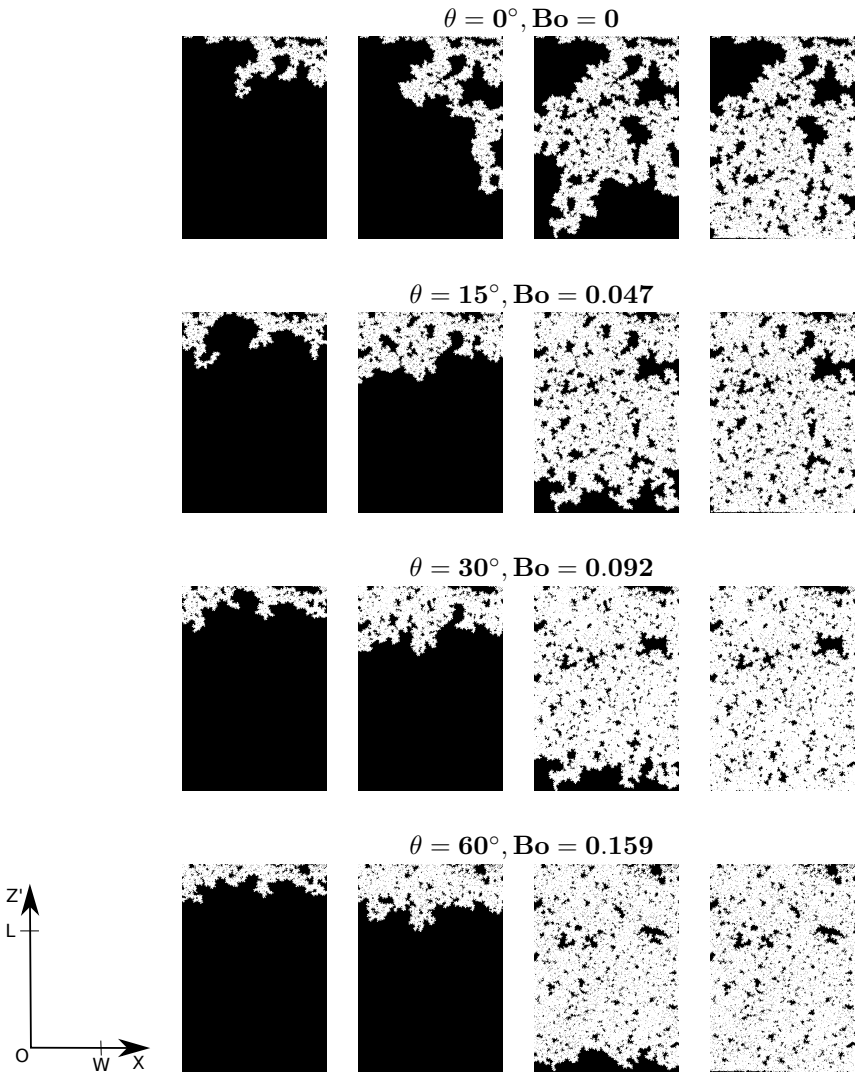

Figure 2. Snapshots from four different experiments. The air invades the saturated porous media from top to bottom, the time evolution for each Bond number goes from right to left. The first two columns show the displacement structure after respectively 8 and 16 % of air has saturated the medium taking 2.7 and 5.4 hours , the two last ones show the break-through and final configurations. The duration of the experiments with increasing inclination is: 18.9h, 25.7h, 26.1h and 26.6h.

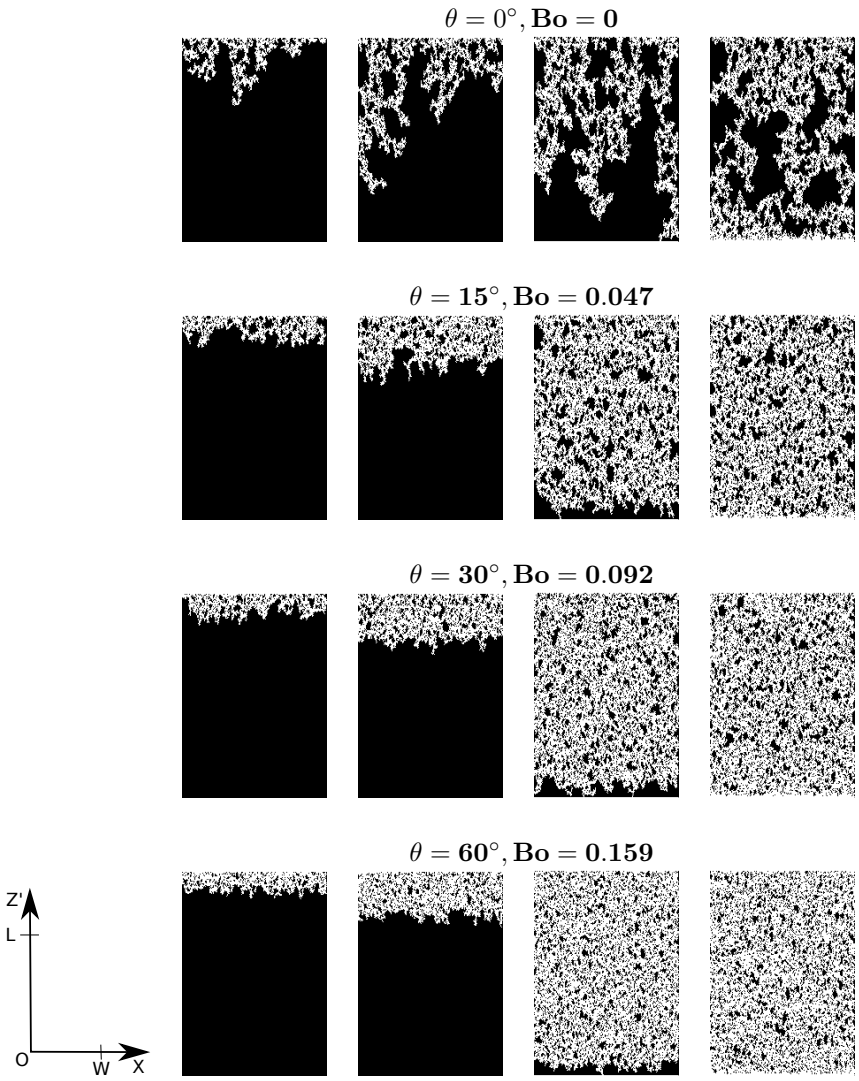

Figure 3. Snapshots from network simulations with Bond numbers comparable to those in set by the inclinations in the experiments. The first two columns show the displacement structure after respectively 8 and 16 % of air has saturated the medium, the two last ones show the breakthrough and final configurations.

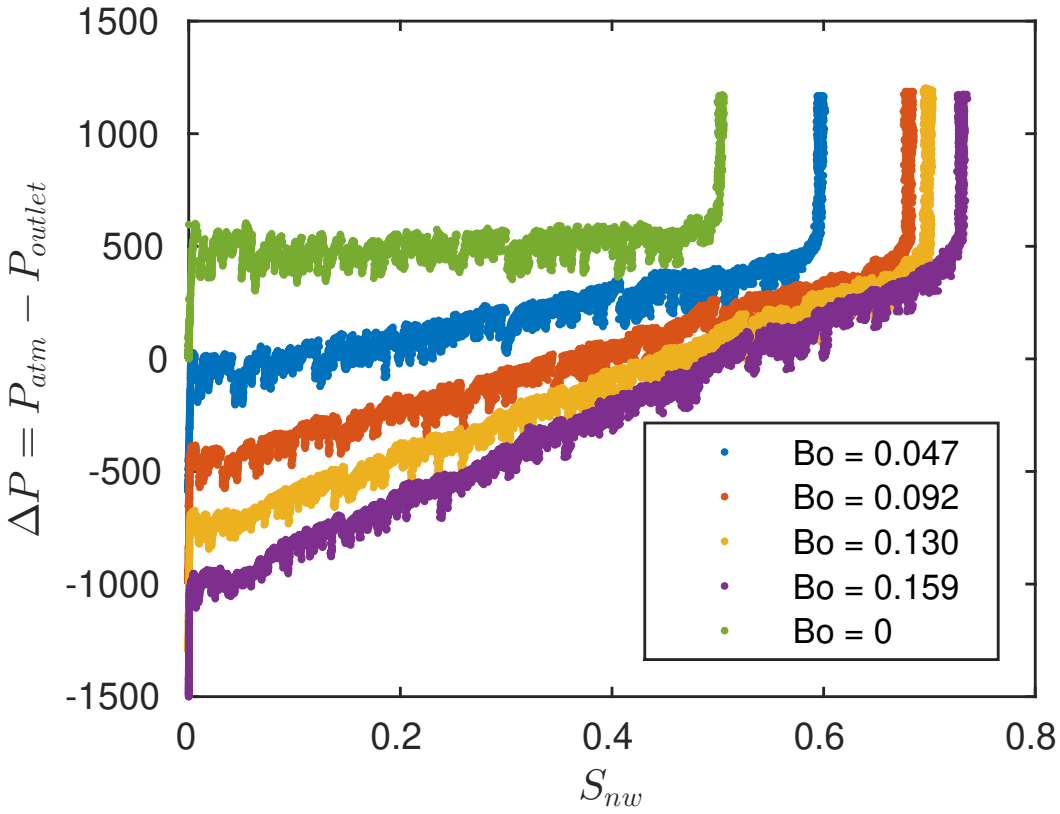

Figure 4. Pressure-saturation curves obtained for five different inclinations of the experimental model. Here S_{nw} is the saturation of non-wetting phase, and ΔP corresponds to the pressure difference between the outlet and the amtmospheric pressure.

Once the invading phase reaches breakthrough, the invasion structure is in contact with the filter prolongating the cell, presenting much smaller pore-throats, so that this filter is not invaded, while pores with higher capillary thresholds are invaded in the cell. leads to an increase of the capillary pressure as the invasion goes on. Once the pores bordering the filter have all been invaded the system is said to has reached its final saturation S_{nw}^F. We observe that there is a consistency between the numerical and the experimental final saturation values as the inclination increases.

5.2 Master curve: Relating the pressure drop and saturation for different Bond numbers

For the case $Bo>0$, i.e. when the lightest fluid penerates from the top and gravity stabilizes the system, and the system is in mechanical equilibrium, the total pressure difference across the porous model is expressed as $\Delta P = \Delta P_c - \Delta P_h$. Here ΔP_c is the capillary pressure accross the interface, given by the Laplace pressure Eq.(9), and ΔP_h is the hydrostatic pressure difference across the wetting phase. For slow drainage where $Ca \ll 1$, this pressure difference is essentially hydrostatic, and can be expressed as $\Delta P_h = \Delta\rho g l \sin\alpha$. Here, $\Delta\rho$ is the density contrast between the fluids, the term $g\sin\alpha$ is the component of gravity parallel to the cell and $l = \Delta z'$ is the distance between the point considered along the two fluids boundary and the outlet, projected along the steepest descent direction. Since gravity stabilizes the front, one can consider a characteristic dis-

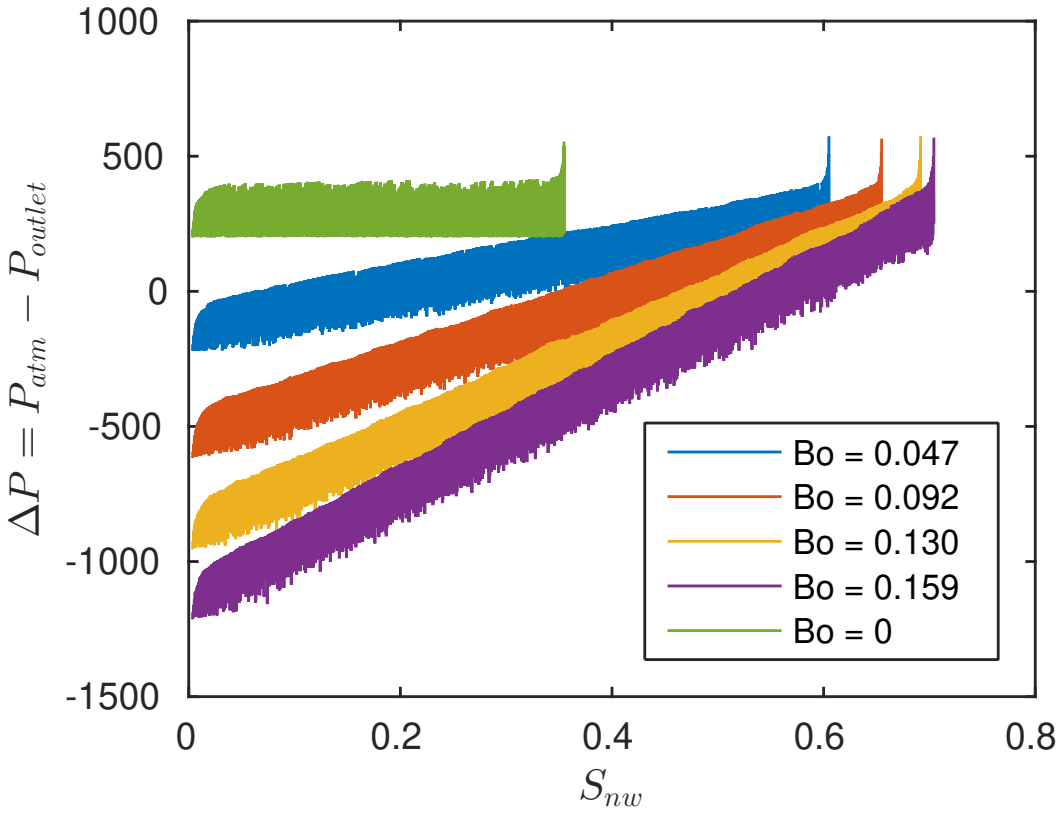

Figure 5. The pressure saturation curves obtained numerically, for a system size with the same aspect ratio $L \times W$ as the experimental system.

tance l as the mean in-plane distance between the outlet and the invasion front. Thereby the measured pressure across the cell can be expressed as:

$$\Delta P = 2\gamma/R - \Delta\rho g l \sin\alpha. \tag{9}$$

Furthermore a functional dependency of the saturation with respect to l can be expressed, by considering the saturation-balance of the total non-wetting phase S_{nw}^{tot} in the entire cell of size $A_{tot} = L \times W$, and approximating the system as transiting from an initial saturation S_{nw}^{0} to a characteristic residual final saturation S_{nw}^{F} after the passage of the drainage front, i.e. above it - cf Fig. 6. Fluctuations along the invasion front are assumed to average out. We denote $A^F = (L-l) \times W$ the area of the region where the invasion front has passed. By volume conservation we get an expression for the total saturation

$$S_{nw}^{tot} A_{tot} = S_{nw}^{F} A^F + S_{nw}^{o}(A_{tot} - A^F)\ . \tag{10}$$

i.e.

$$S_{nw}^{tot} LW = S_{nw}^{F}(L-l)W + S_{nw}^{o} lW\ . \tag{11}$$

Dividing this equation by $S_{nw}^{F} LW$ leads to

$$\frac{l}{L} = \frac{\frac{S_{nw}^{tot}}{S_{nw}^{F}} - 1}{\frac{S_{nw}^{0}}{S_{nw}^{F}} - 1}\ . \tag{12}$$

Since the system is initially fully saturated, $S_{nw}^{0} = 0$. This gives an expression for the distance to the outlet as: $l = L(1 - S_{nw}^{tot}/S_{nw}^{F})9$. Inserting this in Eq. (9) leads to the

following saturation pressure relation:

$$\Delta P = \frac{2\gamma}{R} - \frac{\gamma L}{a^2} Bo\Big(1 - \frac{S_{nw}^{tot}}{S_{nw}^{F}}\Big) \ . \tag{13}$$

This equation has been expressed with the Bond number from Eq. (1). In Fig.7 the rescaled pressure is plotted as a function of the relative-saturation obtained from the experiments in Fig. . Similar results obtained from the numerical modeling are displayed in Fig.8. We here show the envelope of the pressure-saturation curves , i.e. the maximum of the pressure difference reached up to a certain saturation, without displaying the fluctuations related to the Haines jumps. The term $2\gamma/R$, was experimentally obtained by measuring the relative pressure difference of the pressure build up associated with the invasion of the first pore , i.e. it was approximated as the entrance pressure. More precisely, the term $2\gamma/R$ to consider corresponds to the capillary pressure for the characteristic position of the invasion front, separating the initial saturation zone and the final saturation one. The position of this front can be evaluated from its average position, in which case experimentally one can extract l, and measure $2\gamma/R$ from the experimental measure of ΔP and a measure of l for a given time, using Eq. (9). Theoretically, the characteristic position of the front can be defined as the position where the occupancy probability corresponding to the capillary pressure drop is equal to the percolation threshold for the type of network defined by the porous matrix. As demonstrated in (Moura et al., 2015)this corresponds to

$$2\gamma/R = f^{-1}(p_c) \tag{14}$$

with p_c the percolation threshold in terms of occupancy probability, $f(P) = \int_0^P g(P')dP'$ is the cumulative distribution of the normalized capillary threshold distribution (probability density function) $g(P)$, and f^{-1} is the reciprocal function of f. In other words, the constant term in Eq. (13) conrrespond to the capillary pressure threshold corresponding to the percolation threshold in the pore network. We see that by inserting pore-scale description of the system, and taking into account the gravity effect accross the cell, we are able to collapse the Pressure-saturation curves onto a single Master curve: this equation captures properly the entrance pressure, the rise of the pressure drop with the drainage, and the final pressure buildup when the invader is limited by the semi-permeable membrane. This is the case both for the experiments and for the simulations, in all probed effective gravities (i.e. cell angles over the horizontal). This reduced pressure has two terms: one is related to the disorder in the system, the second term is related to the hydrostatic height difference, which decreases as the drainage takes place and the average interface moves down, closer to the outlet.

5.3 Final saturation as function of the Bond number

Previous research has allowed to explicit a functional dependency between final air saturation and the spatial extension of the system size in the absence of gravity, i.e. for the flat case, in the capillary regime (Moura et al., 2015). (Løvoll et al., 2011) extended the analysis to take dynamical effects into account, allowing a broad range of capillary numbers to be permitted, in a viscosity-destabilizing situation, i.e. when the least viscous fluid invades the system, without stabilizing effects of gravity. In this section we propose a scaling relation between the residual saturation (at the end of the drainage) and the Bond number for a gravity stabilized situation, i.e. when the lighter fluid is initially on top of the denser one.

The invaded region in the capillary regime is shown to display a fractal structure (Lenormand et al., 1983; Wilkinson, 1984), with a well established fractal dimension (Mandelbrot, 1982) of $D_c = 1.83$ for a two dimensional (2D) system (Lenormand & Zarcone, 1985). Exploiting together this fractal property of the invaded area and the scaling properties of the invasion front, a functional relationship between the final saturation S_{nw}^F and the Bond number or system size can be obtained. The final saturation of the system S_{nw}^F is attained once all the pores closest to the outlet have been invaded. We first note that

the largest connected clusters of defending fluid, that stay trapped after the invasion interface moved through the system, are built by the motion of this interface. Before they are disconnected of the large cluster connected to the outlet, the boundary of these clusters is part of the mobile interface. Their maximum size is reached when they become disconnected, after what their size does not evolve significantly. Hence, the maximum linear size of the trapped clusters corresponds to the typical size of the interface in the average flow direction. This cutoff length scale l_c corresponds thus to the root mean square width of the mobile front, i.e. $l_c \simeq \sigma$, wich follows the scaling law from Eq. (4) , set by invasion percolation in a gradient, as established by (Birovljev et al., 1991):

$$l_c \sim \sigma \sim aBo^{-\nu/(1+\nu)} \, . \tag{15}$$

Up to this size, the system is fractal with a fractal dimension corresponding to capillary fingering and Invasion Percolation, D_c. Above this size, the mobile front looks like a stright horizontal line. The shape of the trapped clusters above this size is thus not set any more by the selection of smallest thresholds, but by the geometry of the straight line leaving trapped clusters everwhere behind it: it presents the trivial fractal dimension of the space left behind the front, i.e. $D = 2$ in 2D. If the system size is smaller than this characteristic size $aBo^{-\nu/(1+\nu)}$, the system is fractal up to the system's shortest size, W or L. To summarize, the system is fractal with dimension D_c up to a cutoff size

$$l_c = Min(aBo^{-\nu/(1+\nu)}, W, L) \tag{16}$$

The functional relationship between the final saturation and l_c is found by considering a partitioning of the model of dimensions $L \times W$ into square boxes of length l_c . For every such box the displacement structure occupies on average $(l_c/a)^{D_c}$poresAbove this size, the fractal dimension is the trivial fractal dimension $D = 2$, and the number of boxes of size l_c^2 with trapped clusters required to cover the system is simply LW/l_c^2. Moreover, a pores area is a^2, the system's area is LW, and the final saturation is the fraction of the total area occupied by the nonwetting fluid. Hence,

$$S_{nw}^F = \frac{\left(\frac{LW}{l_c^2}\right)\left(\frac{l_c}{a}\right)^{D_c} a^2}{LW} = \left(\frac{l_c}{a}\right)^{D_c-2} \, . \tag{17}$$

Using Eq. (16) hence leads to

$$S_{nw}^F \propto Bo^{[-\nu/(\nu+1)](D_c-2)} \, , \tag{18}$$

where $\nu = 4/3$ is a critical percolation exponent, having the value 4/3 in 2D (Stauffer & Aharony, 2014). This is the case when gravity sets up the cutoff scale, i.e. when $aBo^{-\nu/(1+\nu)} < Min(W, L)$. By contrast, when the system size or gravity is negligible, we predict

$$S_{nw}^F \propto Min(W, L)^{(D_c-2)} \, , \tag{19}$$

This last relation is satisfied by experiments and simulations in horizontal cells where $Bo \ll 1$ for slow drainage where $Ca \ll 1$, as demonstrated by (Moura et al., 2015).

This relation, Eq. (20), holds for Bo >Ca, where the invading fluid from the top has the lower density. In this case, corresponding to the experiments and simulations done here, we obtain a functional dependency between the final saturation and the Bondnumber. In order to check this predicted dependency, the final saturation S_{nw}^F was measured experimentally (circles) and numerically (stars) for a range of Bond numbers, and shown in Fig. 9. From our theoretical prediction we expect

$$S_{nw}^F \propto Bo^{0.097}, \tag{20}$$

This corresponds to the dashed line in this figure. The agreement between both simulations and experiments and this theoretically predicted scaling seems satisfactory. The spread of the final saturation is seen to narrow in as the Bond number increases, which is associated with the finite size effects being suppressed, and the increasingdominance of the width σ as the limiting factor.

6 Discussion

6.1 Extensions in three and one dimensions

This type of argumentation can be extended to three dimensions (3D). Instead of considering partitioning of square boxes, we now consider cubes which on average occupy $(l_c/a)^{D_c}$ pores. This leaves us with the general relation

$$S_{nw}^F \propto Bo^{[-\nu/(\nu+1)](D_c-D)}, \tag{21}$$

where D is 2 or 3 depending on the case considered, 2D or 3D. Here the critical exponent $\nu = 0.88$ in 3D from percolation theory (Adler et al., 1990), and the fractal dimension obtained from invasion percolation is found to be $D_c = 2.5$ (Wilkinson & Willemsen, 1983). Comparative experimental measurements have also been made (Yan et al., 2012; Nsir et al., 2012; Chen et al., 1992) ((Toussaint et al., 2012) for a review), finding compatible D_c values. Hence, we expect in 3D,

$$S_{nw}^F \propto Bo^{0.23}. \tag{22}$$

Data in 3D with detailed capillary pressure relationships and systematically changing Bond number is more scarce than in 2D, as it is easier to change the orientation of the 2D cell than it is to perform 3D experiments where the gravitational field is changed and the wetting properties are kept fixed. To check the consistency between the predicted 3D relation from Eq. (22) and the experiments, the proposed prediction was compared with measurements conducted by (Nouri et al., 2014). Here saturation and pressure was measured using an hanging column apparatus for four different soil types. Namely persian gulf sand (PGS), sandy loam (SL), silty clay (SiC) and silty loam (SiL). For every soil type drainage experiments were performed for four different wetting phases Fig. 10. We determined the final volumetric content of each wetting fluid as function of the soil texture by digitizing the presented data and extracting the resulting final air saturation. We note that the displacement of petroleum by air was extremely low and resulted in very small saturation variations even by applying very high capillary pressure values. The reason for this abnormal behavior is not yet known; we therefore used only the well documented experimental data obtained for kerosene, diesel, water and gasoline. The Bond number was calculated for each fluid pair and soil type, using the given surface tension for each of the four wetting fluids and the density contrast between the wetting fluid and air, the mean grain size diameter (d50) as the typical pore size, and setting $\alpha = \pi/2$. The experimental data from (Nouri et al., 2014) were then analyzed for each soil type separately as shown in Figure 10. This is justified by the large degree of non-uniformity of the different grain-size distributions. The only uniform porous medium is that of the Persian Gulf Sand whose linear trend gives a slope which is the closest to the theoretical one (0.23).

As the process relies on disorder in thresholds a large dispersion from experiment to experiment is expected. Further the capillary number is assumed to be negligible in the derived relation. In these experiments, this approximation is not necessarily perfectly valid. In addition, the wetting angle is probably different between fluid pairs. Furthermore the finite size of the sample will influence the final saturation (Moura et al., 2015).

Eventually, the general Eq. (21) also holds in one dimension (1D), which is an academically trivial case. Indeed, in this case, all pores are along a single line, and are invaded one after the other from the top. Hence, the final saturation is 1. In such case, $D = 1$, and since all cells are occupied behind the front (composed of one pore), the fractal dimension of the invaded cluster is also $D_c = 1$. In this case, $\nu = 1$ (Stauffer & Jayaprakash, 1978) and Eq. (21) predicts $S_{nw}^F = 1$ independently of Bo, which is in agreement with the fact that all cells along the linear network are eventually occupied with the invader, i.e. that indeed $S_{nw}^F = 1$.

6.2 Average capillary pressure

Here, we have considered the capillary pressure as determined experimentally, between the outlet at the wetting fluid and the inlet pressure in the nonwetting one. By contrast, in theoretical or numerical studies, the pressure saturation relationships is often defined as the difference between the average pressure in one fluid at the REV scale, and the average pressure in the other fluid at the same scale (Reeves & Celia, 1996; Hassanizadeh et al., 2002; Hassanizadeh & Gray, 1990, 1993a, 1993b). This quantity can also be approximated for the current simulations and experiments, in order to use in simulations the quantities determined experimentally. Since the variation of the pressure under the approximately horizontal interface is hydrostatic, from Eq. (8) and Eq. (14) the pressure difference at distance z' from the bottom is thus

$$P(z') = P_{outlet} - \Delta\rho g(\sin\alpha)z' = P_a - \Delta P - \Delta\rho g(\sin\alpha)z' = P_a - f^{-1}(p_c) + \Delta\rho g(\sin\alpha)(l - z') \tag{23}$$

with $\Delta P = P_a - P_{outlet}$, and l the front average position.

Hence, averaging over the region of the defending fluid connected to the outlet, one can define the average wetting fluid pressure in this zone as $\bar{P}$, and the difference between the nonwetting fluid and fluid pressure $\Delta\bar{P} = P_a - \bar{P}$, obtaining:

$$\bar{P} = \frac{1}{l}\int_0^l P(z')dz' = P_a - f^{-1}(p_c) + \Delta\rho g(\sin\alpha)\frac{l}{2} = P_a - f^{-1}(p_c) + \frac{a^2 LBo}{2\gamma}\Big(1 - \frac{S_{nw}}{S_{nw}^F}\Big) \tag{24}$$

and

$$\Delta\bar{P} = f^{-1}(p_c) + \frac{a^2 LBo}{2\gamma}\Big(\frac{S_{nw}}{S_{nw}^F} - 1\Big) \tag{25}$$

Eventually, another way to perform the space average of the pressure in both phases is to consider the whole space, including the trapped fluid region behind the front, and not only the connected fluid considered above. This alternative definition of average wetting fluid pressure can then be defined as $\bar{P}' = \frac{1}{L}\int_0^L \Delta P(z')dz'$. In order to evaluate this average, one can approximate the wetting fluid pressure in the trapped clusters above the front, in the zone where $l < z' < L$, as the percolating pressure threshold, $P(z') = P_a - f^{-1}(p_c)$. Thus,

$$\bar{P}' = \frac{l}{L}\bar{P} + (1 - \frac{l}{L})(P_a - f^{-1}(p_c)) = P_a - f^{-1}(p_c) + \Delta\rho g(\sin\alpha)\frac{l^2}{2L} \tag{26}$$

and

$$\Delta\bar{P}' = P_a - \bar{P}' = f^{-1}(p_c) - \Delta\rho g(\sin\alpha)\frac{l^2}{2L} = f^{-1}(p_c) + \frac{a^2 LBo}{2\gamma}\Big(\frac{S_{nw}}{S_{nw}^F} - 1\Big)^2 \tag{27}$$

6.3 Dynamic effects

Dynamic effects also affect the average pressure gradient, and the shape of the interface during drainage. In a situation similar to the one studied so far, i.e. with a low

viscous fluid invading the cell, so that viscosity destabilizes the front, and the lightest fluid entering on top of the densest fluid, so that gravity stabilizes the front, (Méheust et al., 2002) showed that the front root mean square width still follows the same scaling law, with a generalized Bond number $Bo^* = Bo - Ca$. All the other arguments developed above are expected to hold. Since the results only depend on the average pressure gradient and the presence of the disorder, one thus expects that

$$S_{nw}^F \propto (Bo - Ca)^{[-\nu/(\nu+1)](D_c - D)} , \tag{28}$$

when $Bo > Ca$, i.e. when the situation is intrinsically stable. This is expected to hold both in 2D and 3D, replacing D by 2 or 3, and D_c and ν by their proper values for each dimension.

In three dimensions, the Bond number is defined as $Bo = \Delta p_{grav}/\Delta p_{cap}$ where Δp_{grav} is evaluated in the average flow direction, i.e. with $\mathbf{v}$ the average flow velocity, $\Delta p_{grav} = \rho(\mathbf{g}\cdot\mathbf{v})/v$, so that $Bo = \rho(\mathbf{g}\cdot\mathbf{v})a/(v\gamma)$.

Conversely, when $Ca > Bo$, the situation becomes instable, and the front splits in fingers that grow in a ballistic way. In such case, a scaling law can also be obtained between the residual saturation and the system size, as shown in (Løvoll et al., 2011). This study also proposed a relationship betwen pressure and saturation related to this instable situation.

Eventually, the scaling law in Eq. (28) allows to propose a track for future applications: since the residual saturation depends on the capillary number at which a drainage takes place, it can be used as a marker of the flux that took place during this drainage: measuring the residual saturation and knowing the Bond number (characterizing the fluid densities, surface tension and pore sizes), this equation allows to estimate Ca during the drainage. In situations where a drainage took place, this can give a precious estimator to evaluate the conditions at which the flow took place. We propose this as a perspective of future research.

Some limits of this estimation will naturally affect this estimator. Notably, in a few hours, film flow can lower further the residual saturation (as e.g. shown in (Moura et al., 2019)), and for longer times, transport of humidity by the gas phase (evaporation) (Or et al., 2013) will also affect it.

6.4 General pressure-saturation law expected for drainage

Combining Eqs. (13,28,19), one obtains a general approximate law for primary drainage, arising from the hydrostatic effects in the system, the fractal properties of the trapped clusters and of the invasion front, that can be represented by three linear branches: as displayed in Fig.11

When $\Delta P < P_c^t - \frac{\gamma L}{a^2}(Bo - Ca)$, there is no pore invaded and

$$S_{nw}^{tot} \simeq 0 \tag{29}$$

where $P_c^t = f^{-1}(p_c)$ is the capillary pressure corresponding to capillary pressure threshold whose occupancy probability is equal to the percolation threshold for the porous media network the entrance pressure

When $P_c^t - \frac{\gamma L}{a^2}(Bo - Ca) < \Delta P < P_c^t$,

$$\Delta P = P_c^t + \frac{\gamma L}{a^2}(Bo - Ca)\Big(\frac{S_{nw}^{tot}}{[Min(W, L, (Bo - Ca)^{-\nu/(\nu+1)})]^{(D_c - D)}} - 1\Big) , \tag{30}$$

When $\Delta P > P_c^t$, enventually,

$$S_{nw} = S_{nw}^F \simeq [Min(W, L, Bo^{-\nu/(\nu+1)})]^{(D_c - D)} , \tag{31}$$

where ν and D_c are the critical percolation exponent and the capillary fingering dimension for the spatial dimension D (3D or 2D).

This behavior corresponds to the observed one in the experiments and simulations, in Figs. 4,5, and to the behavior studied in (Moura et al., 2015) in the case of $Bo = 0, Ca = 0$.

In addition, for a system with straight boundaries and exit filters, there is also a curvature at the beginning of the curve and at the end, related to the deformation of the invasion front from an initial straight shape to a shape characteristic of percolation invasion in a gradient close to the inlet, and conversely, from such shape to a straight shape against the semipermeable exit filters. Consequently, the entrance pressure, $\frac{2\gamma}{R_{min}}$ with R the minimum curvature of the interface in the largest pore throat size, is always smaller that P_c^t. Such effects of curvature are nonetheless related to the initial and final imposed shape of the interface in tests, and should be absent in an open REV in an open system,with no imposed shape of the front at the entrance and exit of an REV.

7 Conclusions

Pressure-saturation relationships are essentialin soil science, hydrology and for other communities who model multi-phase flow in reservoirs and porous media using Darcy equations. To quantify pressure-saturation curves in the laboratory with the porous plate (or diaphragm) method, researchers generally use soil samples with a height of only several tens of centimetres. The obtained relationships are thus potentially strongly affected by the boundary effects introduced by the semi-permeable membrane, depending on the pore sizes (and on the Bond number associated to it. In our work, we highlight the influence of gravity on the form of pressure-saturation curves during primary drainage. The overall pressure difference between the two fluids is therefore influenced by the hydrostatic pressure difference across the wetting fluid phase. For a system unaffected by boundary effects is then specified by a characteristic capillary pressure that can be obtained from percolation threshold p_c for the occupancy probability and the cumulative distribution of capillary pressure thresholds f as $f^-1(p_c)$, a straight line with a slope given by $\gamma L/a^2 Bo$ and a final saturation, S_{nw}^F. We further show in this study that invasion percolation scheme generates pressure-saturation curves consistent with experimental measurements on a representative volume element (REV), for varying Bond numbers. By using a pore-scale description of the system under the influence of gravity, we are able to collapse the pressure-saturation curves onto a single mastercurve. Furthermore a functional dependency between the final saturation, the strength of the gravitational component (Bond number) the correlation length ν from percolation and the fractal dimension of capillary fingering is obtained for 2D and 3D. For the 2D case we find a good fit with our experimental and numerical results. For the 3D relation we compared with experiments conducted by Nouri et al, which showed compatibility with the predicted relationship. Furthermore, knowing the final air saturation obtained from water retention curves, using the theoretical relation of Eq. (21), it is possible to predict the final non-wetting saturation when other wetting fluids than water are displaced by air during primary gravity stabilized drainage. With these elements together, one predicts an approximate capillary pressure - saturation relation as function of dimension, Capillary and Bond number, and of the system dimension. Such prediction is done between the air pressure and wetting fluid pressure measured at the bottom. The theoretically corresponding difference between the average pressures in both phases is also derived. Knowing the pore-size distribution and the characteristics of the fluid pair and the wetting properties of the system, our results gives a guideline for simulations and upscaling of the saturation from small to large scales.

Acknowledgments

This work was partly supported by the Research Council of Norway through its Centres of Excellence funding scheme, Project No. 262644 (PoreLab), the LIA France-Norway D-FFRACT, the University of Strasbourg PDI program and the CNRS INSU ALEAS program.

References

Adler, J., Meir, Y., Aharony, A., & A.B. Harris, A. (1990). Series study of percolation moments in general dimension. *Phys. Rev. E*, *41*, 9183–9206. doi: 10.1103/PhysRevB.41.9183

Aggelopoulos, C., & Tsakiroglou, C. (2009). A multi-flowpath model for the interpretation of immiscible displacement experiments in heterogeneous soil columns. *Journal of Contaminant Hydrology*, *105*(3), 146 - 160. Retrieved from http://www.sciencedirect.com/science/article/pii/S0169772208002180 doi: https://doi.org/10.1016/j.jconhyd.2008.12.004

Aker, E., Måløy, K., Hansen, A., & Batrouni, G. (1998, 08). A two-dimensional network simulator for two-phase flow in porous media. *Transport in Porous Media*, *32*, 163-186. doi: 10.1023/A:1006510106194

Auradou, H., Måløy, K. J., Schmittbuhl, J., Hansen, A., & Bideau, D. (1999, Dec). Competition between correlated buoyancy and uncorrelated capillary effects during drainage. *Phys. Rev. E*, *60*, 7224–7234. Retrieved from https://link.aps.org/doi/10.1103/PhysRevE.60.7224 doi: 10.1103/PhysRevE.60.7224

Aursjø, O., Knudsen, H. A., Flekkøy, E. G., & Måløy, K. J. (2010, Aug). Oscillation-induced displacement patterns in a two-dimensional porous medium: A lattice boltzmann study. *Phys. Rev. E*, *82*, 026305. Retrieved from https://link.aps.org/doi/10.1103/PhysRevE.82.026305 doi: 10.1103/PhysRevE.82.026305

Birovljev, A., Furuberg, L., Feder, J., Jøssang, T., Måløy, K. J., & Aharony, A. (1991). Gravity invasion percolation in two dimensions: Experiment and simulation. *Physical Review Letters*, *67*(5), 584.

Blunt, M., King, M. J., & Scher, H. (1992, Dec). Simulation and theory of two-phase flow in porous media. *Phys. Rev. A*, *46*, 7680–7699. Retrieved from https://link.aps.org/doi/10.1103/PhysRevA.46.7680 doi: 10.1103/PhysRevA.46.7680

Blunt, M., & King, P. (1990, Oct). Macroscopic parameters from simulations of pore scale flow. *Phys. Rev. A*, *42*, 4780–4787. Retrieved from https://link.aps.org/doi/10.1103/PhysRevA.42.4780 doi: 10.1103/PhysRevA.42.4780

Brooks, R. H., & Corey, A. T. (1964). Hydraulic properties of porous media. *Hydrology Papers*(3).

Bryant, S., & Blunt, M. (1992, Aug). Prediction of relative permeability in simple porous media. *Phys. Rev. A*, *46*, 2004–2011. Retrieved from https://link.aps.org/doi/10.1103/PhysRevA.46.2004 doi: 10.1103/PhysRevA.46.2004

Chandler, R., Koplik, J., Lerman, K., & Willemsen, J. F. (1982, 6). Capillary displacement and percolation in porous media. *J. Fluid Mech.*, *119*, 249–267. Retrieved from http://journals.cambridge.org/article_S0022112082001335 doi: 10.1017/S0022112082001335

Chen, S., Kim, K.-H., Qin, F., & Watson, A. (1992). Quantitative nmr imaging of multiphase flow in porous media. *Magnetic Resonance Imaging*, *10*(5), 815 - 826. Retrieved from http://www.sciencedirect.com/science/article/pii/0730725X9290417X doi: https://doi.org/10.1016/0730-725X(92)90417-X

Clotet, X., Santucci, S., & Ortín, J. (2016, Jan). Experimental study of stable imbibition displacements in a model open fracture. ii. scale-dependent avalanche dynamics. *Phys. Rev. E*, *93*, 012150. Retrieved from https://link.aps.org/

doi/10.1103/PhysRevE.93.012150 doi: 10.1103/PhysRevE.93.012150

Ewing, R. P., & Berkowitz, B. (1998). A generalized growth model for simulating initial migration of dense non-aqueous phase liquids. *Water Resources Research*, *34*(4), 611-622. doi: 10.1029/97WR03754

Fiorentino, E.-A., Toussaint, R., & Jouniaux, L. (2017). Two-phase lattice boltzmann modelling of streaming potentials: Influence of the air-water interface on the electrokinetic coupling. *Geophysical Journal International*, *208*(2), 1139-1156. doi: 10.1093/gji/ggw417

Furuberg, L., Feder, J., Aharony, A., & Jøssang, T. (1988, Oct). Dynamics of invasion percolation. *Phys. Rev. Lett.*, *61*, 2117–2120. Retrieved from http://link.aps.org/doi/10.1103/PhysRevLett.61.2117 doi: 10.1103/PhysRevLett.61.2117

Furuberg, L., Måløy, K. J., & Feder, J. (1996, Jan). Intermittent behavior in slow drainage. *Phys. Rev. E*, *53*, 966–977. Retrieved from http://link.aps.org/doi/10.1103/PhysRevE.53.966 doi: 10.1103/PhysRevE.53.966

Glass, R., Conrad, S., & Yarrington, L. (2001). Gravity-destabilized nonwetting phase invasion in macroheterogeneous porous media: Near-pore-scale macro modified invasion percolation simulation of experiments. *Water Resources Research*, *37*(5), 1197-1207. doi: 10.1029/2000WR900294

Haines, W. B. (1930, 1). Studies in the physical properties of soil. v. the hysteresis effect in capillary properties, and the modes of moisture distribution associated therewith. *The Journal of Agricultural Science*, *20*, 97–116. Retrieved from http://journals.cambridge.org/article_S002185960008864X doi: 10.1017/S002185960008864X

Hassanizadeh, S., Celia, M., & Dahle, H. (2002). Dynamic effect in the capillary pressuresaturation relationship and its impacts on unsaturated flow. *Vadose Zone Journal*, *1*, 38–57.

Hassanizadeh, S., & Gray, W. (1990). Mechanics and thermodynamics of multiphase flow in porous media including interphase boundaries. *Adv. Water Resour.*, *13*, 169–186.

Hassanizadeh, S., & Gray, W. (1993a). Thermodynamic basis of capillary pressure in porous media. *Water Resour. Res.*, *29*(10), 3389–3405.

Hassanizadeh, S., & Gray, W. (1993b). Toward an improved description of the physics of two-phase flow. *Adv. Water Resour.*, *16*, 53–67.

Jankov, M., Løvoll, G., Knudsen, H., Måløy, K. J., Planet, R., Toussaint, R., & Flekkøy, E. G. (2010). Effects of pressure oscillations on drainage in an elastic porous medium. *Transport in Porous Media*, *84*(3), 569-585. doi: 10.1007/s11242-009-9521-z

Joekar Niasar, V., Hassanizadeh, S. M., Pyrak-Nolte, L. J., & Berentsen, C. (2009). Simulating drainage and imbibition experiments in a high-porosity micromodel using an unstructured pore network model. *Water Resources Research*, *45*(2). Retrieved from https://agupubs.onlinelibrary.wiley.com/doi/abs/10.1029/2007WR006641 doi: 10.1029/2007WR006641

Kallel, W., van Dijke, M. I. J., Sorbie, K. S., & Wood, R. (2017). Pore-scale modeling of wettability alteration during primary drainage. *Water Resources Research*, *53*(3), 1891-1907. Retrieved from https://agupubs.onlinelibrary.wiley.com/doi/abs/10.1002/2016WR018703 doi: 10.1002/2016WR018703

Kokkinaki, A., O'Carroll, D. M., Werth, C. J., & Sleep, B. E. (2013). Coupled simulation of dnapl infiltration and dissolution in three-dimensional heterogeneous domains: Process model validation. *Water Resources Research*, *49*(10), 7023-7036. doi: 10.1002/wrcr.20503

Lenormand, R., & Zarcone, C. (1985, May). Invasion percolation in an etched network: Measurement of a fractal dimension. *Phys. Rev. Lett.*, *54*, 2226–2229. Retrieved from https://link.aps.org/doi/10.1103/PhysRevLett.54.2226 doi: 10.1103/PhysRevLett.54.2226

Lenormand, R., Zarcone, C., & Sarr, A. (1983, 10). Mechanisms of the displacement of one fluid by another in a network of capillary ducts. *Journal of Fluid Mechanics*, *135*, 337–353. Retrieved from http://journals.cambridge.org/article_S0022112083003110 doi: 10.1017/S0022112083003110

Løvoll, G., Jankov, M., Måløy, K. J., Toussaint, R., Schmittbuhl, J., Schäfer, G., & Méheust, Y. (2011, Jan 01). Influence of viscous fingering on dynamic saturation–pressure curves in porous media. *Transport in Porous Media*, *86*(1), 305–324. Retrieved from https://doi.org/10.1007/s11242-010-9622-8 doi: 10.1007/s11242-010-9622-8

Løvoll, G., Méheust, Y., Toussaint, R., Schmittbuhl, J., & Måløy, K. J. (2004, Aug). Growth activity during fingering in a porous hele-shaw cell. *Phys. Rev. E*, *70*, 026301. Retrieved from https://link.aps.org/doi/10.1103/PhysRevE.70.026301 doi: 10.1103/PhysRevE.70.026301

Måløy, K. J., Feder, J., & Jøssang, T. (1985, Dec). Viscous fingering fractals in porous media. *Phys. Rev. Lett.*, *55*, 2688–2691. Retrieved from https://link.aps.org/doi/10.1103/PhysRevLett.55.2688 doi: 10.1103/PhysRevLett.55.2688

Måløy, K. J., Furuberg, L., Feder, J., & Jøssang, T. (1992, Apr). Dynamics of slow drainage in porous media. *Phys. Rev. Lett.*, *68*, 2161–2164. Retrieved from http://link.aps.org/doi/10.1103/PhysRevLett.68.2161 doi: 10.1103/PhysRevLett.68.2161

Mandelbrot, B. (1982). *The fractal geometry of nature*. San Francisco: W.H. Freeman.

Méheust, Y., Løvoll, G., Måløy, K. J., & Schmittbuhl, J. (2002, Nov). Interface scaling in a two-dimensional porous medium under combined viscous, gravity, and capillary effects. *Phys. Rev. E*, *66*, 051603. Retrieved from http://link.aps.org/doi/10.1103/PhysRevE.66.051603 doi: 10.1103/PhysRevE.66.051603

Misztal, M., Hernandez-Garcia, A., Matin, R., Srensen, H., & Mathiesen, J. (2015). Detailed analysis of the lattice boltzmann method on unstructured grids. *Journal of Computational Physics*, *297*, 316-339. doi: 10.1016/j.jcp.2015.05.019

Moura, M., Fiorentino, E.-A., Måløy, K. J., Schäfer, G., & Toussaint, R. (2015). Impact of sample geometry on the measurement of pressure-saturation curves: Experiments and simulations. *Water Resour. Res.*, *51*(11), 8900–8926. Retrieved from http://dx.doi.org/10.1002/2015WR017196 doi: 10.1002/2015WR017196

Moura, M., Flekkø, E. G., Måløy, K. J., Schäfer, G., & Toussaint, R. (2019). Connectivity enhancement due tofilm ow in porous media. *Phys. Rev. Fluids*, *submitted*.

Moura, M., Måløy, K., Flekkøy, E., & Toussaint, R. (2017). Verification of a dynamic scaling for the pair correlation function during the slow drainage of a porous medium. *Physical Review Letters*, *119*(15). doi: 10.1103/PhysRevLett.119.154503

Moura, M., Måløy, K. J., & Toussaint, R. (2017). Critical behavior in porous media flow. *EPL*, *118*(1). doi: 10.1209/0295-5075/118/14004

Nayagum, D., Schäfer, G., & Mos, R. (2004). Modelling two-phase incompressible flow in porous media using mixed hybrid and discontinuous finite elements. *Computational Geosciences*, *8*(1), 49-73. Retrieved from http://dx.doi.org/10.1023/B%3ACOMG.0000024446.98662.36 doi: 10.1023/B:COMG.0000024446.98662.36

Nordhaug, H. F., Celia, M., & Dahle, H. (2003, 10). A pore network model for calculation of interfacial velocities. *Advances in Water Resources*, *26*, 1061-1074. doi: 10.1016/S0309-1708(03)00100-3

Nouri, M., Homaee, M., & Bybordi, M. (2014, 05). Quantitative assessment of lnapl retention in soil porous media. *Soil and Sediment Contamination: An Interna-*

tional Journal, *23*.

Nsir, K., Schäfer, G., di Chiara Roupert, R., & Mercury, L. (2018). Pore scale modelling of dnapl migration in a watersaturated porous medium. *Journal of Contaminant Hydrology*, *215*, 39 - 50. Retrieved from http://www.sciencedirect.com/science/article/pii/S0169772217302905 doi: https://doi.org/10.1016/j.jconhyd.2018.07.001

Nsir, K., Schäfer, G., di Chiara Roupert, R., Razakarisoa, O., & Toussaint, R. (2012). Laboratory experiments on DNAPL gravity fingering in water-saturated porous media. *International Journal of Multiphase Flow*, *40*(0), 83 - 92.

Or, D., Lehmann, P., Shahraeeni, E., & Shokri, N. (2013). Advances in soil evaporation physicsa review. *Vadose Zone Journal*, *12*(4).

Paterson, L. (1984, Apr). Diffusion-limited aggregation and two-fluid displacements in porous media. *Phys. Rev. Lett.*, *52*, 1621–1624. Retrieved from https://link.aps.org/doi/10.1103/PhysRevLett.52.1621 doi: 10.1103/PhysRevLett.52.1621

Planet, R., Santucci, S., & Ortín, J. (2009, Mar). Avalanches and non-gaussian fluctuations of the global velocity of imbibition fronts. *Phys. Rev. Lett.*, *102*, 094502. Retrieved from https://link.aps.org/doi/10.1103/PhysRevLett.102.094502 doi: 10.1103/PhysRevLett.102.094502

Reeves, P., & Celia, M. (1996). A functional relationship between capillary pressure, saturation, and interfacial area as revealed by a porescale network model. *Water Resources Research*, *32*(8), 2345–2358.

Sapoval, B., Rosso, M., & Gouyet, J.-F. (1985). The fractal nature of a diffusion front and the relation to percolation. *Journal de Physique Lettres*, *46*(4), 149–156.

Schneider, L., Roupert, R., Schaefer, G., & Helluy, P. (2015, 08). Highly gravity-driven flow of a napl in water-saturated porous media using the discontinuous galerkin finite-element method with a generalised godunov scheme: Highly gravity-driven flow of a napl in water-saturated porous media. *Computational Geosciences*, *19*, 1-22. doi: 10.1007/s10596-015-9494-7

Sheng, Q., & Thompson, K. (2013). Dynamic coupling of pore-scale and reservoir-scale models for multiphase flow. *Water Resources Research*, *49*(9), 5973-5988. Retrieved from https://agupubs.onlinelibrary.wiley.com/doi/abs/10.1002/wrcr.20430 doi: 10.1002/wrcr.20430

Singh, M., & K. Mohanty, K. (2003, 01). Dynamic modelling of drainage through three-dimensional porous materials. *Chemical Engineering Science*, *58*, 1-18. doi: 10.1016/S0009-2509(02)00438-4

Sleep, B., Beranger, S., Reinecke, S., & Filion, Y. (2015, 10). Dnapl accumulation in wells and dnapl recovery from wells: Model development and application to a laboratory study. *Advances in Water Resources*, *85*.

Stauffer, D., & Aharony, A. (2014). *Introduction to percolation theory.* Taylor & Francis.

Stauffer, D., & Jayaprakash, C. (1978). Critical exponents for one-dimensional percolation clusters. *Physics Letters*, *64A*(5), 433–434.

Tørå, G., Oeren, P.-E., & Hansen, A. (2012, 03). A dynamic network model for two-phase flow in porous media. *Transport in Porous Media*, *92*. doi: 10.1007/s11242-011-9895-6

Toussaint, R., Løvoll, G., Méheust, Y., Måløy, K. J., & Schmittbuhl, J. (2005). Influence of pore-scale disorder on viscous fingering during drainage. *Europhys. Lett.*, *71*(4), 583-589. Retrieved from http://dx.doi.org/10.1209/epl/i2005-10136-9 doi: 10.1209/epl/i2005-10136-9

Toussaint, R., Måløy, K., Méheust, Y., Løvoll, G., Jankov, M., Schaefer, G., & Schmittbuhl, J. (2011). Two-phase flow: Structure, upscaling, and consequences for macroscopic transport properties. *Vadose Zone Journal*,

11. Retrieved from http://dx.doi.org/10.2136/vzj2011.0123 doi: 10.2136/vzj2011.0123

Toussaint, R., Måløy, K., Méheust, Y., Løvoll, G., Jankov, M., Schäfer, G., & Schmittbuhl, J. (2012). Two-phase flow: Structure, upscaling, and consequences for macroscopic transport properties. *Vadose Zone Journal*, *11*(3). doi: 10.2136/vzj2011.0123

van Genuchten, M. T. (1980). A closed-form equation for predicting the hydraulic conductivity of unsaturated soils. *Soil Sci. Soc. Am. J.*, *44*, 892–898.

Wilkinson, D. (1984). Percolation model of immiscible displacement in the presence of buoyancy forces. *Physical Review A*, *30*(1), 520.

Wilkinson, D. (1986, Aug). Percolation effects in immiscible displacement. *Phys. Rev. A*, *34*, 1380–1391. Retrieved from https://link.aps.org/doi/10.1103/PhysRevA.34.1380 doi: 10.1103/PhysRevA.34.1380

Wilkinson, D., & Willemsen, J. F. (1983). Invasion percolation: a new form of percolation theory. *J. Phys. A: Math. Gen.*, *16*(14), 3365-3376. Retrieved from http://iopscience.iop.org/0305-4470/16/14/028 doi: 10.1088/0305-4470/16/14/028

Yan, J., Luo, X., Wang, W., Toussaint, R., Schmittbuhl, J., Vasseur, G., ... Zhang, L. (2012, may). An experimental study of secondary oil migration in a three-dimensional tilted porous medium. *AAPG bulletin*, *96*(5), 773–788. Retrieved from http://dx.doi.org/10.1306/09091110140 doi: 10.1306/09091110140

Yang, Z., Méheust, Y., Neuweiler, I., Hu, R., Niemi, A., & Chen, Y.-F. (2019). Modeling immiscible two-phase flow in rough fractures from capillary to viscous fingering. *Water Resources Research*, *55*(3), 2033-2056. doi: 10.1029/2018WR024045

Zhang, Z., & Smith, J. E. (2001). The velocity of dnapl fingering in water-saturated porous media: laboratory experiments and a mobileimmobilezone model. *Journal of Contaminant Hydrology*, *49*(3), 335 - 353. Retrieved from http://www.sciencedirect.com/science/article/pii/S0169772201000973 doi: https://doi.org/10.1016/S0169-7722(01)00097-3

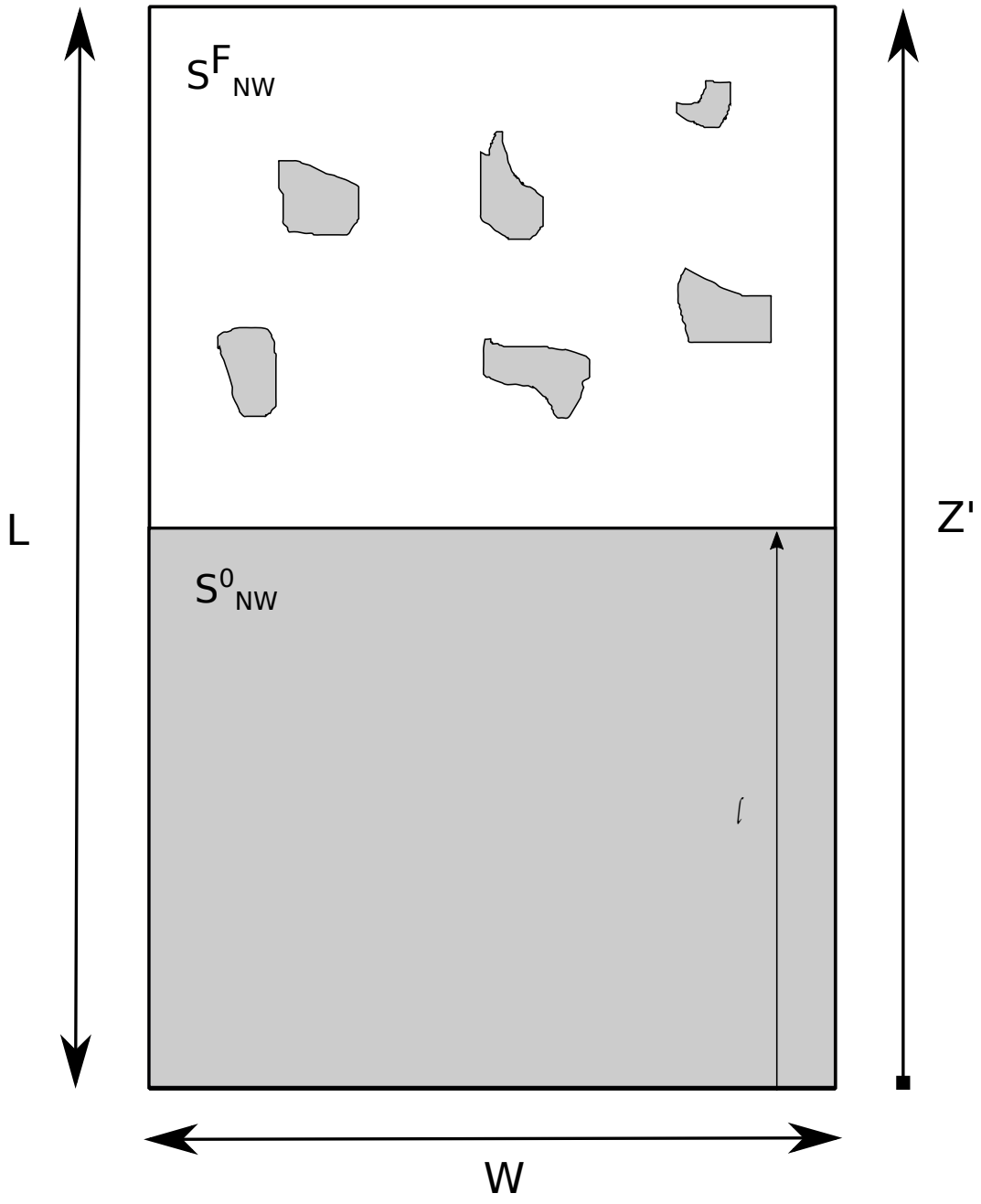

Figure 6. Schematics of of a fully saturated porous medium, which has been drained until the average front position is in a distance l from the outlet.

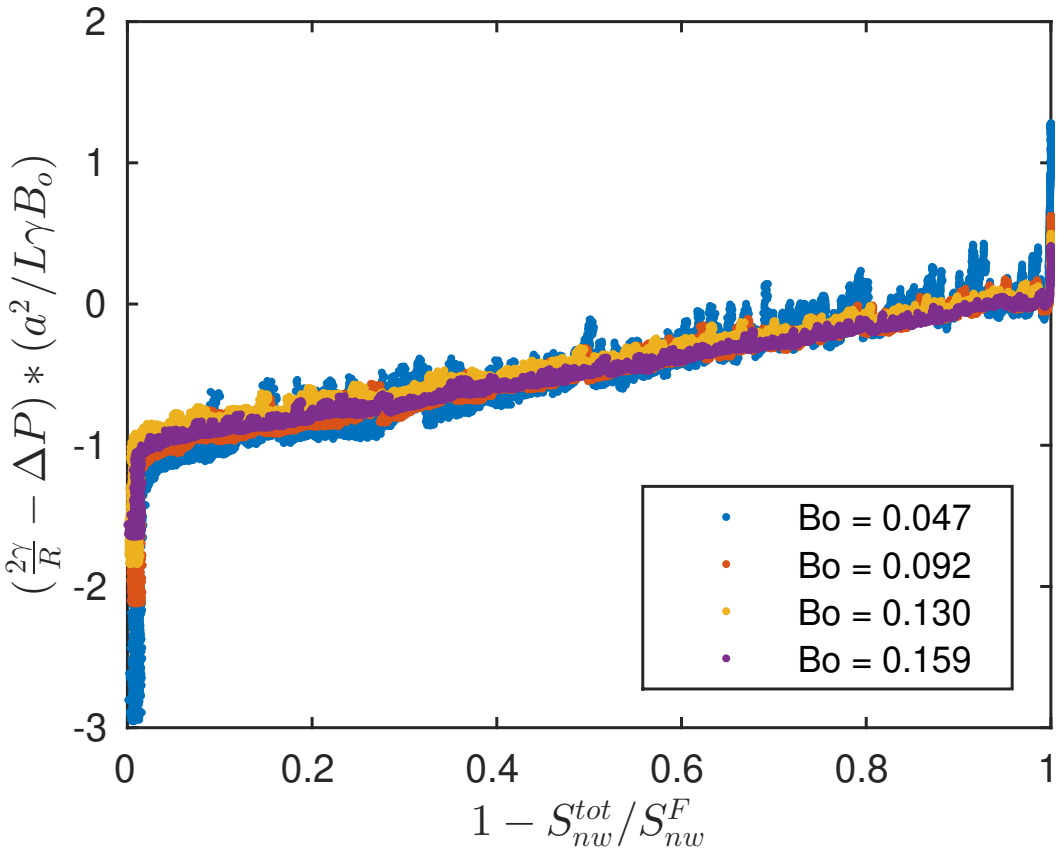

Figure 7. Data collapse of pressure as function of the relative saturation,for the experimentally obtained datasets.

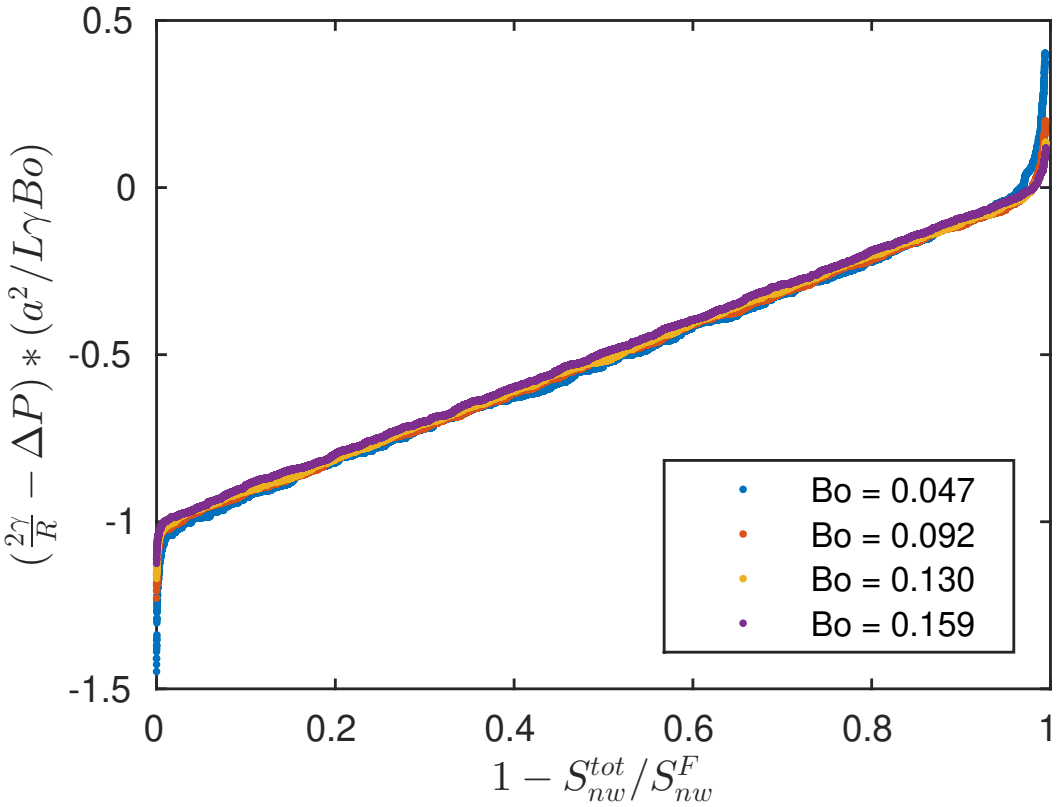

Figure 8. Data collapse of pressure as function of the relative saturation.numerically obtained datasets

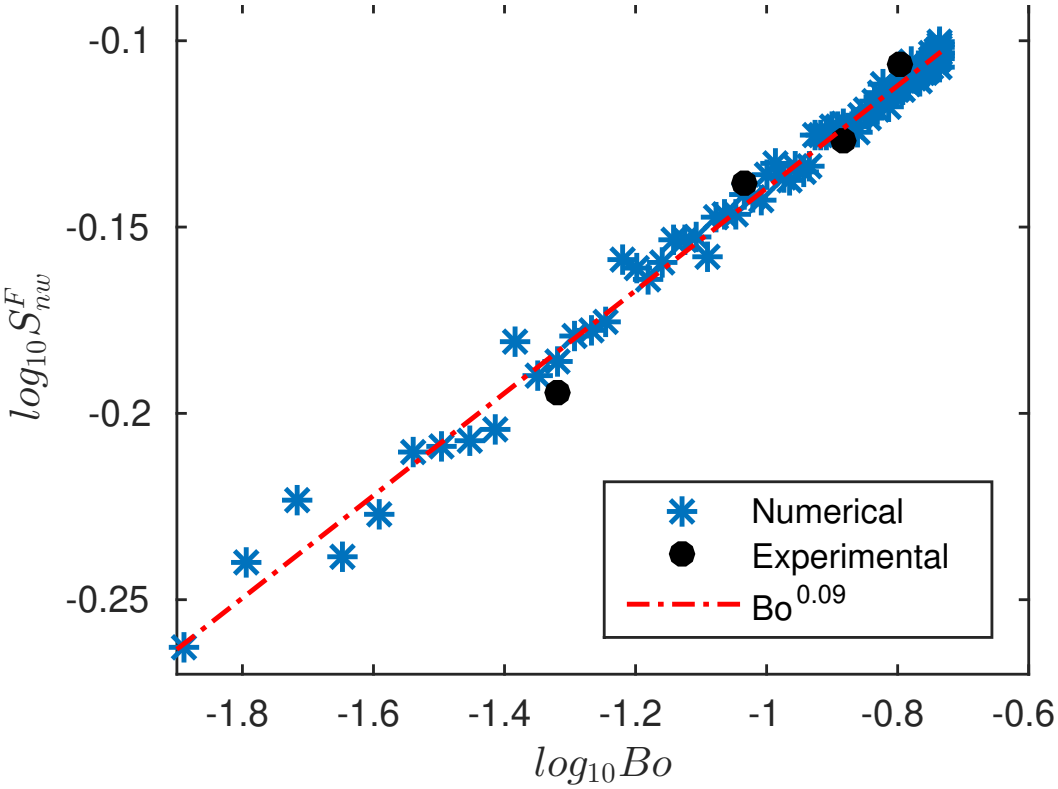

Figure 9. The final saturation as a function of the Bond number is plottet both for the experimental and numerical results together with the predicted 2D relation $S^F_{nw} = Bo^{0.09}$

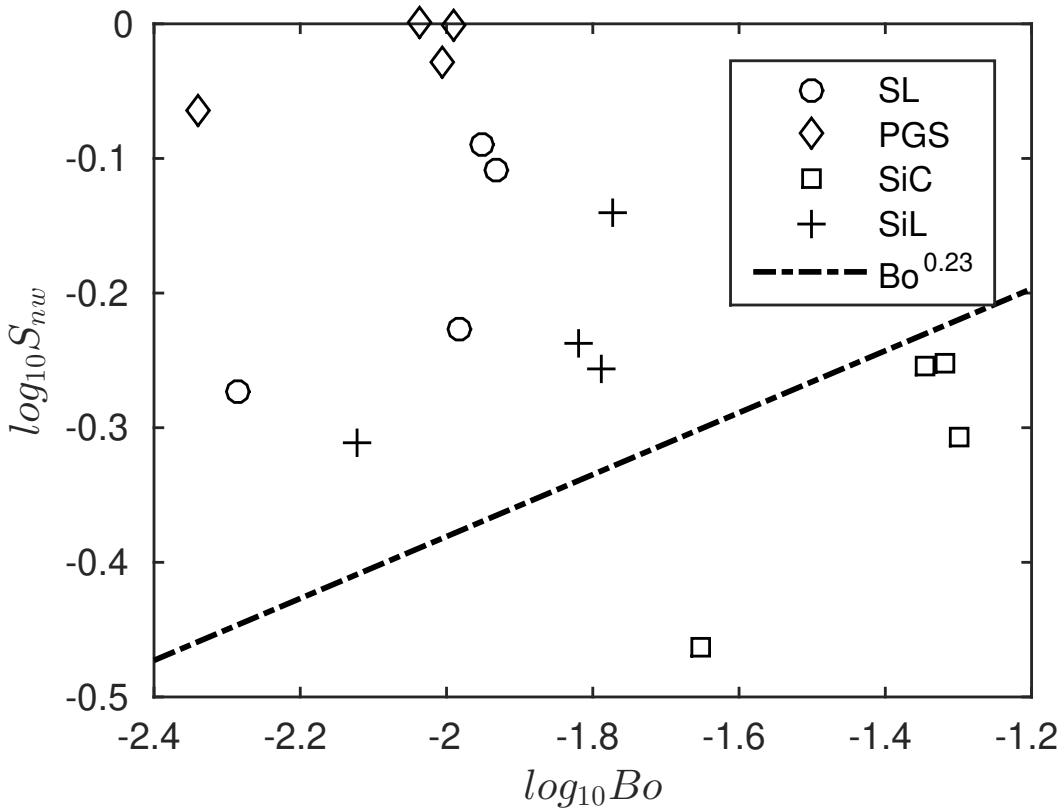

Figure 10. Shows the final saturation and its corresponding Bond number for four different soil samples. The Bond number was here varied by changing the wetting phase. The striped line indicate the power law slope obtained from the theoretical prediction.

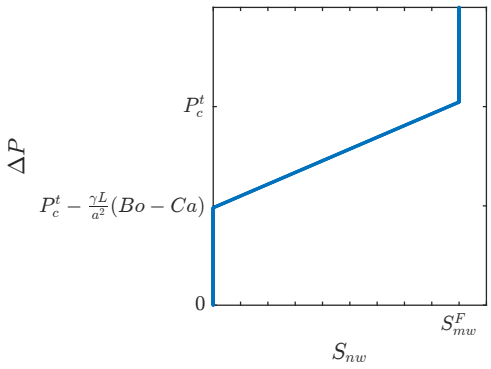

Figure 11. Figure shows our modeled general pressure-saturation law represented by three linear branches.

Paper 2: Avalanche dynamics under the influence of gravity

Avalanche dynamics and pressure variations during drainage in gravity stabilized flow

Monem Ayaz*
Universit de Strasbourg, Institut de Physique du Globe de Strasbourg, UMR7516, 67084 Strasbourg, France
Université de Strasbourg, CNRS, LHyGeS UMR 7517, 67084 Strasbourg, France. and
PoreLab, The Njord center, Department of Physics, University of Oslo, Norway

Renaud Toussaint
Universit de Strasbourg, Institut de Physique du Globe de Strasbourg, UMR7516, 67084 Strasbourg, France and
PoreLab, The Njord center, Department of Physics, University of Oslo, Norway

Knut Jørgen Måløy
PoreLab, The Njord center, Department of Physics, University of Oslo, Norway

Gerhard Schäfer
Université de Strasbourg, CNRS, LHyGeS UMR 7517, 67084 Strasbourg, France.

We experimentally study slow drainage in a quasi two-dimensional Hele-shaw cell. The setup construction allows for tuning of the gravitational component. During experiments the pressure in the fluid phase is measured coupled with optical monitoring. We show by correlating the two measured quantities that the intermittent evolution of the pressure signal can be related to the invasion of multiple pores in a burst like fashion. Furthermore we investigate the influence of gravity on its statistics, the distribution of waiting times $p(w_t)$ and avalanche size $p(s)$ is calculated from the optical signal for five different inclinations and we find a linear relationship between the size of the burst in the pressure signal and the volume invaded during invasion of multiple pores. Further we are able to extract the average shape of the pressure variation around a burst and compare it to theoretical considerations.

PACS numbers: 47.56.+r, 47.61.Jd, 05.40.-a

I. INTRODUCTION

Studies of fluid invasion, displacement of one fluid by another one in a porous medium, has revealed a variety of pattern-forming procesess [1–3] governed by the interplay between viscous, capillary and gravitational forces. Pore-scale studies have revealed a variety of phenomena and mechanisms by which such systems evolve, and has shown to exhibit complex behavior characterized by their rich intermittent dynamics and their ability to exhibit long ranging correlations. [4, 5]. Many systems respond to a slowly changing external condition not in a smooth way but in the terms of a series of discrete events or bursts spanning a broad range of sizes [6]. Such avalanches are observed for many different systems ranging from earthquakes [7] occuring when slowly moving tectonics plate slide along each other, to the tearing of paper [8]. Other examples is the motion of a front between two immiscible fluids as it invades a porous medium [4, 9, 10].

Studies of drainage in the capillary regime, where the fluid pressure difference between two fluids is solely responsible for the displacement dynamics, have displayed pressure evolution in terms of avalanches, also referred to in the literature as Haines jumps[11–13]. Here the pressure signal is characterized by slow build ups followed by drops in pressure. On a pore level this slow build up corresponds to a slow deformation of the interface between the two into the porous body. Once the pressure difference between the two fluids along the interface reaches critical capillary threshold value, the interface becomes unstable, resulting in the invasion of multiple pores, and as a result the invaded fluid is redistributed along the interface. It is noteworthy that even if the displacement dynamics is a highly non-local mechanism, it is well modeled by invasion percolation (IP), being a stochastic growth model [14].

The influence of gravity in such systems has shown to lead to long range correlations along the interface [3, 15], reducing the spread between the two phases, in effect spatially limiting the front of the invading phase. Moreover varying the effective gravity changes how much and how the pore-space is explored by the fluid front. This can be of importance for the burst dynamics as the number of pores in which the interface is redistributed is decreased with an increase in the effective gravity.

Målœy et al reported on experiments [13] with complementary simulations where the bursty dynamics of the displacement front was measured and successfully modeled by a modified invasion percolation algorithm. Here the notion of a capacative interface volume was introduced, $K = dV/dp_{cap}$, where V is the fluid typically displaced in a typical pore for a change in pressure difference between the two fluids dp_{cap}. Furthermore

* auayaz@fys.uio.no

$\Delta P = -\sum_i V_i/(n_f K)$. The total change in capillary pressure ΔP is proportional to the sum over all the pore volumes V_i invaded during a burst. Here n_f is the length of the interface perimeter, measured in number of pores.

We show in this study that the pressure signal obtained during slow drainage, with its characteristic periods of pressure build up followed by a sudden decompression, can be optically related to the rapid invasion of multiple pores in an avalanche behavior. We further investigate how tuning of the gravitational component affects the bursty behavior. Lastly we validate the use of linear relationship between the total change in capillary pressure and the displaced volume, and we are able to experimentally determine a characteristic relaxation time for a typical burst, and compare with theoretical considerations.

II. EXPERIMENTAL METHOD

A. The setup

The porous network is constructed by pouring poly-disperse glass beads $1.0mm < d < 1.2mm$i n size onto the sticky side of an adhesive contact paper, the monolayer of beads is then clamped between two Plexiglas plates, which is sealed off with a rectangular layer of silicon glue. The Plexiglas plate has milled inlet and outlet channels, allowing for injection and withdrawal of the respective fluid phases. From below a pressure cushion forces the porous structure to stay confined. The dimensions of the rectangular system is: Length $L = 14.5cm$, width $W = 10cm$ and thickness of $d = 1mm$. The porous medium is initially saturated with a wetting fluid which is composed of 80% glycerol and 20% water by weight, having a dynamic viscosity of $\nu = 4.25 \cdot 10^{-5} m^2/s$, density of $\rho_w = 1.205 g/cm^3$ with surface tension $\gamma = 0.064 N/m$. The invading fluid used is air and is withdrawn into the system through the outlet channel by a syringe pump at a constant flow rate of $0.004 ml/min$. The system is resting on a lightbox which can be tilted by an angle α over the horizontal, allowing for tuning of the gravitational component along the average flow direction $g \sin \alpha$. Furthermore the 2D porosity of the system was measured to be $\phi = 0.66$ by performing an image analysis, projecting the beads shape on a plane, and computing the fraction of the area uncovered by this projection.

During the experiments the relative pressure difference between the non-wetting and wetting phase is measured by a Honeywell 26PCAFG6G flow-through pressure sensor connected to the model outlet, making measurements every $\Delta t \approx 0.2s$.

The dynamical evolution of the displacement structure is captured by images at fixed time lapse $\approx 10s$ with a NIKON D7100 SLR camera, which is mounted perpendicularly to the model. An Aladdin AL-1600 syringe pump is used to provide constant flow rates, the fluid is withdrawn from the system with a discharge rate of Q = $6.6 \cdot 10^{-11} m^3/s$.

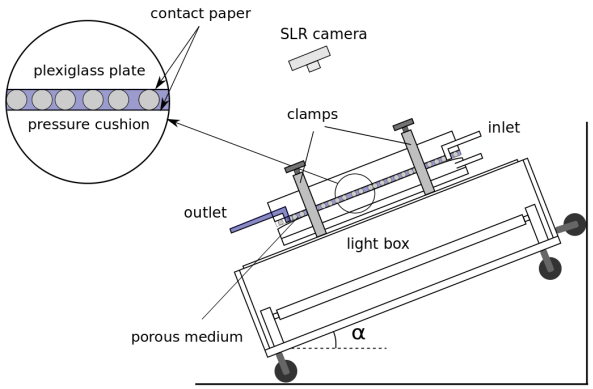

FIG. 1. Schematics of the experimental setup. Two plexiglass plates are sandwiched between a monolayer of polydisperse glass-beads.

III. RESULTS

A. Extracting the signals

From the image sequence captured during the experiments, growth of displacement structure is extracted, by performing image subtraction between sequential images and thereafter thresholding (see Fig. 2). The signal $I(t)$ was retrieved, by summing over all pixels corresponding to the newly invaded area and dividing by the area corresponding to the average pore-size. A subset of this signal is shown as the topmost graph in Fig. 3.

The pressure drop across the model is at any time such that it maintains the constraint set by the flow rate. Measured as the difference between the atmospheric pressure p_{atm} and the pressure in the wetting phase at the outlet $p(t) = p_{outlet} - p_{atm}$. As we are interested in studying the pressure drops related to the invasion of multiple pores, the linear hydrostatic drift $p_{drift}(t)$ is subtracted from the pressure signal, giving us $p_c(t) = p(t) - p_{drift}(t)$. In order to extract the corresponding rate of change in the pressure-measurements the derivative $\dot{p}_c$ is introduced. A one-to-one relation is made by pairing the optical signal with the nearest pressure measurement in time, giving an uncertainty in synchronization of up to 0.2s. We further observe that the derivative corresponds well with the optical signal.

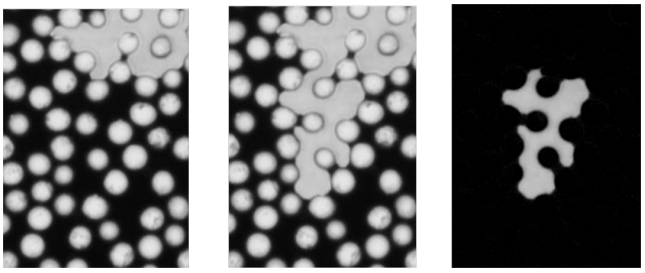

FIG. 2. The first two image shows the displacement caused by a burst, here the lighter colored fluid(air) is seen to invade the wetting fluid which is darker colored. The last image shows the growth obtained by performing an image subtraction between the two gray-scale images.

B. Correlation

To measure the significant relationship between the optical and pressure measurements, the correlation between the signal was calculated using the normalized cross-correlation function $CC(\Delta t)$ as defined below

$$CC(\Delta t) = \left\langle \frac{(\dot{p}_c(t) - \mu_{\dot{p}_c})(I(t+\Delta t) - \mu_I)}{\sigma_{\dot{p}_c}\sigma_I} \right\rangle_t \qquad (1)$$

where μ_I and $\mu_{\dot{p}_c}$ are the averages, σ_I and $\sigma_{\dot{p}_c}$ the standard deviations of the respective signals.The result is shown onFig. 4.

We first notice the maximum correlation to exist in the absence of any phase shift between the signals $\dot{p}_c(t)$ and $I(t)$. It has a negative sign as $\dot{p}_c(t)$ is negative during pressure drops, we find this zero-shift to be $CC(0) = -0.89$. We notice further that on Fig. 4 this peak is followed by a positive correlation which peaks close to 30 seconds, as the signal $I(t)$ is strictly positive this means that we have optical activity present in the system while the pressure again starts to build up in the wetting phase, this activity can be related to snap-off of capillary bridges [16] or the possible gradual drainage of pores through secondary drainage by filmflow. The newly displaced pores take some time to reconfigure their meniscii, which can also lead to activity.
The build up phase shows a gradual increase in correlation with an average time of $\sim 100s$, this increase in correlation is related to the linear increase in pressure up to threshold where the meniscii is deformed into the porous structure. Next the average relaxation time after a sudden burst is estimated to be around 200s, after which the signals once again become uncorrelated, this sets a time-scale for the secondary activity in terms of snap-off and film-flow [16]

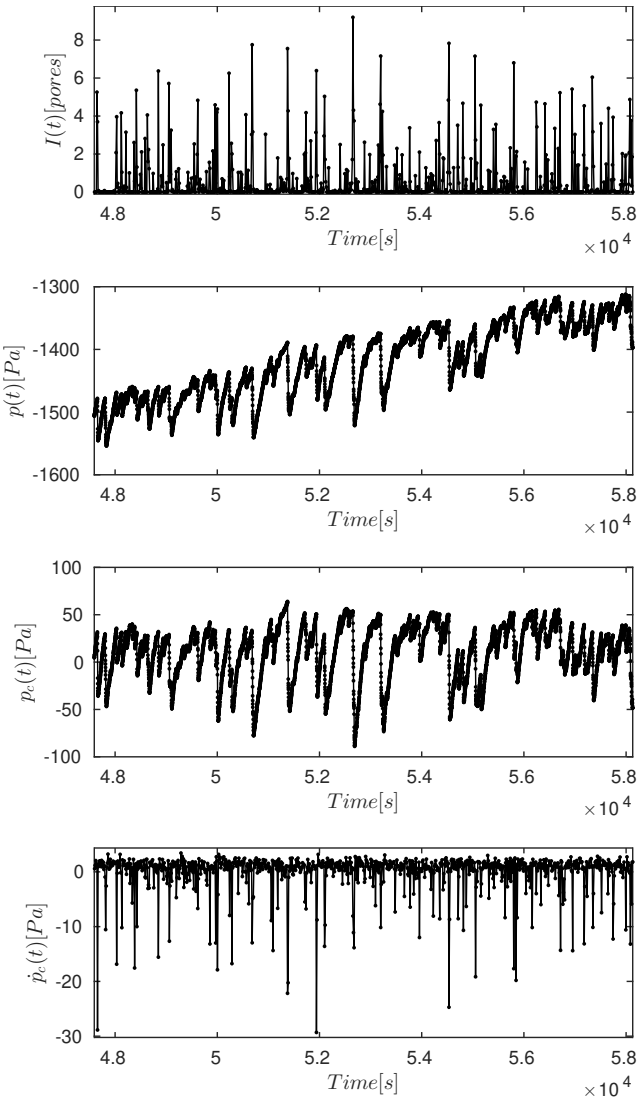

FIG. 3. The topmost graph shows the amplitude of the invaded area extracted from the images. the following two graphs show the measured signal $p(t) = p_{outlet} - p_{atm}$ and $p_c(t) = p(t) - p_{drift}(t)$ where the hydrostatic drift has been subtracted from the signal. The bottom shows the derivative $\dot{p}_c(t)$.

C. Statistics under the influence of gravity

Complex systems are characterized by their power-law distributions over a broad range of scales in time and space. The distribution of waiting times $p(w_t)$ and avalanche size $p(s)$ is calculated from the derivative $\dot{p}_c(t)$ for four different inclinations. We define the size of an avalanche S as the integrated domain existing below a defined clip level c, see Fig. 5, for an avalanche of duration $\Delta t = t_1 - t_0$ the size of the resulting avalanche $S = \mid p_c(t_1) - p_c(t_0) \mid = \mid \int_{t_0}^{t_1} \dot{p}_c(t)dt \mid$ gives us the pressure drop over the integration domain.

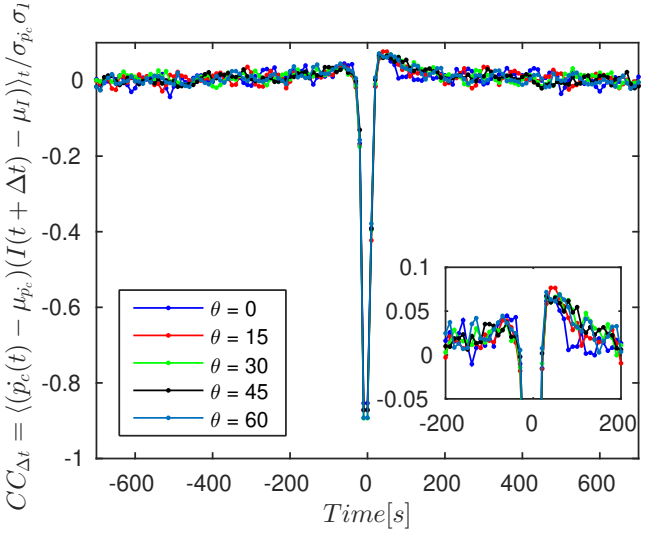

FIG. 4. Cross-correlation between the signal $I(t)$ obtained from the images and the pressure difference $\Delta p_c(t)$. The inset shows a zoom of the graph.

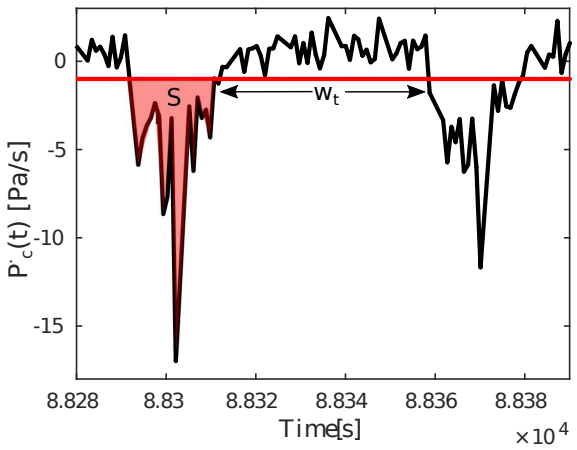

FIG. 5. a zoom of the signal $\dot{p}_c(t)$, the avalanche size S is determined as the integrated domian below a clip level, the waiting time w_t is defined as time between successive avalanches.

Futher we define the waiting time as the period between successive pore-invasion events. The avalanche size $p(s)$ is found to be well fitted to a power-law with an exponential cut-off

$$p(s) \propto s^{-\alpha} e^{s/s^*} \tag{2}$$

with $\alpha \simeq 1.6$ and $s^* \simeq 40Pa$. For the waiting time distribution $p(w_t)$ we expect similar to the avalanche size distribution it to follow a power law with an exponential cutoff. We found a scaling relation on the form $p(w_t) \sim w_t^{-\alpha} e^(w_t/w_t^*)$ here the power law exponent was found to be $\alpha = 1.65$.

The presence of gravity sets up hydrostatic pressure differences which suppress the maximum height difference between two points along the front [15], acting as a stabilizing force on the system. This leads to a reduction of the interface perimeter between the fluid pair. Similarly the presence of disorder acts as a destabilizing force [3] acting on a smaller length and time scale. From $p(s)$ and $p(w_t)$ we observe the large waiting time where the interface is pinned, and subsequent avalanches to occur for the larger inclination. This can be understood as: When the hydrostatic pressure differences along the front pores increases the advantageous pores with positions closer to the inlet get harder to invade, resulting in larger waiting times. This longer build up is not seen to result in larger avalanches.

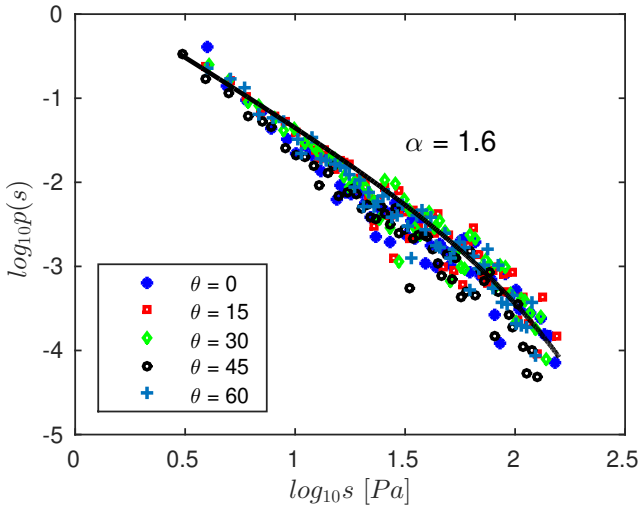

FIG. 6. Avalanche size distribution for different inclinations. The datapoints are fitted with the function $p(s) \propto s^{-\alpha} e^{-s/s^*}$, where $\alpha = 1.6$ and $s^* = 40Pa$.

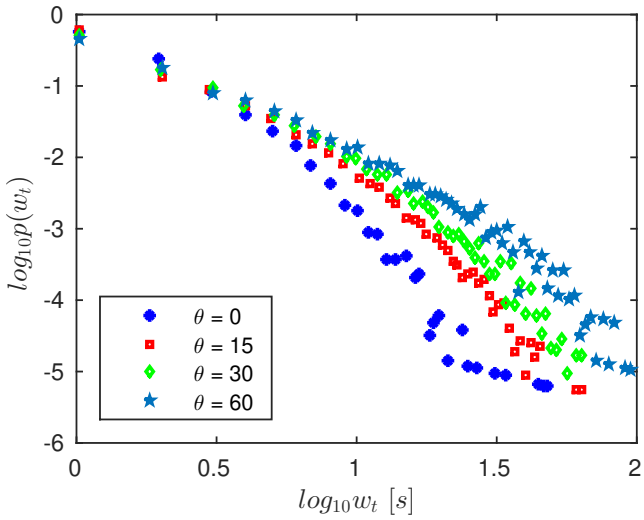

FIG. 7. Waiting time distribution for varying inclinations, obtained from the pressure signal $p_c(t)$.

D. Relationship between the capillary pressure and the total displaced area

As the constant withdrawal rate is much slower than the local flux during a burst, the displaced wetting phase must be reconfigured at the interface between the fluids, causing the interface to quickly readjust to larger radii of curvature. Hence the ability of the interface to facilitate for the displaced volume, is what drives the Haines jumps.
Furuberg et al. [17]. introduced the notion of a volume capacitance, $K = dV/dp_{cap}$, as the rate of change in the average volume of wetting fluid received in a front pore with the capillary pressure. It was assumed to be constant for a given system. We evaluate their assumption by measuring the relationship between the capillary pressure drop and the displaced area. The former is found by integrating the signal $\dot{p_c}(t)$ over a threshold. Similarly the displaced area is found by integrating connected regions in its respective time series. A linear relation between the two quantities is found as displayed in Fig. 8. We notice the larger inclinations to have tendency for a smaller spread compared to larger inclinations.

The characteristic time scale Γ of a burst was proposed roughly approximated as follows: The meniscus positioned at the typically the largest possible distance L from the region where the burst occurs will relax most slowly, we estimate this distance to be the system width. As the flow of fluid is driven by the pressure gradient of the order p_{cap}/L, the velocity close to the meniscus is then given by Darcy's law:

$$u = \frac{\kappa_0}{\mu\phi}\frac{p_{cap}}{L} \tag{3}$$

where μ is the dynamic viscosity of the wetting phase, ϕ the porosity and κ_0 the permeability defined by the Carman-Kozeny relation [18]:

$$\kappa_0 = \frac{a^2}{180}\frac{\phi^3}{(1-\phi)^2} \tag{4}$$

We require further that Eq.3 be equal to the backcontracting meniscus velocity given by the capillary pressure volume relation $\Delta V = K\Delta P_{cap}$, for an approximated linear length traveled of $\Delta x = \Delta V/a^2$, where a is the average pore-throat size. Setting the velocities equal to each other gives.

$$\frac{dp_{cap}}{dt} = \frac{-a^2\kappa_0 p_{cap}}{\mu K L\phi} \tag{5}$$

This gives us a separable differential equation, which has an exponential solution on the form, $p_{cap}(t) = Ce^{-a^2\kappa_0 t/\mu LK\phi}$, where C is an integration constant. The expression gives us a characteristic relaxation time $\Gamma = (\mu LK\phi)/\kappa_0 a^2$. The value of K for an typical pore was measured from the pressure-measurements and found to be $K = 3.33\cdot 10^{-12}m^5/N$, we notice that this value is independent of gravity and the system size. As the interface fluctuates close to its pore-throat during invasion, a is approximated by the mean pore-throat size. Inserting for the parameters in the expression for Γ gives us a relaxation time of $\approx 3s$.

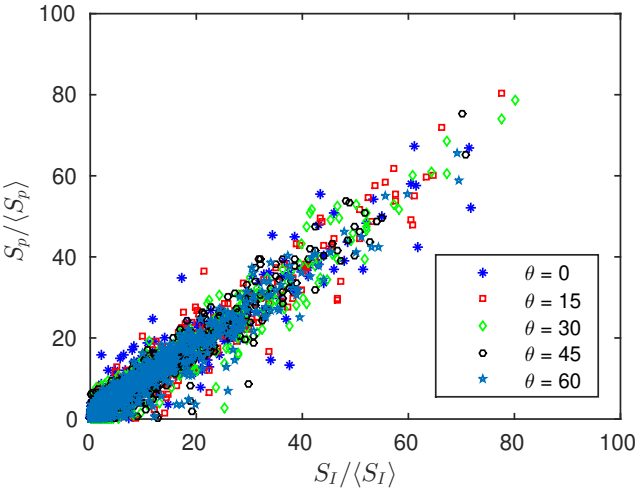

FIG. 8. We find there to be a linear relationship between the size of the pressure drops S_p and its corresponding displaced volume S_I .

The burst shape was experimentally obtained by investigating independent bursts where the pumping rate have been subtracted from the pressure signal as displayed in Fig. 9, for the horizontal case where gravity does not influence the system. The bursts are well fitted to an exponential relaxation with a characteristic relaxation time, measured to be $\Gamma \approx 8s$.

IV. CONCLUSION

We study experimentally burst dynamics during drainage in a gravity stabilized setting, in a quasi two-dimensional confinement, where the viscous forces are negligible for the displacement. We are able to correlate pressure and optical signal, and obtained an average build-up and relaxation time for the bursts. Furthermore a linear relationship between the total pressure drop and the volume being displaced during a burst is obtained. Lastly we find the individual bursts to be well fitted to an exponentially decaying function, in agreement with theoretical considerations.

ACKNOWLEDGMENTS

We would like to thank the support from the University of Oslo and University of Strasbourg. This work

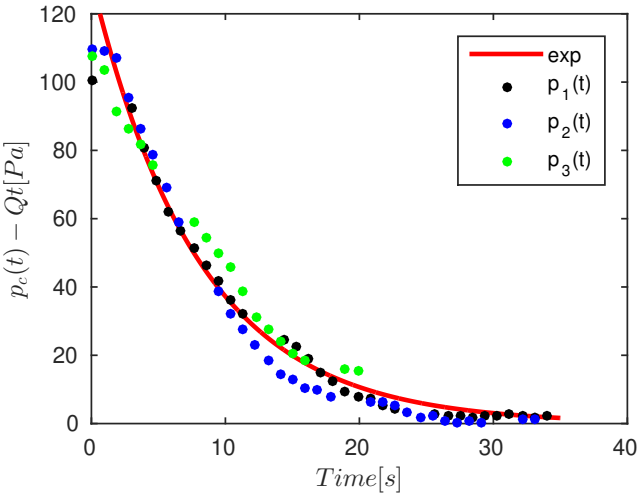

FIG. 9. Pressure signal from three independent bursts are here displayed. The pumping rate has been withdrawn from the signal. Further the datapoints have been fitted to an exponentially decaying function.

was partly supported by the Research Council of Norway through its Centres of Excellence funding scheme, Project No. 262644 (PoreLab), the LIA France-Norway D-FFRACT, the University of Strasbourg PDI program and the CNRS INSU ALEAS program.

[1] K. J. Måløy, J. Feder, and T. Jøssang, Phys. Rev. Lett. **55**, 2688 (1985).
[2] R. Lenormand, C. Zarcone, and A. Sarr, Journal of Fluid Mechanics **135**, 337 (1983).
[3] Y. Méheust, G. Løvoll, K. J. Måløy, and J. Schmittbuhl, Phys. Rev. E **66**, 051603 (2002).
[4] X. Clotet, S. Santucci, and J. Ortn, Physical Review E **93** (2016), 10.1103/PhysRevE.93.012150.
[5] M. Moura, K. J. Mly, and R. Toussaint, EPL (Europhysics Letters) **118**, 14004 (2017).
[6] J. P. Sethna, K. A. Dahmen, and C. R. Myers, Nature **410**, 242 (2001).
[7] R. Shcherbakov, D. L. Turcotte, and J. B. Rundle, Geophysical Research Letters **31** (2004), 10.1029/2004GL019808.
[8] M. Stojanova, S. Santucci, L. Vanel, and O. Ramos, Phys. Rev. Lett. **112**, 115502 (2014).
[9] S. Santucci, R. Planet, K. J. Måløy, and J. Ortín, EPL (Europhysics Letters) **94**, 46005 (2011).
[10] R. Planet, S. Santucci, and J. Ortín, Phys. Rev. Lett. **102**, 094502 (2009).
[11] W. B. Haines, The Journal of Agricultural Science **20**, 97 (1930).
[12] L. Furuberg, J. Feder, A. Aharony, and T. Jøssang, Phys. Rev. Lett. **61**, 2117 (1988).
[13] K. J. Måløy, L. Furuberg, J. Feder, and T. Jøssang, Phys. Rev. Lett. **68**, 2161 (1992).
[14] R. Chandler, J. Koplik, K. Lerman, and J. F. Willemsen, J. Fluid Mech. **119**, 249 (1982).
[15] A. Birovljev, L. Furuberg, J. Feder, T. Jssang, K. J. Mly, and A. Aharony, Phys. Rev. Lett. **67**, 584 (1991).
[16] M. Moura, E. G. Flekkøy, K. J. Måløy, G. Schäfer, and R. Toussaint, Phys. Rev. Fluids **4**, 094102 (2019).
[17] L. Furuberg, K. J. Måløy, and J. Feder, Phys. Rev. E **53**, 966 (1996).
[18] P. Carman, Chemical Engineering Research and Design **75**, S32 (1997).

Paper 3: Snap-off displacement during slow drainage in a gradient

Snap-off displacement during slow drainage

Monem Ayaz*
Institut de Physique du Globe de Strasbourg, University of Strasbourg, France. Université de Strasbourg, CNRS, LHyGeS UMR 7517, 67084 Strasbourg, France. and PoreLab, The Njord center, Department of Physics, University of Oslo, Norway

Renaud Toussaint
PoreLab, The Njord center, Department of Physics, University of Oslo, Norway and Institut de Physique du Globe de Strasbourg, University of Strasbourg, France.

Knut Jørgen Måløy
PoreLab, The Njord center, Department of Physics, University of Oslo, Norway

Gerhard Schäfer
Université de Strasbourg, CNRS, LHyGeS UMR 7517, 67084 Strasbourg, France.

We investigate the connectivity of the secondary flow networks that emerge during slow drainage of a two-dimensional synthetic porous medium. Our experimental setup allows to vary the effective gravity imposed on the system. Optical monitoring of the invasion process allows us to identify capillary bridges and map their connectivity. Furthermore a novel algorithm was designed to detect their rupture. Occurrences of snap-off are dynamically measured in the reference frame of the displacement front and its statistical distribution measured. Moreover the connectivity problem is translated to a graph object.

PACS numbers: 47.56.+r, 47.61.Jd, 05.40.-a

I. INTRODUCTION

The study of displacement of one fluid by another in a porous confinement is a well studied problem, both from a fundamental and an applied perspective. An increased understanding of these processes are of interest in hydrology and soil-sciences [1]. From an applied perspective an increased understanding can be of importance for the control of migration of pollutants through ground water aquifers and CO_2 sequestration in reservoir rock.

The pioneering work of Lenormand et al. [2], made use of a single layered transparent etched porous network to conduct displacement experiments with immiscible fluid phases. Here the gravitational and viscous forces were well controlled parameters. This quasi two dimensional(2D) confinement has been well explored in the wake of their work [3–5]. Fluid displacement in porous network has been observed to occur by two main mechanisms: Either as pore-filling displacement where the advancement occurs when the threshold pressure for the pore-throat and its adjacent pore is met, or as secondary displacement that does not modify the structure of the bulk pores being invaded. Among this, displacement by snap-off occurs along sets of film and bridges of wetting fluid, when pore-filling type motion is not possible due to topological reasons. [2]

Much emphasis has been on the characterization and understanding of the displacement structure [6] that arise from varying flow conditions and its dependence on the fluid pair, geometrical properties of the confining porous body and the flow rate with which the system is driven [7]. The structures obtained have been categorized in a phase diagram[8] consisting of three flow regimes namely; Viscous fingering [3, 5], stable displacement and capillary fingering [9]

The many islands of wetting fluid left behind by the displacement front are characteristic of the displacement structure that arise from slow drainage. This effect is especially prominent for 2D, and of less importance for 3D systems. A recent study by Moura et al. revealed how a series of connected capillary bridges formed by thin films can conduct wetting fluid from a seemingly entrapped fluid back to the bulk on the system scale [10]. An increased understanding of these pathways and the mechanism by which they rupture is important for understanding and ultimately controlling entrapment in porous media.

The use of graph theory to study complex networks have received a lot of attention. It allows to study the connection topology in various topics ranging from the internet[11] to fracture networks [12–14]. Properties and behaviors of complex systems has uncovered surprising resemblance among the topology of various systems. For instance, a particular set of networks are said to be scale-free, meaning that the probability that a node of a network has k connections follows a scale-free distribution $P(k) \sim k^{-\gamma}$ with the exponent γ. The characteristic feature of such graphs is the presence of nodes with very large number of connections compared

* auayaz@fys.uio.no

to the average.
We will in this paper study the distribution of snap-off events in time and space, and utilize network theory to calculate measures in order to characterize the network emerging from secondary migration of wetting fluid.

II. EXPERIMENTAL SETUP

The porous network is constructed by pouring spherical glass beads, $1mm$ in size onto the sticky side of an adhesive contact paper, the monolayer of beads is then clamped between two Plexiglas plates, with milled inlet and outlet channels, allowing for injection and withdrawal of the respective fluid phases. The distance L between the two channels is 14.5 cm, while the width W of the model is 11.5 cm. From below a pressure cushion pressurized by 3 meter water column forces the beads to stay confined. The porous medium is initially saturated with a wetting fluid which is composed of 80% glycerol and 20% water by weight, having a kinematic viscosity of $\nu = 4.25 \cdot 10^{-5} m^2/s$, density of $\rho_w = 1.205 g/cm^3$ with surface tension $\gamma = 6.4 \cdot 10^{-2} Nm^{-1}$. The saturating fluid is withdrawn from the outlet channel by a syringe pump providing constant flow rates. The system is resting on a lightbox which can be tilted allowing for the tuning of the gravitational component $g \sin\theta$. Fig.1

At the outlet boundary, there exists a sponge permitting the continuation of pores to be invaded once the system has reached break-through. Final saturation of the non-wetting phase is achieved once all the pores bordering the sponge has been invaded. Optical monitoring of the invasion process is made with a NIKON D7100 SLR camera and a 20mm focal objective, capturing images with the time resolution $\Delta t = 10s$. The images have a spatial resolution of 30 pix per pore.

A. Identifying capillary bridges and their ruptures

We define a capillary bridge to be a trapped film of fluid stuck between two glass beads, which is not available for invasion by regular pore-filling mechanism where the threshold pressure associated to the pore throat size can be overcome. Instead, the observed mechanism of removal of this bridge is thrgough an unstable rupturing event, also referred to as snap-off [2].

Our routine for identifying capillary bridges is based on firstly pinpointing all the pore-throats in the system. This is achieved by Delaunay triangulating over the porous network, with the centroids of the glass beads as vertices. Hence, acquiring the set of corresponding triangulated edges is equivalent to finding all the pore-throat sizes in the system. We define the position of the pore-throat as the midpoint of the respective edge Fig.2.

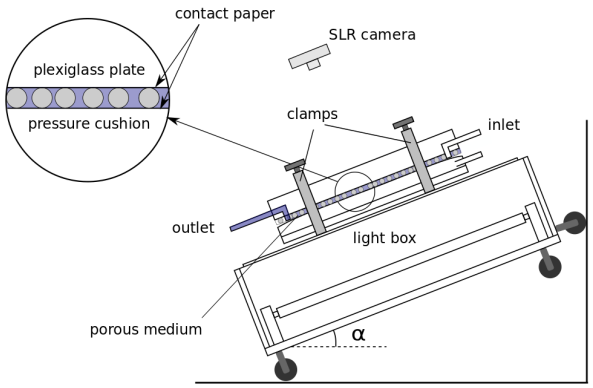

FIG. 1. Schematics of the experimental setup. Two plexiglass plates are sandwiched between a monolayer of polydisperse glass-beads.

For every time-step, the midpoint of the pore-throats is assessed, by evaluating its gray-scale value. The two phases are clearly distinguishable as the wetting phase is dyed with nigrosin. By applying a mask over all the trapped clusters of wetting fluid. The pore-throats are found to be in one of three possible scenarios: 1) The entry pressure to the adjacent pore has been overcome in which case the pore-throat is invaded 2)The pore-throat can be situated in one of the trapped clusters or the bulk. 3) Lastly the pore-throat can be a capillary bridge, in which case the pore on both sides have been invaded by alternative invasion paths. Fig.2 shows the implementation of our technique, the green dot marks the midpoint of the capillary bridges and the striped blue line the edge along the pore-throat with which it lies.

III. RESULTS

Drainage experiments were performed at low withdrawal rate of 0.02 ml/min under the influence of gravity in the capillary regime. Here the lighter non wetting fluid (air) invades the saturated cell from the top. This leads to a gravity stabilized configuration [4, 15]. As the invading front propagates through the system it sheds behind residual wetting fluid, in terms of clusters spanning multiple pores and capillary bridges. During the experiments pore-invasion caused by the possible continuous flow along the edges of the system or the confining plate was not detected on the time scale of the experiment. This was checked by conducting an experiment where the system was left to run for a much longer times. No pore-invasion caused by the above mentioned effects were observed.

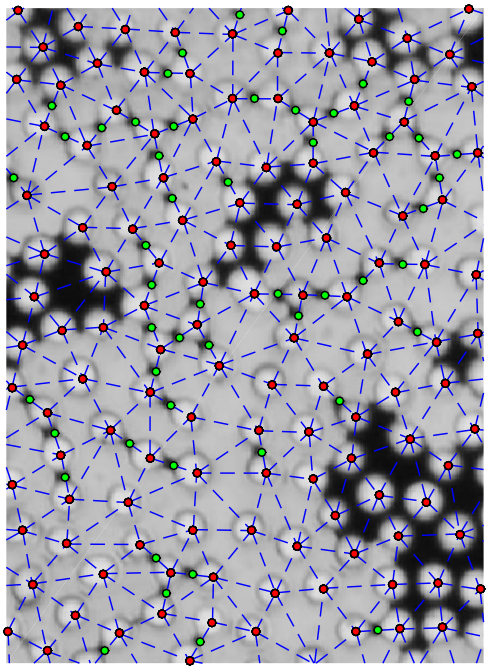

FIG. 2. Image crop, the bead centers are represented by red dots, green dots represents the center of the capillary bridges. Dashed blue grid represents the Delaunay triangulation, by which the capillary bridges are identified.

A. Snap-off

Once the capillary bridges have been identified, snap-off events can easily be detected, this is achieved by dynamically checking for sudden changes in grayscale value above some threshold on the pixels related to pore-throats which are identified to be capillary bridges. This analysis is performed for varying inclinations ranging from $[0, 60^{\circ}]$ as shown in Fig 3. Here we plot the normalized probability distribution of snap-of events occurring in the reference frame of the mean front position $z - \bar{z}$, where z is the upwards coordinate along the cell starting from the cell bottom and $\bar{z}$ defines the average front position.

The front is defined as the set of pores bordering the largest cluster (i.e the bulk) of the wetting phase at any time. The algorithm was implemented once the front was well defined and terminated once it reached breakthrough to avoid any finite-size effects. We notice that most of the activity occurs close to the mean front position $(z - \bar{z}) = 0$. Secondly we notice that an increasing inclination, leads to a flatter front[15], restricting the area where events typically occur. The front width and activity area behave in a coupled manner in space. In the inset figure We rescale the obtained distributions with the front width, which is predicted by IP to be $\sigma \sim Bo^{-\nu/1+\nu}$. [1, 4, 15] Here ν is a critical exponent of

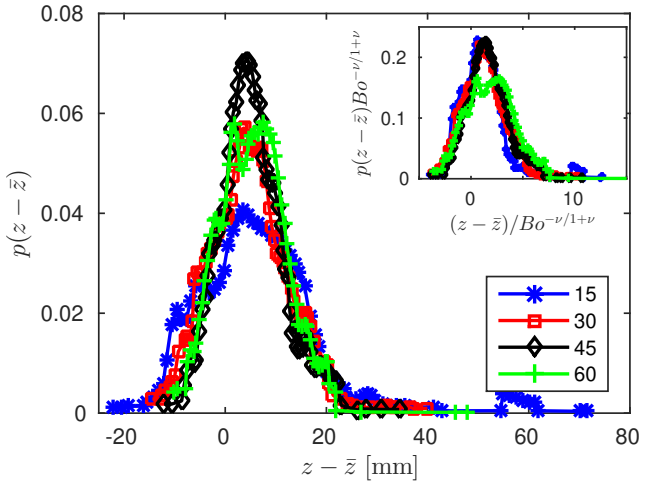

FIG. 3. Snap-off distribution position. In the mean interface position $z - \bar{z}$. The inset shows the rescaled probability distribution function(pdf) with the predicted front width σ from percolation theory.

the correlation length, having the value 4/3 for two dimensions. Bo is the Bond number defined to be the typical ratio of gravitational and capillary forces over pore $\Delta\rho g a^2/\gamma$. where $\Delta\rho$ is the density contrast between the two fluids, a is the typical pore size, γ is the surface tension between the two fluids and $g \sin\theta$ is the gravitational term parallel to the average flow direction. In effect giving the strength of the gravitational field on the porous body.

B. Gravitational dependence

Increasing the gravitational component, sets up stabilizing hydrostatic pressure differences along the front. Hence tuning this parameter in effect changes how much and the sequence by which the pore-space is explored by the invading fluid [15]. In Fig.4 the effect of gravity on the length of capillary bridges once the experiment has been terminated is probed. We see that the number of pores invaded are inconsequential for the shape of the distribution, which is well fitted by Gaussian of the form $p(l) \propto e^{(l-\mu)^2/2\sigma^2}$, where $\mu = 0.29mm$ and $\sigma = 0.05mm$. The inset figure shows the distribution of capillary bridges that end up snapping off with fit parameters for a Gaussian; $\mu = 0.36mm$ and $\sigma = 0.08mm$. This shift between the two bell curves indicates that the larger capillary bridges on average are more unstable, and hence rupture.

We define objects composed of capillary-pathways and trapped cluster which are connected by fluid paths, these structures are seen to branch out in space, the question of directional growth with respect to gravity

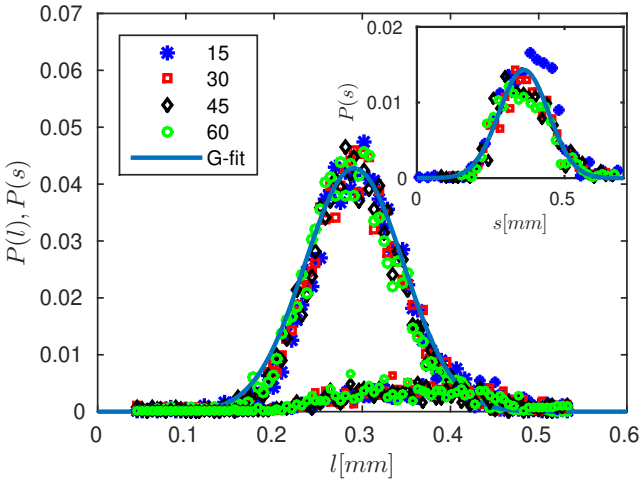

FIG. 4. Distribution $p(l)$ of the capillary bridges of length l in the system once the system has reached break-through, fitted together with a Gaussian. also displayed is the distribution $p(s)$, which are the bridges that end up rupturing, we see that only small portion of bridges snap-off. The inset figure shows the distribution $p(s)$

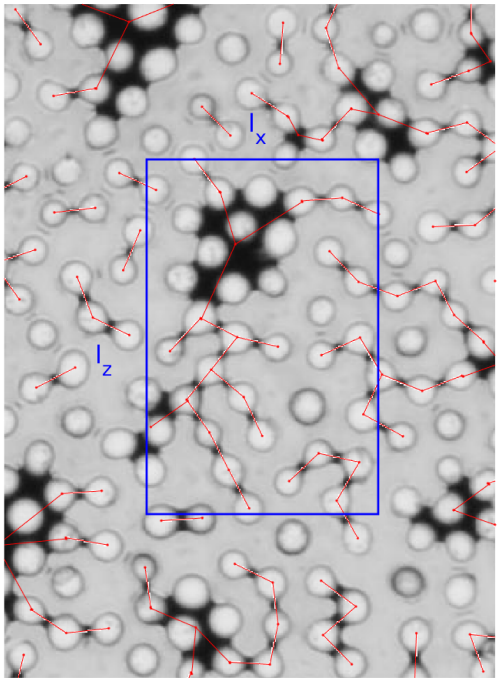

FIG. 5. The blue rectangle shows the use of a bounding box to enclose one of the disconnected subset of the graph.The tran

is studied. Such objects can be characterized by their extension in the l_x direction transverse to the flow direction and l_z parallel to the flow direction. To study this we utilize a bounding box which is the smallest rectangle that encloses the subgraph as displayed in Fig.5. The distribution for the two respective spatial direction are displayed in Fig. 6 which lie ontop of each other. We observe that there is no noticeable asymmetry in the elongations of the subset of the graph. For capillary network consisting of more than one capillary bridge we observe the distribution to be power law distributed $P(l_{x,z}) \sim X^{-\alpha}$, with $\alpha = 2.1$. For extensions smaller than 1mm we observe the distribution to display a dip, which corresponds to the projection of single segments in all direction with no marked preferential direction.

C. Waiting-time distribution

The waiting time distribution between snap-off events is calculated to probe the system for temporal correlations. We observe in Fig.7 the function to have a power-law like behavior $T_w^{-\alpha}$ over the short time region with an exponent of $\alpha = 1.7$. If the generation of snap-off events are uncorrelated the waiting times between consecutive events are expected to obey a exponential distribution. Such a power-law distribution indicate the presence of temporal *memory*. [16]

D. Network Characterization

Networks are an excellent framework to study complex systems. Hence we transform the set of connected capillary bridges and trapped islands into a graph object. We connect pathways of liquid bridges to trapped islands by a node positioned at its center of mass. Each edge corresponds to the length of a capillary bridge or the distance to its neighboring island of defending fluid. These objects gives us the topology of trapped fluid, as shown in Fig.11. Different colors here represent disconnected subsets of the graph. We observe there to be some vertices with a high *node degree* k, defined as the number of edges incident to a given vertex. These nodes are observed to be the centers of the trapped islands. We also measure the average node degree $\langle k \rangle$ in the system together with the maximum node degree k_{max} ,as displayed in Tab.10. We observe these two quantities to not systematically change with an increasing inclination imposed on the system. The size of the clusters defined in terms of the number of nodes are displayed in Fig. 8.

In order to characterize our transformed system we measure typical measures related to networks. The clustering coefficient C_ν is a measure of the local

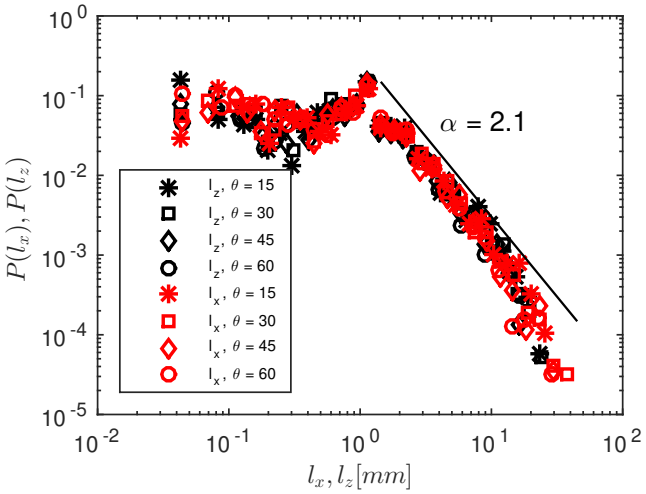

FIG. 6. The spatial extent of the disconnected subsets of the graph was measured both in the direction along the flow direction l_z and transverse to the flow l_x, their distribution are found to be lying on-top of each other.

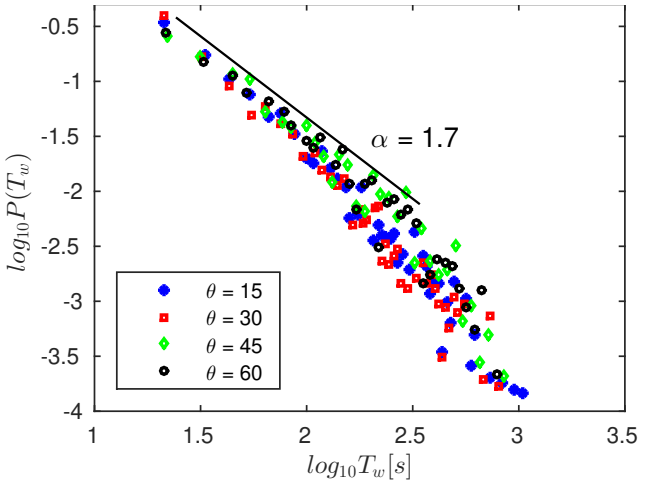

FIG. 7. Waiting-time distribution for successive snap-off events. The solid line has the slope of $\alpha = 1.7$

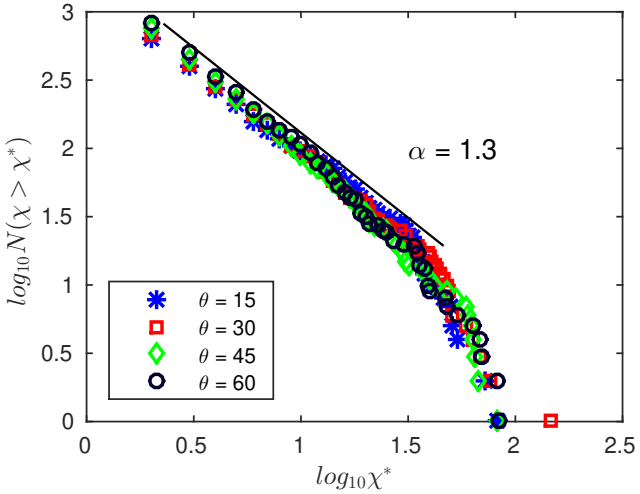

FIG. 8. The cumulative node-size distribution for the disconnected graph subsets.

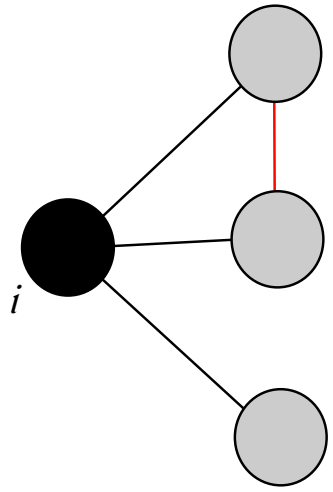

FIG. 9. Here the node i (black node) is connected to its three neighboring nodes, giving it a degree value of $k_i = 3$, further, among the neighboring nodes there is one connection indicated by the red edge, giving $t_i = 1$

connectivity for a given node i, with node degree k_i and t_i number of links between neighbors of node i, see Fig. 9.

$$\langle C \rangle = \frac{1}{N} \sum_{\nu \in G} C_\nu = \frac{1}{N} \sum_{i}^{N} \frac{2t_i}{k_i(k_i - 1)} \qquad (1)$$

Here N is the number of nodes in the graph G. The resulting clustering coefficient is displayed in Table.10. By construction the clustering coefficent is $C_i = 0$ if none of the neighbors of node i are connected, and $C_i = 1$ if all of the neighbors are connected. We can find the global clustering coefficient $\langle C \rangle$ by averaging over the local coefficients. The obtained values are found to rather low, reflecting the fact that fluid pathways created during drainage dont have many alternative paths, making the network prone to *network attacks* in terms of snap-offs.

Efficiency, E is a measure of the range connectivity of a network. [17] defined the efficency of the path between two vertices as the inverse of their distance measured from the graph topology, such that if there is no path connecting i and j, then $d(i, j) = \infty$. In effect making this measure well suited for graphs which are not fully connected. Given all possible paths between nodes i and j the shortest path, d_{ij} , is found based on the smallest number of edges traversed. The efficiency

θ	Nodes	clustering (C_i)	k_{max}	$\langle k \rangle$	Efficiency (E)
15	4011	0.0023	17	1.68	0.0013
30	4240	0.0021	18	1.69	0.0013
45	4246	0.0023	16	1.65	0.0011
60	4630	0.0031	17	1.68	0.0010

FIG. 10. The table shows the calculated measures for the graphs obtained for different inclinations. k_{max} is the node with the highest degree in the graph, similarly $\langle k \rangle$ gives the mean degree in the system.

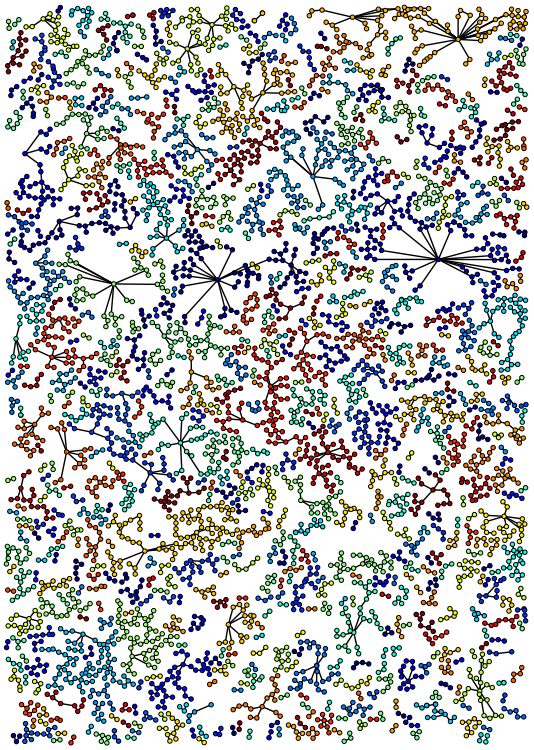

FIG. 11. The graph shows the translated problem of fluid connectivity once the system is fully drained the. The different colors represent disconnected subsets.The network is obtained for an inclination of 60°

can then be defined as [17]

$$E = \frac{1}{N(N-1)} \sum_{i,j} \frac{1}{d_{i,j}} \tag{2}$$

We observe the total number of nodes in the system to increase as the effective gravity increases. This can be understood as; Gravity stabilization forces the front-width to become more spatially limited, which in return reduces the size of the trapped clusters. As more of the pore-space is displaced the trapped clusters shrink in size replacing the area of defending fluid with

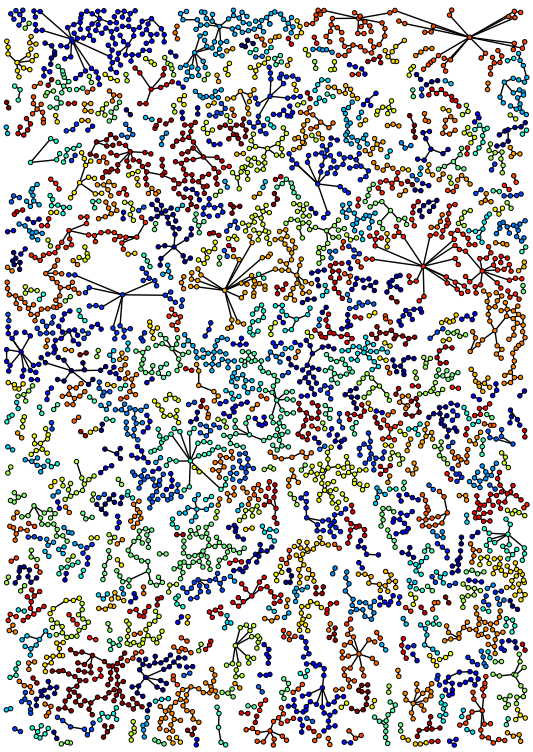

FIG. 12. The graph shows the translated problem of fluid connectivity once the system is fully drained the. The different colors represent disconnected subsets.The network is obtained for an inclination of 45°

area where capillary bridges can be formed. What is less expected is the maximum node degree and the average degree remains more or less constant. One would perhaps expect more trapped area to correspond to more connectivity in term of pathways formed by capillary bridges.

IV. CONCLUDING REMARKS

In this study we have examined the pore-scale mechanism of snap-off. We calculated the snap-off distribution in the reference frame of the mean front position $\bar{z}$. We find it to scale with the front width $\sigma = Bo^{-0.57}$,dependency given by percolation theory. We find the mean life time of capillary bridges that snap-off to be very small compared to the time scale of the experiments. We have further looked at the branching of capillary bridges in the graph framework. This has been used characterize the system by calculating associated measures.

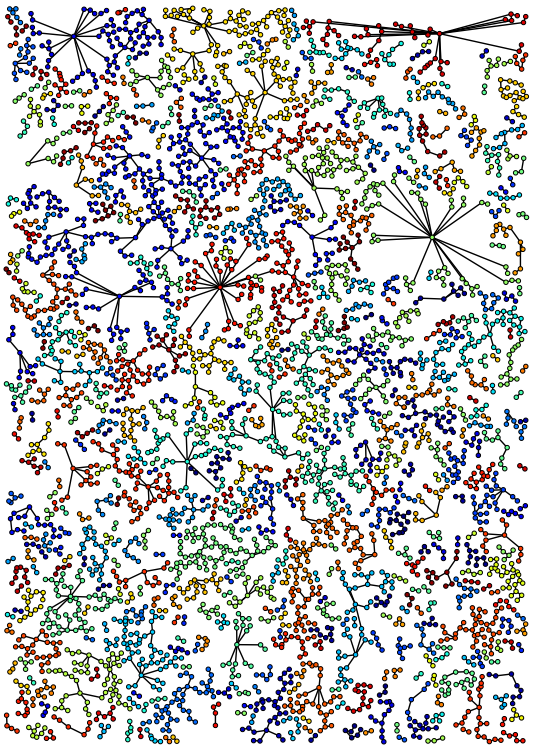

FIG. 13. The graph shows the translated problem of fluid connectivity once the system is fully drained the. The different colors represent disconnected subsets.The network is obtained for an inclination of 30°

ACKNOWLEDGMENTS

We would like to thank the support from the University of Oslo and University of Strasbourg. This work was partly supported by the Research Council of Norway through its Centres of Excellence funding scheme, Project No. 262644 (PoreLab), the LIA France-Norway D-FFRACT, the University of Strasbourg PDI program and the CNRS INSU ALEAS program.

[1] R. Toussaint, K. Måløy, Y. Méheust, G. Løvoll, M. Jankov, G. Schäfer, and J. Schmittbuhl, Vadose Zone Journal **11** (2012), 10.2136/vzj2011.0123.
[2] R. Lenormand, C. Zarcone, and A. Sarr, Journal of Fluid Mechanics **135**, 337 (1983).
[3] K. J. Måløy, J. Feder, and T. Jøssang, Phys. Rev. Lett. **55**, 2688 (1985).
[4] Y. Méheust, G. Løvoll, K. J. Måløy, and J. Schmittbuhl, Phys. Rev. E **66**, 051603 (2002).
[5] G. Løvoll, Y. Méheust, R. Toussaint, J. Schmittbuhl, and K. J. Måløy, Phys. Rev. E **70**, 026301 (2004).
[6] R. Lenormand, Proc. R. Soc. Lond. A **423**, 159 (1989).
[7] G. Løvoll, M. Jankov, K. J. Måløy, R. Toussaint, J. Schmittbuhl, G. Schäfer, and Y. Méheust, Transport in Porous Media **86**, 305 (2011).
[8] R. Lenormand, E. Touboul, and C. Zarcone, Journal of Fluid Mechanics **189**, 165187 (1988).
[9] R. Lenormand and C. Zarcone, Physical review letters **54**, 2226 (1985).
[10] M. Moura, E. G. Flekkø, K. J. Måløy, G. Schäfer, and R. Toussaint, Phys. Rev. Fluids **submitted** (2019).
[11] R. Albert, H. Jeong, and A.-L. Barabasi, Nature **401**, 130 (1999).
[12] C. Andresen, A. Hansen, R. Le Goc, P. Davy, and S. Hope, Frontiers in Physics **1**, 7 (2013).
[13] S. Hope, S. Kundu, C. Roy, S. Manna, and A. Hansen, Frontiers in Physics **3**, 72 (2015).
[14] L. Valentini, D. Perugini, and G. Poli, Physica A: Statistical Mechanics and its Applications **377**, 323 (2007).
[15] A. Birovljev, L. Furuberg, J. Feder, T. Jssang, K. J. Mly, and A. Aharony, Phys. Rev. Lett. **67**, 584 (1991).
[16] S. Santucci, K. T. Tallakstad, L. Angheluta, L. Laurson, R. Toussaint, and K. J. Mly, Philosophical Transactions of the Royal Society A: Mathematical, Physical and Engineering Sciences **377**, 20170394 (2019).
[17] V. Latora and M. Marchiori, Phys. Rev. Lett. **87**, 198701 (2001).

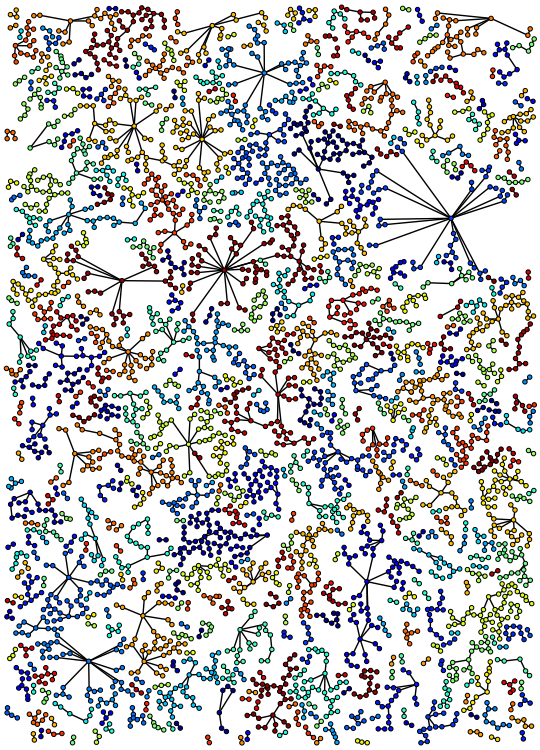

FIG. 14. The graph shows the translated problem of fluid connectivity once the system is fully drained the. The different colors represent disconnected subsets.The network is obtained for an inclination of 15°

Paper 4: Frictional fluid dynamics and plug formation in multiphase millifluidic flow

Frictional Fluid Dynamics and Plug Formation in Multiphase Millifluidic Flow

Guillaume Dumazer,[1] Bjørnar Sandnes,[2,*] Monem Ayaz,[1] Knut Jørgen Måløy,[1] and Eirik Grude Flekkøy[1]
[1]Department of Physics, University of Oslo, P.O. Box 1048 Blindern Oslo, Norway
[2]College of Engineering, Swansea University, Bay Campus, Swansea SA1 8EN, United Kingdom
(Received 10 March 2016; published 7 July 2016)

We study experimentally the flow and patterning of a granular suspension displaced by air inside a narrow tube. The invading air-liquid interface accumulates a plug of granular material that clogs the tube due to friction with the confining walls. The gas percolates through the static plug once the gas pressure exceeds the pore capillary entry pressure of the packed grains, and a moving accumulation front is reestablished at the far side of the plug. The process repeats, such that the advancing interface leaves a trail of plugs in its wake. Further, we show that the system undergoes a fluidization transition—and complete evacuation of the granular suspension—when the liquid withdrawal rate increases beyond a critical value. An analytical model of the stability condition for the granular accumulation predicts the flow regime.

DOI: 10.1103/PhysRevLett.117.028002

Complex multiphase flows in channels and tubes occur in a range of geophysical, biological, and engineered processes. Examples include transport of blood cells suspended in plasma through the cardiovascular network [1,2], conveying of powders and granular materials in civil and chemical engineering [3,4], and transport of oil, gas, and sand through sub-sea pipelines [5]. Even the simple case of two-phase air and water flow through tubes and capillaries displays complex flow behavior, with commonly observed transitions between stratified, bubbly, slug, and annular flow depending on the flow rates of the respective phases [6–8]. Hydraulic and pneumatic conveying of particulates and granular materials similarly show a range of flow regimes ranging from bed load, to slug flow, and dilute flow depending on granular loading and fluid flow rate [3,9–13].

The flow of dense granular suspensions has proved challenging to characterize due in part to the frictional contact interactions between grains, and between grains and the confining boundaries. Examples of complex flow behavior associated with frictional fluid dynamics include shear thinning, shear thickening, shear banding, plug growth, and normal stresses [14–18]. Several factors need to be taken into account in order to describe the rheology of dense granular suspensions corresponding to vanishing values for viscous and inertial numbers [16,19]. The extended contact time between particles introduces Coulomb friction as a dominating dissipation mechanism [15,17]. Gravity has been shown to play an important part in inducing granular contact dynamics below close packing densities, leading to system spanning contact networks and yield stresses [14].

Discontinuous shear thickening (DST), where increased shear rate causes a sudden jump in the stress producing solidlike behavior is a striking example of complex frictional fluid dynamics. Recent studies have pointed to both frictional contact dynamics as well as dilation and confinement as the dominating mechanisms for DST [17,18,20]. Dilation is the expansion of the granular packing due to shear, which, when confined by system boundaries, causes additional normal stress and friction.

The role of the confining geometry is therefore of fundamental importance in governing the frictional fluid flow behavior at the point where system-spanning contact networks emerge. These grain-grain contact networks mediate imposed stresses through force chains within the packing [20,21], amplifying the stresses on the boundaries, leading to nonlinear frictional responses [22,23]. The flow dynamics of granular particles approaching the jamming transition can be described by nonlocal rheological effects in part due to the confinement [24,25]. In experimental systems, the boundaries are often the confining plates of a rheometer or a flow cell, or the solid walls of a tube. Note, however, that in the case of multiphase flows, the meniscus between immiscible fluids constitutes another type of system boundary. Here the capillary forces acting at the fluid-fluid-grain contact lines impose confining stresses on the granular phase [26].

It is therefore perhaps not surprising to find that multiphase granular or frictional flow in confined geometries are a rich source of spectacular flow instabilities and pattern formation processes. For the case of granular suspension flow in 2D Hele-Shaw geometries these include viscous fingers in granular suspensions [27,28], labyrinths and frictional fingers [26,29,30], stick-slip gas bubbles [30–32], and gas driven fracturing in saturated granular packings [28,30,33–38]. The complexity of flow behavior stems from the variety of forces at play (pressure, viscous, capillary, frictional, and gravitational) in addition to effects associated with the confining geometry and inherent system disorder.

Here we focus on a simple model system of confined, multiphase frictional flow: a 1.0 m long glass tube filled with a mixture of glass beads and water, where the tube diameter ($D = 2.0$ mm) is close to the capillary length of

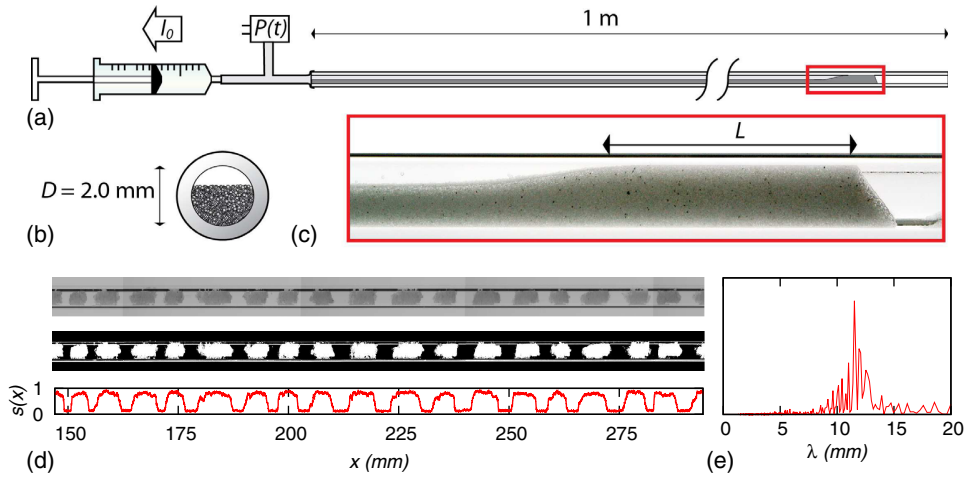

FIG. 1. (a) Schematic of the experimental setup. A syringe pump withdraws water at constant rate I_0 from a horizontal glass tube initially filled with a mixture of water and sedimented grains. Liquid pressure is measured at the tube outlet. (b) Schematic of the tube's intial cross section, and (c) close-up of accumulation front shortly after start of withdrawal. (d) Granular plugs obtained after drainage at low withdrawal rate (top), same picture after thresholding showing granular matter in white (middle), and normalized filling fraction parameter $s(x)$ estimating the density of granular matter from the thresholded picture (bottom). (e) Spatial power spectral density obtained for the signal $s(x)$ as a function of the inverse spatial frequency λ.($I_0 = 0.1$ mL $\cdot$ min^{-1}, $\varphi \approx 0.5$, $d = [150\text{–}200]$ μm).

the liquid. The granular material settles out of suspension, and the gas invasion dynamic is governed in part by the Coulomb friction associated with granular accumulation fronts ahead of the meniscus [23,29]. We show that capillary and frictional forces combine to produce a characteristic flow pattern whereby plugs of grains are shed by the moving interface, and that the system undergoes a transition from frictional to viscous flow as the flow rate increases.

Figure 1(a) illustrates the experiment: A syringe pump withdraws water at a controlled flow rate I_0 from one end of the horizontal tube, driving invasion of air at atmospheric pressure from the opposite open end. The glass beads form a uniform sedimented layer along the tube with well-defined granular filling fraction $\varphi = \phi_0/\phi_c$, where ϕ_0 is the volume fraction of grains in the grain-water mixture, and ϕ_c corresponds to random close packing in the sedimented layer. φ thus corresponds to the fraction of the tube cross-sectional area taken up by the layer of grains [Fig. 1(b)]. The experiment is imaged against a LED screen, and variations in illumination intensity are corrected by subtracting a reference image. Figure 1(c) shows a close-up of a granular accumulation front, and Fig. 1(d) shows an example of the trail of granular plugs left behind the invading meniscus after the tube is fully drained. Images are thresholded to isolate the granular fraction, and the filling fraction is measured by a normalized variable $s(x,t)$ such that $s = 1$ and 0 for a fully packed and empty tube, respectively, and $s(x, t = 0) = s_0$ corresponds to the initial filling height.

The spatial structure obtained is analyzed with the power spectral density of $s(x)$; see Fig. 1(e). The power spectrum maximum gives a scale $\lambda_0 \simeq 11.5$ mm, and corresponds to the averaged spatial period $\langle L_{\text{plug}} + L_{\text{gap}} \rangle$ of one plug and one gap. The average plug size measured after smoothing the function $s(x)$ gives $\langle L_{\text{plug}} \rangle \approx 5.9$ mm which is consistent with the maximum $\lambda_0 \approx 2\langle L_{\text{plug}} \rangle$ corresponding to an initial filling fraction $\varphi \approx 0.5$.

At a slow withdrawal rate, the viscous pressure drop along the tube is small, such that the pressure imposed by the pump is mainly balanced by the capillary pressure at the gas-liquid-grain interface. As the invading meniscus meets the granular bed, capillary forces act to sweep the grains along, and an accumulation front develops ahead of the interface as seen in Fig. 1(c). Inside the front, stress is transferred through grain-grain contacts, and a portion of the horizontally imposed stress is redirected towards the confining boundaries of the tube. We adopt a Janssen stress distribution model where the redirected stress σ_r is proportional to the applied horizontal stress σ_h, $\sigma_r = K\sigma_h$, where K is the Janssen coefficient [22,23,29]. The gas pressure P required to move the accumulation front increases exponentially with the front length L:

$$P \approx \sigma_0(\varphi, \mu, K) \exp(4\mu K L/D), \tag{1}$$

where μ is the static friction coefficient and the prefactor σ_0 is a function of filling fraction and the frictional properties of the granular material [23,29,39].

Figure 2(a) shows close-up images at different stages of formation of a single plug, with Fig. 2(b) representing a spatiotemporal diagram of the filling fraction parameter $s(x,t)$, where time develops from top to bottom. The unperturbed initial sedimented state corresponds to intermediate values of s (gray, upper left). The bright area illustrates the motion of the accumulation front, and the

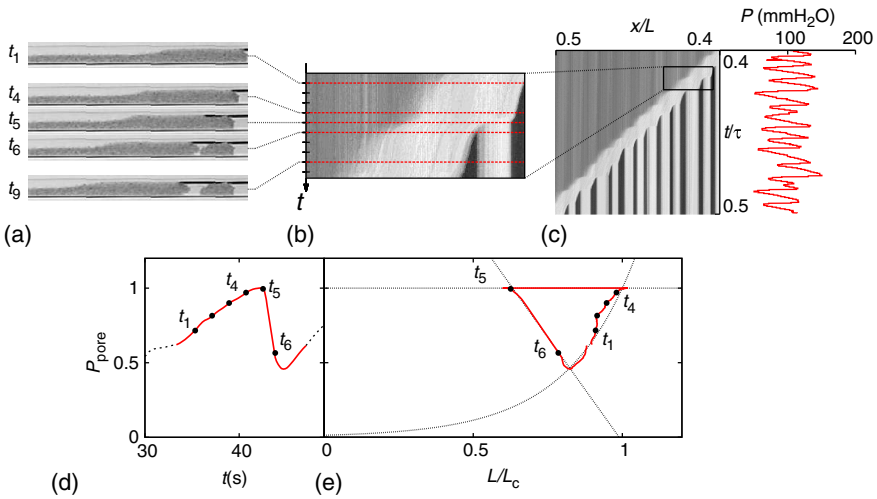

FIG. 2. Plug formation for $I_0 = 0.3$ mL $\cdot$ min^{-1}, $\varphi = 0.5$, and $d = [200–300]$ μm. (a) Images and (b) spatiotemporal diagram $s(x, t)$ of the formation of a single plug: slow compaction (t_1–t_4); rapid air percolation with plug splitting (t_4–t_5); viscous slip (t_5–t_6); and the next slow compaction ($t > t_6$). (c) A full $s(x, t)$ diagram over several plug formation cycles with corresponding measured liquid pressure. The pressure increases gradually during the slow compaction phase, then drops rapidly during the slip phase. (d) and (e) Pressure as a function of time and plug length, respectively, for a single plug formation corresponding to (a) and (b). Conceptual trajectory according to Eqs. (1) and (2) (dotted line) plotted together with measured pressure and front length (red line, data markers).

plug formation corresponds to the appearance of a vertical, static column flanked by dark zones corresponding to empty tube sections. The system cycles through repeated plug forming events where the moving interface sheds a series of plugs separated by gaps as illustrated in the full spatiotemporal diagram in Fig. 2(c). The interface travels from right to left, and the diagonal outlines the progression of the interface whose speed is given by the slope $\Delta X/\Delta t \propto [4/(\pi D^2)]\Delta V/\Delta t$ determined by the pumping rate $I_0 = \Delta V/\Delta t$, ΔV being the volume withdrawn from the tube during the time interval Δt. The plugs form in an intermittent, stick-slip fashion as evident from the sawtooth pressure curve [Fig. 2(c)], indicating that the dynamics is dominated by frictional interactions.

Figure 2(d) shows the pressure evolution during the formation of the plug depicted in Fig. 2(a), with a corresponding trajectory of pressure versus plug length illustrated in Fig. 2(e). The period t_1 to t_4 corresponds to the slow accumulation or compaction phase where the pressure increases according to Eq. (1). As the accumulation front grows to a critical length L_c, the gas pressure reaches the capillary pore throat pressure, $P_{\text{pore}} \propto \gamma/d$, and the meniscus begins to invade the pore space between the grains. γ is the liquid-air interfacial tension, and we assume that typical pore sizes are proportional to average bead diameter d. Air percolates relatively quickly through the packing (t_4 to t_5), giving rise to a Darcy flow of the displaced water. The flow acts to destabilize the packing, and the plug splits, leaving behind the percolated section as a static plug (t_5).

The meniscus now moves quickly, driven by release of elastic energy stored in the system due to the underpressure in the liquid, and the fluidized granular front grows linearly with decreasing pressure (t_5 to t_6). The decreasing slope $\Delta P/\Delta L$ is given by the system's compressiblity, $\beta V_0 = -\Delta V/\Delta P$, where V_0 is the total system volume. Together with the granular material mass balance as sedimented grains accumulate onto the granular front, $\phi_c \Delta L = \phi_0(\Delta L + \Delta X)$, this gives

$$\frac{\Delta P}{\Delta L} = -\frac{\pi D^2}{4\beta V_0}\frac{\phi_c - \phi_0}{\phi_0}. \tag{2}$$

The motion comes to a halt when the pressure is fully relaxed, and a new cycle of pressure increase and slow accumulation ensues.

Figure 3 illustrates the flow dynamics over 5 orders of magnitude of the withdrawal rate I_0. So far we have considered the slow withdrawal regime where the dynamics is governed by frictional forces ($I_0 \leq 0.1$ mL $\cdot$ min^{-1}). A transitional regime with larger granular fronts and fewer plugs occurs as the withdrawing rate increases ($0.3 \leq I_0 \leq 1$ mL $\cdot$ min^{-1}). The larger pumping rate increases the viscous forces on the granular material. The granular suspension forms a larger fluidized accumulation front, and the shedding of plugs becomes irregular and infrequent.

Increasing the pumping rate beyond $I_0 \geq 3$ mL $\cdot$ min^{-1} results in a suspended granular phase along the entire length of the tube, and a full evacuation of the granular mixture with no plug formation. The viscous forces dominate the transport regime and no frictional grain-grain contacts have time to form in the fluidized material. Propagating fluctuations of the suspension density explain shades of light levels in the

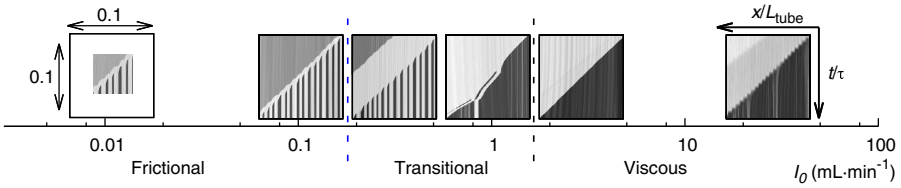

FIG. 3. Spatiotemporal $s(x,t)$ diagrams obtained for different withdrawal rates $I_0 \in [0.01, 30]$ mL $\cdot$ min^{-1}. (Grain size $d = [75, 100]$ μm and $\varphi = 0.50 \pm 0.05$ for all experiments). The diagrams feature reduced units x/L_{tube} and t/τ with $\tau = L_{\text{tube}}\pi D^2/(4I_0)$, and display a tenth of the tube's length, $L_{\text{tube}}/10$, i.e., a total recording time $\tau/10$, so that enough details are captured. At $I_0 = 0.01$ mL $\cdot$ min^{-1} the recording time was limited to 0.065τ. The dashed lines demarcate the boundaries between frictional, transitional, and viscous flow regimes.

fluidized granular material that can be observed in the $s(x,t)$ diagrams for $I_0 \geq 3$ mL $\cdot$ min^{-1}.

A stability condition for a granular front of plug length L_{plug} can be derived considering a balance between the competing frictional and viscous forces, where the transition from frictional to viscous dynamics upon increased I_0 occurs once the viscous drag exceeds the frictional resistance that must be overcome to move the plug. The fluid pressure due to Darcy flow is

$$\delta P_{\text{visc}} = \frac{\eta}{k}\frac{4I_0}{\pi D^2} L_{\text{plug}}, \tag{3}$$

where η is the liquid viscosity and the permeability k can be related to average grain size using the Kozeny-Carman equation, $k = (d^2/180)(1-\phi_c)^3/\phi_c^2$.

The gravitationally induced frictional stress associated with an accumulation front of length L_{plug} is given by Eq. (1). The prefactor σ_0 can be expressed as

$$\sigma_0 = D\phi_c \Delta\rho g \left((1 + \cos^2\theta\varphi^2)\frac{\mu}{\tan\theta} + \frac{1}{4K} \right), \tag{4}$$

where we have used the expression derived in Ref. [23] adapted for cylindrical confinement [39]. The frictional stress is an increasing function of the filling fraction φ and granular friction μ, θ being the angle of repose, and $\Delta\rho$ the density contrast between grains and liquid.

Plug formation is prevented when fluid forces exceed frictional stress in the plugs. We define a dimensionless number as the ratio between viscous and frictional forces: $N = \delta P_{\text{visc}}/\delta P_{\text{fric}}$ such that $N = 1$ marks the transition between plug formation and a fluidized packing. Rearranging Eqs. (1), (3), and (4), we get the following transition flow rate:

$$I_{0,N=1} = \frac{k\pi D^2}{4\eta L_{\text{plug}}}\sigma_0 \exp(4\mu K L/D), \tag{5}$$

where the permeability $k \propto d^2$.

The exploration of pumping rates $I_0 \in [0.01\text{–}30]$ mL$\cdot$min^{-1} and bead sizes $d \in [50 - 300]$ μm, shows a frictional regime at low pumping rates and large bead sizes, and a viscous regime at large pumping rates and small bead sizes as shown in the phase diagram in Fig. 4. The transition flow rate $I_{0,N=1}$ (5) is plotted together with the experimental results (blue dashed line). The model matches the data well considering the simplistic assumptions. The model assumes maximum friction in jammed plugs, which can be considered as an upper limit, and explains the higher transitional flow rates predicted than observed experimentally.

In conclusion, we have demonstrated that three-phase gas-liquid-grain flow in narrow tubes produce complex flow patterns due to the interaction between capillary, frictional, and viscous forces. The formation of granular plugs at low flow rate is governed by frictional stress associated with grain-grain and grain-tube contacts. The plug formation cycles through three stages: slow compaction, pore invasion, and viscous slip. Increasing the flow rate results in viscous forces fluidizing the packing, and a transition to suspension flow is observed. Reducing the

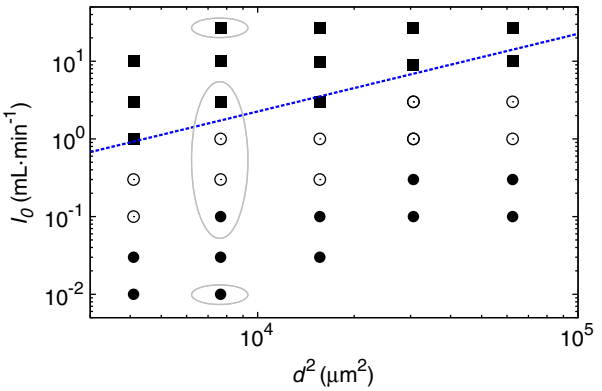

FIG. 4. Phase diagram of I_0 plotted against d^2 featuring the different granular transport regimes observed: Viscous suspension flow (solid squares), frictional plug formation (solid circles), and a transitional regime (open circles). Glass beads were sieved to the following size ranges: [53–75], [75–100], [100–150], [150–200], and [200–300] μm, with pumping rates ranging from 0.01–30 mL $\cdot$ min^{-1}. Encircled markers correspond to observations in Fig. 3. The blue dashed line represents the theoretical transition flow rate $I_{0,N=1}$ [Eq. (5)] where we have used $L_{\text{plug}} = 5.9$ mm [Fig. 1(e)], $\mu = 0.47$ [29], $K = 0.6$ [23], $\theta = 25°$, $\phi_c = 0.6$, $\Delta\rho = 1.463 \times 10^3$ kg m^{-3}.

grain size leads to lower permeability and increased fluid pressure on the grains, thus lowering the flow rates required to bring on the transition from frictional to viscous dynamics.

Our results provide new insight into how frictional interactions and competing forces lead to the emergence of complex flow patterning in multiphase flows. The experiment represents a quasi 1D representation of a larger family of flow patterning dynamics occurring in 2D Hele-Shaw flows [26–38], where a similar fluidization transition is observed [30], and where stick-slip bubbles [30,31] are analogues to the plug formation observed in the 1D tube system.

The authors thank Benjy Marks, Jon Alm Eriksen, and Renaud Toussaint for discussions. The work was supported by the Norwegian Research Council through the FRINAT Grant No. 213462/F20. B. S. acknowledges support from EPSRC Grant No. EP/L013177/1 and Sêr Cymru National Research Network in Advanced Engineering and Materials Grant No. NRN141.

*Corresponding author.
b.sandnes@swansea.ac.uk

[1] D. Gidaspow and J. Huang, Ann. Biomed. Eng. **37**, 1534 (2009).
[2] J. B. Freund and M. M. Orescanin, J. Fluid Mech. **671**, 466 (2011).
[3] O. Molerus, Powder Technol. **88**, 309 (1996).
[4] F. B. Soeypan, S. Cremaschi, C. Sarica, H. J. Subramani, and G. E. Kouba, AlChE J. **60**, 76 (2014).
[5] J. Tronvoll and E. Fjær, Int. J. Rock Mech. Min. Sci. Geomech. Abstr. **31**, 393 (1994).
[6] k. A. Triplett, S. M. Ghiaasiaan, S. I. Abdel-Khalik, and D. L. Sadowski, Int. J. Multiphase Flow **25**, 377 (1999).
[7] M. Suo and P. Griffith, J. Basic Eng. **86**, 576 (1964).
[8] L. Cueto-Felgueroso and R. Juanes, Phys. Rev. Lett. **108**, 144502 (2012).
[9] M. Houssais, C. P. Ortiz, D. J. Durian, and D. J. Jerolmack, Nat. Commun. **6**, 6527 (2015).
[10] M. Strauss, S. McNamara, and H. J. Herrmann, Granular Matter **9**, 35 (2007).
[11] C.-Y. Wen and H. P. Simons, AIChE J. **5**, 263 (1959).
[12] J. E. Hilton and P. W. Cleary, Chem. Eng. Sci. **66**, 231 (2011).
[13] O. Durán, B. Andreotti, and P. Claudin, Phys. Fluids **24**, 103306 (2012).
[14] A. Fall, F. Bertrand, G. Ovarlez, and D. Bonn, Phys. Rev. Lett. **103**, 178301 (2009).
[15] R. Blumenfeld, S. F. Edwards, and M. Schwartz, Eur. Phys. J. E **32**, 333 (2010).
[16] F. Boyer, E. Guazzelli, and O. Pouliquen, Phys. Rev. Lett. **107**, 188301 (2011).
[17] R. Seto, R. Mari, J. F. Morris, and M. M. Denn, Phys. Rev. Lett. **111**, 218301 (2013).
[18] E. Brown and H. M. Jaeger, Rep. Prog. Phys. **77**, 046602 (2014).
[19] M. Trulsson, B. Andreotti, and P. Claudin, Phys. Rev. Lett. **109**, 118305 (2012).
[20] E. Lerner, G. Düring, and M. Wyart, Proc. Natl. Acad. Sci. U.S.A. **109**, 4798 (2012).
[21] T. S. Majmudar and R. P. Behringer, Nature (London) **435**, 1079 (2005).
[22] H. A. Janssen, Z. Ver. Dtsch. Ing. **39**, 1045 (1895).
[23] B. Marks, B. Sandnes, G. Dumazer, J. A. Eriksen, and K. J. Måløy, Front. Phys. **3**, 41 (2015).
[24] O. Pouliquen and Y. Forterre, Phil. Trans. R. Soc. A **367**, 5091 (2009).
[25] P. G. Rognon, T. Miller, B. Metzger, and I. Einav, J. Fluid Mech. **764**, 171 (2015).
[26] B. Sandnes, H. A. Knudsen, K. J. Måløy, and E. G. Flekkøy, Phys. Rev. Lett. **99**, 038001 (2007).
[27] C. Chevalier, A. Lindner, and E. Clément, Phys. Rev. Lett. **99**, 174501 (2007).
[28] C. Chevalier, A. Lindner, M. Leroux, and E. Clément, J. NonNewton. Fluid **158**, 63 (2009).
[29] H. A. Knudsen, B. Sandnes, E. G. Flekkøy, and K. J. Måløy, Phys. Rev. E **77**, 021301 (2008).
[30] B. Sandnes, E. G. Flekkøy, H. A. Knudsen, K. J. Måløy, and H. See, Nat. Commun. **2**, 288 (2011).
[31] B. Sandnes, E. G. Flekkøy, and K. J. Måløy, Eur. Phys. J. Spec. Top. **204**, 19 (2012).
[32] J. A. Eriksen, B. Marks, B. Sandnes, and R. Toussaint, Phys. Rev. E **91**, 052204 (2015).
[33] R. Holtzman and R. Juanes, Phys. Rev. E **82**, 046305 (2010).
[34] F. Stauffer, X.-Z. Kong, and W. Kinzelbach, Adv. Water Resour. **32**, 1180 (2009).
[35] G. Varas, V. Vidal, and J.-C. Geminard, Phys. Rev. E **83**, 011302 (2011).
[36] R. Holtzman, M. L. Szulczewski, and R. Juanes, Phys. Rev. Lett. **108**, 264504 (2012).
[37] A. Islam, S. Chevalier, I. B. Salem, Y. Bernabe, R. Juanes, and M. Sassi, Int. J. Multiphase Flow **58**, 279 (2014).
[38] J. Oppenheimer, A. C. Rust, K. V. Cashman, and B. Sandnes, Front. Phys. **3**, 60 (2015).
[39] See Supplemental Material at http://link.aps.org/supplemental/10.1103/PhysRevLett.117.028002 for detailed derivation of the frictional stress.

Paper 5: Self-Structuring of granular material under capillary bulldozing

EPJ Web of Conferences **140**, 09016 (2017) DOI: 10.1051/epjconf/201714009016
Powders & Grains 2017

Self-Structuring of Granular material under Capillary Bulldozing

Guillaume Dumazer[1,⋆], *Bjørnar* Sandnes[2], *Monem* Ayaz[1,3], *Knut Jørgen* Måløy[1], and *Eirik* Flekkøy[1]

[1] *Physics Department, University of Oslo, P. O. Box 1048 Blindern Oslo, Norway*
[2] *College of Engineering, Swansea University, Bay Campus, Swansea SA1 8EN, UK*
[3] *Institut de Physique du Globe de Strasbourg, Université de Strasbourg/EOST, CNRS, 5 rue Descartes, F67084 Strasbourg Cedex, France*

Abstract. An experimental observation of the structuring of a granular suspension under the progress of a gas/liquid meniscus in a narrow tube is reported here. The granular material is moved and compactifies as a growing accumulation front. The frictional interaction with the confining walls increases until the pore capillary entry pressure is reached. The gas then penetrates the clogged granular packing and a further accumulation front is formed at the far side of the plug. This cyclic process continues until the gas/liquid interface reaches the tube's outlet, leaving a trail of plugs in the tube. Such 1D pattern formation belongs to a larger family of patterning dynamics observed in 2D Hele-Shaw geometry. The cylindrical geometry considered here provides an ideal case for a theoretical modelling for forced granular matter oscillating between a long frictional phase and a sudden viscous fluidization.

1 Introduction

Transport of oil, water and sand in sub-sea pipelines [1], of blood cells suspended in plasma [2, 3] give two extreme examples of the broad range of situations featuring the multiphase transport of granular material in confined geometries. Pneumatic transport offers a well established field for the transport of granular particles immersed in a single phase [4]. Such a two phase system shows a broad range of flow regimes depending on the filling fraction and flow rate. Plug flow, fluidized flow, bubbly flow, turbulent fluidization, cluster flow, annular flow and suspended flow gives the variety of flow regimes in vertical pneumatic conveying [5]. Such observed flow regimes involve the competing effects of viscosity and friction [6–8], respectively destabilizing and stabilizing the granular phase.

The case of dense granular suspension has recently been actively studied as it features complex rheological behaviour such as shear thinning, shear thickening, yield stress and shear banding [9–12]. The frictional interaction and contact time between granular particle and the viscous interaction with the carrying fluid are the two factors determining the behaviour of dense suspensions. The geometrical confinement is then another key factor as it produces extra frictional forces on the granular flow. The frictional interaction with boundaries induces contacts network spanning over a large part of the system.

In multiphase flows, the existence of one or several meniscii introduce capillary forces as a third factor. Consequently such flows provide a rich source of instabilities and pattern formation processes [13–15].

To simplify the geometrical complexity, we observed the progress of a gas/liquid meniscus along a tube filled with sedimented granular mixture of liquid and glass beads [16]. The confinement chosen is approaching a one-dimensional geometry. We are reporting here the response of a confined granular material under capillary bulldozing.

2 Materials and Methods

A long horizontal tube of size $L = 1.0$ m with constant diameter $D = 2$ mm is filled with a sedimented mixture of liquid and glass beads, with reduced filling fraction $\varphi = \phi_0/\phi_c$, defined as the ratio between the volume fraction ϕ_0 of grains in the grain-water mixture, and the random close packing ϕ_c. Glass beads are sieved to control the polydispersity. The tube is pumped at constant withdrawing rate I_0 and the pressure at the tube's outlet is recorded, see Fig. 1 (a). The tube's diameter is chosen to not exceed the capillary length of the liquid used, ensuring that the meniscus fills the tube's aperture, without spreading along the tube, see Fig. 1 (b). The inner surface of the tube were treated with a silanization solution to achieve an hydrophobic coating ensuring a contact angle $\geq 90^o$ between the meniscus and the confining walls. The experiment is imaged against an LED screen. At the early stages of the withdrawing, the meniscus progresses along the tube, perturbs the sedimented granular material, see Fig. 1 (b), and forms a growing accumulation front, see Fig. 1 (c). At slow withdrawing rates the capillary

⋆e-mail: guillaume.dumazer@fys.uio.no

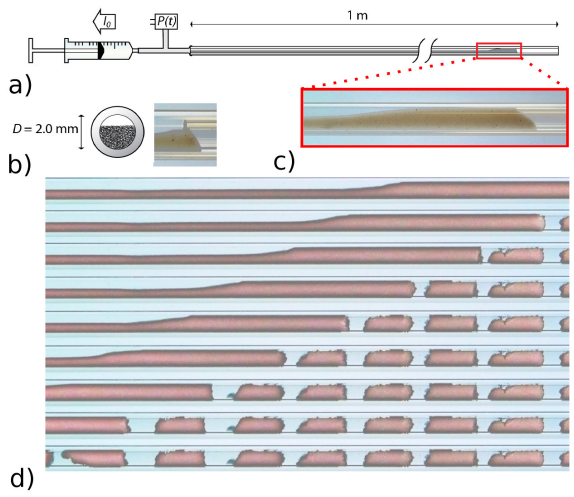

Figure 1. (a) Schematic view of the experimental setup. The sedimented glass beads and liquid mixture is withdrawn by a syringe pump at constant withdrawing rate I_0, withdrawing pressure is recorded at the tube's outlet. (b) (left) initial cross-section schematics, and (right) zoom over the meniscus just after the withdrawing starts. (c) accumulation front after start of withdrawal. (d) series of pictures showing the accumulation front progress, and the trail of plugs left behind, time develops downwards.

bulldozing leads to the intermittent splitting of the growing accumulation front, and a series of granular plugs are left in the tube, see Fig. 1 (d).

3 Plus Formation

The formation of a single plug is imaged after correcting the variations of illumination by subtracting a blank image of the screen, see Fig. 2 (a). Images are then thresholded to clearly distinguish the glass beads from the background. The number of glass beads' pixels are counted as a function of tube's axis x. Repeating this operation for every image recorded during the experiment we get a dimensionless signal $s(x,t)$ with 0 value for no glass beads, 1 value for a fully filled tube's cross-section, s_0 value for unperturbed sedimented glass beads. By mapping $s(x,t)$ with a colorscale on a spatio-temporal diagram with time developing downwards, and tube's axis horizontally, we get a useful visualization of a single plug formation, see Fig. 2 (b). The formation of a single plug can be decomposed into 4 steps: (i) driven by the syringe pump the meniscus progresses against the sedimented grains which slowly compactifies into a growing accumulation front (t_1, t_2). The frictional interaction between the granular material and the confining wall increases. The Janssen's description of stress in confined granular material [14, 17, 18] suggests here an exponential increase of the pressure with the accumulation front length $P \approx \sigma_0(\varphi, \mu, D) \exp(L/\lambda)$. In this description a slice of compacted granular material is considered. The radial stress σ_{rr} normal to the cylindrical confining walls is assumed to be proportional to the longitudinal stress σ_{xx}, $\sigma_{rr} = K\sigma_{xx}$ with the Janssen's coefficient K. The frictional length $\lambda = D/(4\mu K)$ is derived from the force balance over the slice of granular material. (ii) the pressure imposed by the syringe pump reaches the pore pressure of the compacted granular material, $P_{pore} = 4\gamma/d_{pore}$ with the surface tension γ, allowing the meniscus to bend into interstitial pores of diameter d_{pore}. Air quickly percolates through the compacted glass beads and the liquid is pushed away towards the tube's outlet (t_3, t_4). The rapid liquid flow can be considered as a Darcy flow. The viscous forces acting on the compacted grains counteract the frictional interactions, which eventually leads to destabilize the still-immersed packing, and to split the drained glass beads which forms a plug (t_4). (iii) the elastic energy stored in the system during the slow compaction phase is released and the accumulation front rapidly grows (t_4, t_5) before settling down as the next slow compaction phase starts (t_5, t_6). This cycling process is repeated until the meniscus reaches the tube's outlet. The intermittent nature of the plugs formation can be seen from the spatio-temporal diagram obtained over a larger fraction of the tube, see Fig. 3 left for the smallest withdrawing rates.

4 Flow Regimes

The formation of plugs corresponds to an instability resulting from the competition between frictional and viscous forces. At low withdrawing rates the granular material settles easily and frictional forces can be established among granular particles as well as with the confining walls. Increasing the withdrawing rate corresponds to increasing the viscous forces in the system. Viscous drag on particles prevent frictional interactions to be established and the granular packing gets fluidized more easily. We observed the various behaviours of the confined glass beads for larger values of withdrawing rates $I_0 \in [0.01, 30]$ mL.min^{-1}, and reported in Fig. 3 the corresponding spatio-temporal diagrams obtained. As the withdrawing rate is lower than ≈ 0.3 mL.min^{-1} the frictional forces are large enough to form the pattern of granular plugs separated by gaps. Larger withdrawing rate, $I_0 \in [0.3, 3]$ mL.min^{-1} weakens frictional interactions. The accumulation front is getting larger as stronger fluidizations occur, and fewer plugs are formed. Another flow regime is obtained for large flow rate $I_0 \leq 3$ mL.min^{-1}. The viscous forces dominates and prevent any frictional interactions between grains. Glass beads get suspended and no plugs are left in the tube. These three distinct regimes are denoted respectively the frictional, transitional and viscous flow regimes.

5 Phase Diagram

The size of the glass beads influences the balance between friction and visosity. Small glass beads get easily suspended whereas large glass beads are more stable under viscous flow. The viscous drag of a flow through a porous media is indeed proportional to its permeability. A bed

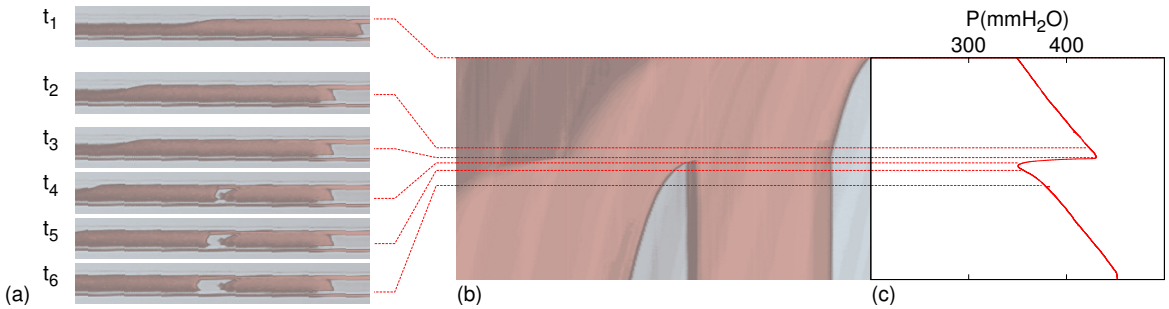

Figure 2. Focus over one plug formation obtained for $I_0 = 0.01$ mL.min^{-1}, filling fraction $\varphi = 0.5$, beads size $d = [75 - 100]$ μm illustrated by (a) images and (b) spatio-temporal diagram. (c) pressure measured at the tube's outlet in mmH$_2$O during the plug formation.

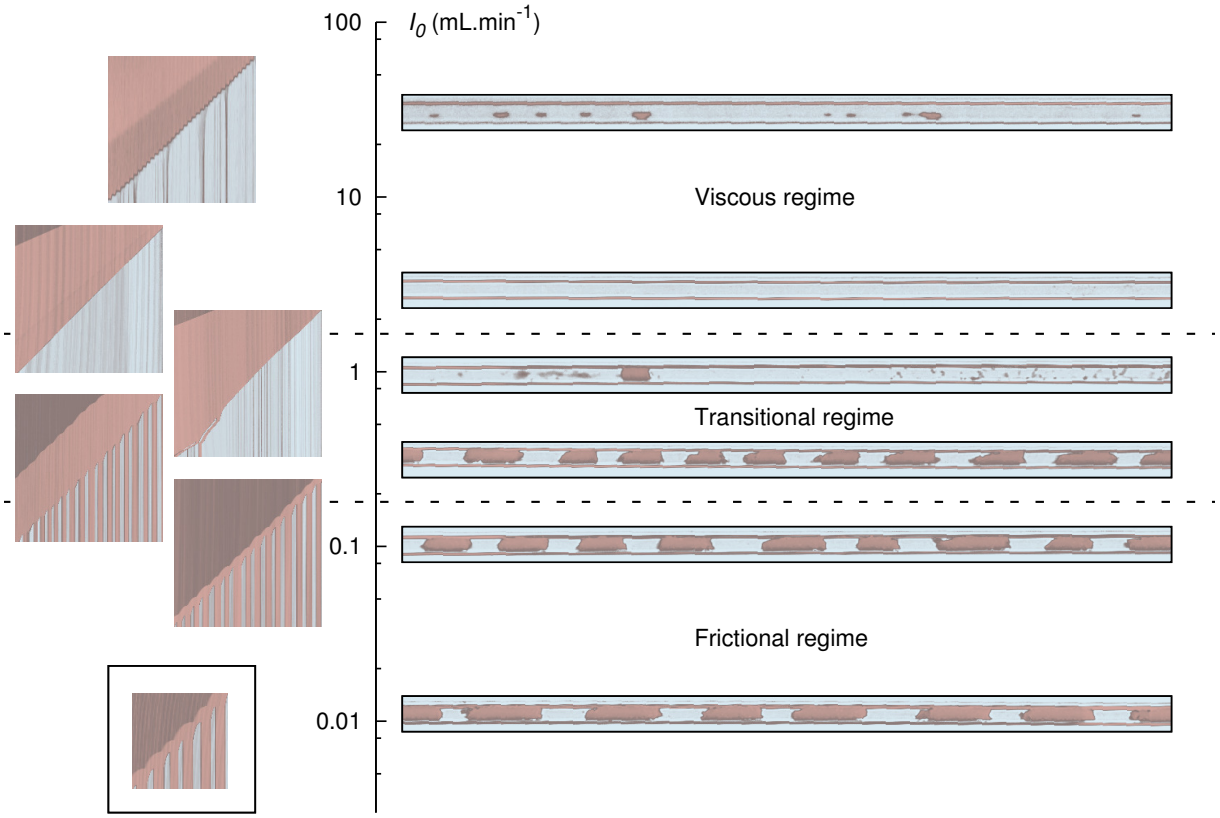

Figure 3. (left column) spatio-temoral diagrams obtained with withdrawing rate increase in the range [0.01 – 30] mL.min−1. The reduced units correspond here to a fraction of the total withdrawing time τ required to empty the tube of size L at withdrawing rate I_0. The same filling fraction $\varphi = 0.5$ and beads size $d = [75, 100]$ μm is used for all observations. Note that at the lowest withdrawing rate $I_0 = 0.01$ mL.min^{-1}, the total withdrawing time τ exeeds the recording time so a smaller fraction of the total spatiotemporal diagram is shown. (right column) corresponding images of the final states obtained. Frictional, transitional and viscous flow regimes are distinguished by the dashed lines according to the qualitative differences in the observations.

of granular particles has a permeability increasing as the particles size decreases, as suggested by the the theoretical Carman-Kozeny relationship. So glass beads were sieved into 5 size ranges [53 – 75], [75 – 100], [100 – 150], [150 – 200], and [200 – 300] μm. A systematic exploration of the three flow regimes described above has been conducted for every size ranges. Figure 4 gives a phase diagram summarizing the observations with squared beads size horizontally, and imposed flow rate vertically. Observations corresponding to frictional, transitional, or viscous flow regime are pointed respectively with disks, open circles, and solid squares.

6 Conclusion

We observed the self structuring of a confined granular material and liquid mixture under capillary stress. A gas/liquid meniscus driven along a narrow tube by a

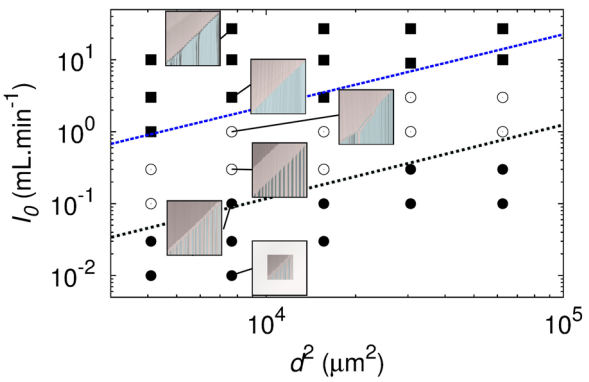

Figure 4. Phase diagram featuring the various flow regimes obtained when varying the withdrawing rate $I_0 \in [0.01, 30]$ mL.min^{-1}, and the bead sizes $d \in [53-75]$, $[75-100]$, $[100-150]$, $[150-200]$, and $[200-300]$ μm obtained after sieving. Disks, circles and squares represent respectively frictional, transitional and viscous flow regime. Spatio-temporal diagrams observed in fig 3 are indicated. Dashed lines are used for flow regime demarcations.

syringe pump bulldozes sedimented glass beads and forms regular granular plugs spaced with empty gaps, or suspends and evacuates the granular material from the tube. Three flow regimes are put in evidence as determined by the imposed flow rate as well as the granular particles sizes. The simplified quasi one-dimensional setup presented here provides a useful tool to interprete the complex behaviour of confined granular material in 2D Hele-Shaw cells under capillary stress [13–15].
The complexity of the patterns observed in confined frictional fluid derives from a mixture of capillary, frictional and viscous interactions. Our setup is constraining the frictional fluid by reducing one degree of freedom in comparison to regular Hele-Shaw cells. A subsequent structuring is still occurring as the confinement preserves the internal fluid self-structuring.

Acknowledgements

This work has been supported by the Norwegian Research Council through the FRINAT Grant No. 213462/F20. B. S. ackowledges support from EPSRC Grant No. EPL/013177/1 and Sêr Cymru National Research Network in Advanced Engineering and Materials Grant No. NRN141.

References

[1] J. Trondvoll and E. Fjær, Int. J. Rock Mech. Min. Sci. Geomech. Abstr. **31**, 393 (1994)
[2] D. Gidaspow and J. Huang, Ann. Biomed. Eng. **37**, 1534 (2009)
[3] J. B. Freund and M. M. Orescanin, J. Fluid Mech. **671**, 466 (2011)
[4] O. Molerus, Powder Technol. **88**, 309 (1996)
[5] E. Rabinovich and H. Kalman, Powder Technol. **207**, 119 (2011)
[6] M. Strauss, S. McNamara, and H. J. Herrmann, Granular Matter **9**, 35 (2007)
[7] S. Shaul and H. Kalman, Powder Technol. **256**, 310 (2014)
[8] F. B. Soeypan, S. Cremaschi, C. Sarica, H. J. Subramani, and G. E. Kouba, AlChE J. **60**, 76 (2014)
[9] F. Boyer, E. Guazzelli, and O. Pouliquen, Phys. Rev. Lett. **107**, 188301 (2011)
[10] A. Fall, F. Bertrand, G. Ovarlez, and D. Bonn, Phys. Rev. Lett. **103**, 178301 (2009)
[11] R. Seto, R. Mari, J. F. Morris, and M. M. Denn, Phys. Rev. Lett. **111**, 218301 (2011)
[12] E. Brown and H. M. Jaeger, Rep. Prog. Phys. **77**, 046602 (2014)
[13] B. Sandnes, E. G. Flekkøy, H. A. Knudsen, K. J. Måløy, and H. See, Nat. Comm. **2**, 288 (2011)
[14] H. A. Knudsen, B. Sandnes, E. G. Flekkøy, and K. J. Måløy, Phys. Rev. E **77**, 023301 (2008)
[15] C. Chevalier, A. Lindner, M. Leroux, and E. Clément, J. NonNewton. Fluid **158**, 63 (2009)
[16] G. Dumazer, B. Sandnes, M. Ayaz, K. J. Måløy, and E. G. Flekkøy, Phys. Rev. Lett. **117**, 028002 (2016)
[17] H. A. Janssen, Z. Ver. Dtsch. Ing. **39**, 1045 (1895)
[18] B. Marks, B. Sandnes, G. Dumazer, J. A. Eriksen, and K. J. Måløy, Front. Phys. **3**, 41, (2015)